ASSESSMENT METHODOLOGY FOR DIAGONALLY CRACKED REINFORCED CONCRETE DECK GIRDERS

3.0 LABORATORY TESTING 121

3.1 SPECIMEN FABRICATION AND MATERIALS 121
3.2 CONTROL TESTS 127
3.2.1 Test Method 127
3.2.2 Support Condition Evaluation 129
3.2.3 Loading Protocol 133
3.2.4 Experimental Results 134
3.3 INCREASED LOADING RATE TEST 162
3.3.1 Test Method 162
3.3.2 Experimental Results 164
3.4 MOVING SUPPORT TESTS 164
3.4.1 Test Method 164
3.4.2 Experimental Observation 165
3.5 INFLUENCE OF FLEXURAL BAR DETAILS 165
3.5.1 Test Method 165
3.5.2 Experimental Results 165
3.6 SUMMARY OBSERVATIONS FROM CONTROL LABORATORY TESTS: 166
3.7 LOW-CYCLE FATIGUE TESTS 167
3.7.1 Test Method 168
3.7.2 Experimental Results 168
3.7.2.1 Low-Cycle Fatigue Specimen 5IT12L22 172
3.7.2.2 Low-Cycle Fatigue Specimen 6T6L22 172
3.7.2.3 Low-Cycle Fatigue Specimen 6IT6L22 174
3.7.2.4 Low-Cycle Fatigue Specimen 7IT6L22 175
3.7.2.5 Low-Cycle Fatigue Specimen 9IT12L22 176
3.7.2.6 Low-Cycle Fatigue Specimen 9T12L24 176
3.7.2.7 Low-Cycle Fatigue Specimen 10T24L24 178
3.7.3 Conclusions 179
3.8 HIGH-CYCLE FATIGUE TESTS 179
3.8.1 Test Method 180
3.8.2 Experimental Results 182
3.8.3 Results 191
3.8.4 Debonded Stirrup Specimens 199
3.8.4.1 Debonded Stirrup Test Results 199
3.8.5 Conclusions 203
3.9 MOVING LOAD TESTS 203

List of Figures

Figure 3.1: Typical specimen configuration 122
Figure 3.2a: Schematic of test frame with specimen for typical test 128
Figure 3.2b: Test frame with specimen for typical test 128
Figure 3.3: Typical instrumentation on test specimen 129
Figure 3.4: Setup for support condition evaluation 130
Figure 3.5: Roller conditions at opposite end of specimen for support condition evaluation 130
Figure 3.6: Displacement sensors to measure support component motions under lateral load applied to the base of the beam web 131
Figure 3.7: Horizontal displacements at supports for applied lateral force at base of beam web 131
Figure 3.8: Equivalent lateral stiffness of support for different amounts of vertical reaction 132
Figure 3.9: Estimated amount of free horizontal displacement required at supports for typical specimen with yielding flexural reinforcing steel 133
Figure 3.10: Control loading protocol (horizontal lines represent holding of load to mark and measure cracks) 134
Figure 3.11a: Load-displacement plot at midspan for Group 1 specimens 135
Figure 3.11b: Load-displacement plot at midspan for Group 2 specimens 136
Figure 3.11c: Load-displacement plot at midspan for Group 3 specimens 137
Figure 3.11d: Load-displacement plot at midspan for Group 4 specimens 138
Figure 3.11e: Load-displacement plot at midspan for Group 5 specimens 139
Figure 3.11f: Load-displacement plot at midspan for Group 6 specimens 140
Figure 3.11g: Load-displacement plot at midspan for Group 7 specimens 141
Figure 3.11h: Load-displacement plot at midspan for Group 8 specimens 142
Figure 3.11i: Load-displacement plot at midspan for Group 9 specimens 143
Figure 3.11j: Load-displacement plot at midspan for Group 10 specimens 144
Figure 3.11k: Load-displacement plot at midspan for Group 10 and 11 moving-load specimens 145
Figure 3.11l: Load-displacement plot at midspan for Group 11 moving-load specimens 146
Figure 3.12a: Digital photographs at failure for Group 1 specimens 147
Figure 3.12b: Digital photographs at failure for Group 2 specimens 148
Figure 3.12c: Digital photographs at failure for Group 3 specimens 149
Figure 3.12d: Digital photographs at failure for Group 4 specimens 150
Figure 3.12e: Digital photographs at failure for Group 5 specimens 151
Figure 3.12f: Digital photographs at failure for Group 6 specimens 152
Figure 3.12g: Digital photographs at failure for Group 7 specimens 153
Figure 3.12h: Digital photographs at failure for Group 8 specimens 154
Figure 3.12i: Digital photographs at failure for Group 9 specimens 155
Figure 3.12j: Digital photographs at failure for Group 10 specimens 156
Figure 3.12k: Digital photographs at failure for Group 11 specimens 157
Figure 3.13: Approach used to determine self-weight at the failure location for different specimens 160
Figure 3.14a: Crack motion for specimen C4T12 (unbonded stirrups) 161
Figure 3.14b: Crack motion for specimen IT18 161
Figure 3.15: Loading histories for specimen tested at higher loading rates 163
Figure 3.16: Typical applied force - stirrup strain response from low cycle fatigue specimen 9T12, part 4 171
Figure 3.17: Typical applied force - crack motion response from low cycle fatigue specimen 9T12, part 2 171
Figure 3.18: Instrumentation for damage sequencing of stirrups for specimen 6T6L22 173
Figure 3.19a: Schematic of high-cycle fatigue test setup 181
Figure 3.19b: Image of high-cycle fatigue test setup 181
Figure 3.20: Example strain ranges during HCF test (specimen 3IT12 south end) 185
Figure 3.21: Example strain gage means during HCF test (specimen 6IT10 North end) 185
Figure 3.22: Example load and crack motion sensor ranges during HCF test (specimen 3IT12) 186
Figure 3.23: Example load and crack motion sensor means during HCF test (specimen 5IT12-B1) 186
Figure 3.24: Increasing strain range in specimen 9T12-B4, having cut and straight bars during HCF test 191
Figure 3.25: Measured strain comparing two interval tests for specimen 6IT10 192

Figure 3.26: Example of debris associated with bond damage around stirrup legs: a) specimen 6T10; b) specimen 3IT12 193
Figure 3.27: Strain gage and associated crack motion sensor at the eventual failure crack in specimen 6IT10. Note that after many cycles, less strain is needed to achieve the same crack movement 193
Figure 3.28: Changes in strain range and crack range for specimen 3IT12 over a 2,000,000 cycle HCF test. 194
Figure 3.29: Ductile fracture of stirrup at ultimate strength: a) sensor GS8 on specimen 3IT18; b) another example from specimen 3IT12 195
Figure 3.30: Fracture surface on east leg of stirrup from high-cycle fatigue specimen 3IT18 at 9 in. below sensor GS2 195
Figure 3.31: Fracture surfaces on west leg of stirrup from high-cycle fatigue specimen 3IT18 at 2 in. above sensor GS7 196
Figure 3.32: Detail from specimen 3IT18 load and crack motion sensor means. Note the change after 1,750,000 cycles 197
Figure 3.33: Detail from specimen 3IT18 Load and crack motion sensor ranges. Note the change after 1,750,000 cycles 197
Figure 3.34: Detail from specimen 3IT18 South strain gage means. Note the change after 1,750,000 cycles. 198
Figure 3.35: Detail from specimen 3IT18 South strain gage ranges. Note the change after 1,750,000 cycles 198
Figure 3.36: Crack pattern and instrument locations for 5IT12-B4 and 7IT12 specimens 200
Figure 3.37: Load-midspan displacement plots for 5IT12-B4 and 7IT12 specimens 201
Figure 3.38b: Stirrup strains and crack displacements for 5IT12-B4 and 7IT12 specimens: a) stirrup strains in the north-end side; b) crack displacements 202

List of Tables

Table 3.1: Concrete Mix Design (5.5-bag Mix) 123
Table 3.2: Concrete Mix Design (5-bag Mix) 123
Table 3.3: Concrete properties at 28 days 124
Table 3.4: Concrete and steel properties for each specimen on the day of test 125
Table 3.4 (continued): Concrete and steel properties for each specimen on the day of test 126
Table 3.5: Salient test results for laboratory specimens 158
Table 3.5 (continued): Salient test results for laboratory specimens 159
Table 3.6a: Time to peak load at a bent cap for different span lengths and vehicle speeds 162
Table 3.6b: Loading rates for different test load increments 163
Table 3.7: Loading levels and number of cycles for low-cycle fatigue tests 169
Table 3.8: Average strain range for low-cycle fatigue tests (strain is microstrain) 170
Table 3.9: Precrack stage crack widths for HCF specimens 180
Table 3.10: Stirrup strain ranges at the beginning and completion of HCF testing 183
Table 3.11: Crack displacement ranges at the beginning and completion of HCF testing 184
Table 3.12a: Stirrup strain ranges during HCF interval tests 187
Table 3.12a (continued): Stirrup strain ranges during HCF interval tests 188
Table 3.12a (concluded): Stirrup strain ranges during HCF interval tests 189
Table 3.12b: Crack displacement ranges during fatigue interval tests 190

3.0 LABORATORY TESTING

Forty-four (44) laboratory tests were conducted to evaluate the behavior of large-sized lightly-reinforced RC girders with vintage proportions and properties. Member proportions were based on a database of cracked bridges within the ODOT inventory as described in Higgins, *et al*. (*2004*). Typical member cross-section was 48 in. overall height with a 14 in. wide stem and included a 6 in. thick deck portion that was 3 ft wide, as shown in Figure 3.1. Complete details for each of the specimens are described below and are contained in Appendix A1.

Two loading configurations were considered: T (deck in flexural compression) and inverted-T (IT) (deck in flexural tension). The T configuration reflects shear in the presence of positive moment, as at simply supported ends of a bridge. The IT configuration reflects shear in the presence of negative moment, as over continuous support locations such as bents and piers.

Several different loading protocols were investigated: incrementally increasing load amplitudes with unloading, high-cycle fatigue after initial diagonal cracking, and low-cycle fatigue. Different stirrup spacing, as well as anchorage and flexural bar cutoff details were included in the study.

Typical tests were performed under static conditions, although one test was performed to simulate loading rates associated with a heavy vehicle traveling over a bridge of typical span length. A series of tests was performed by changing the support conditions after significant cracking was imposed on the specimen in the initial support configuration. Finally, a series of tests was performed with a moving load on specimens representing a portion of a main girder from a typical vintage RCDG bridge. Each of these test series is described below.

3.1 SPECIMEN FABRICATION AND MATERIALS

Beam specimens used in the laboratory testing phase were produced by Morse Bros. Prestressed Concrete Group of Harrisburg, OR, a ready-mix/precast/prestressed concrete supplier. Formwork was constructed to allow four beam specimens to be cast at a time. To construct the 44 specimens used in the testing program, 11 groups of beams were produced. Specimens were designed by OSU and constructed according to OSU approved shop drawings that were prepared by Morse Bros. Shop drawings for the specimens are contained in Appendix A1.

Prior to concrete placement, the as-fabricated reinforcing cages were inspected and verified to correspond with shop drawings. Lifting locations required for specimen handling were carefully detailed to minimize supplemental force transfer at the interface between the deck and stem. This was accomplished by wrapping the lifting loops with foam or using PVC pipe to prevent concrete bearing on lifting inserts as detailed in the shop drawings.

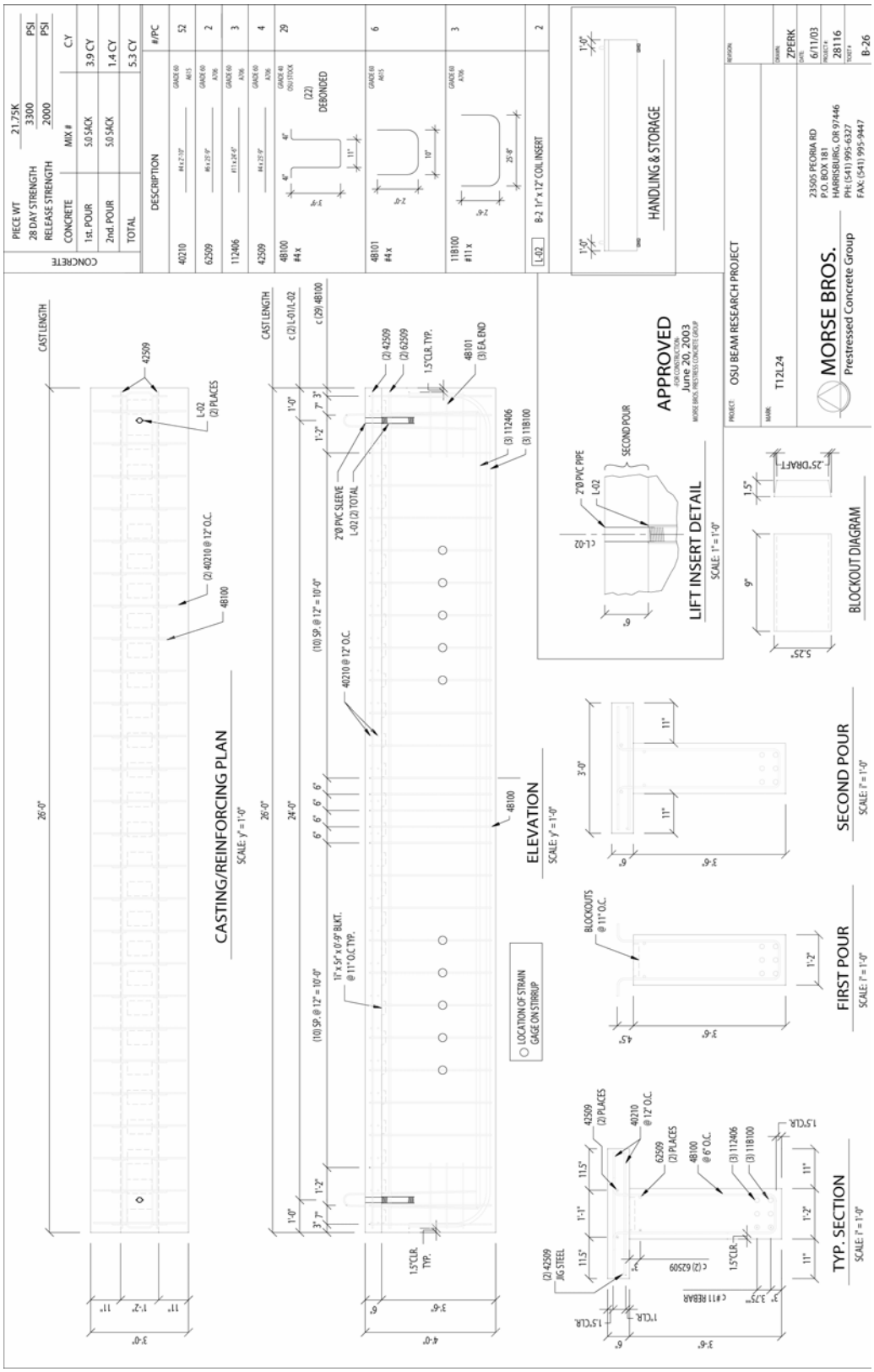

Figure 3.1: Typical specimen configuration

To reflect 1950's construction practice of cast in-place conventionally reinforced concrete deck-girder bridges, beam specimens were cast in two separate operations. In the first operation, the beam stems were cast and shear keys, spaced 11 in. on-center, were stamped into the web after concrete placement and consolidation as shown in Figure 3.1. Dimensions of the shear keys were 9 in. x 5.25 in. x 1.5 in. (length x width x depth) and were based on design details for bridges constructed in the mid-1950's. Beam stems were allowed to cure for 7 days prior to placing concrete for the deck. All beams were allowed to cure a minimum of 28 days before shipment to the laboratory for testing.

Beam specimens also reflected 1950's vintage AASHTO Class-A concrete consisting of cement, sand, aggregate, and water (*AASHTO 1953; AASHTO 1957*). A slight amount of air-entraining admixture was added to obtain desired workability and material properties. Concrete was batched on-site and transported to the formwork in a ready-mix truck. The amount of cement and the water-cement ratio were adjusted to provide a relatively low compressive strength typical of the specified 3300 psi concrete strength of the time. For the first set of beams (Cast 1) a 5.5-bag mix design was used with a mix ratio of 1:2.6:7.1:7 (Water: Cement: Coarse Aggregate: Fine Aggregate). This produced a 28-day strength of approximately 4500 psi. The remaining beams were cast using a 5 bag mix having a ratio of 1:3:11.4:10. Mix designs for both the 5.5 bag mix and 5 bag mix can be seen in Table 3.1 and 3.2.

Table 3.1: Concrete Mix Design (5.5-bag Mix)

Type I Cement	515	lb/yd^3
1/2" Coarse Aggregate	707	lb/yd^3
3/4" Coarse Aggragate	713	lb/yd^3
Fine Aggregate	1400	lb/yd^3
Water	200	lb/yd^3

Table 3.2: Concrete Mix Design (5-bag Mix)

Type I Cement	471	lb/yd^3
1/2" Coarse Aggregate	705	lb/yd^3
3/4" Coarse Aggregate	1052	lb/yd^3
Fine Aggregate	1539	lb/yd^3
Water	155	lb/yd^3

Compressive strengths of concrete for each specimen were determined by 6 x 12 in. cylinder breaks on the day-of-test using a 300 kip capacity concrete testing machine. Modulus of rupture and split cylinder tests were performed 28 days after casting for each group of specimens to determine tensile strength of the concrete. Testing procedures for concrete compression test, concrete split cylinder test, and modulus of rupture test were performed in accordance with ASTM C39, ASTM C496, and ASTM C78, respectively. Loading rates for the compression test, concrete split cylinder test, and modulus of rupture test were performed in the range of 1000 lbs/sec, 250 lbs/sec, and 30 lbs/sec, respectively. Compression tests on the day-of-test also included measurement of cylinder strains for stem concrete to obtain compressive stress-strain curves. The compressive stress-strain curves for each specimen is shown in Appendix A2.

Concrete properties at 28 days for each group of specimens are summarized in Table 3.3 and properties on the day-of-test are shown in Table 3.4. The average concrete strength for all groups was 4332 psi with a COV of 12.4% and average peak strain at the peak stress, ε'_c, from the concrete stress-strain curves was 0.0040 in/in with a COV of 14.7%. The average concrete strength for the specimens was higher than the design specified concrete strength of 3300 psi. The average peak strain was high compared to a typical strain of about 0.002 in/in for concrete having 4000 psi strength.

Table 3.3: Concrete properties at 28 days

Group	f'_c (psi)	f_{ct} (psi)	β_{ct}	f_r (psi)	β_r
1	4485	460	6.9	490	7.3
2	3160	364	6.5	455	8.1
3	3870	369	5.9	310	5.0
4	3600	344	5.7	388	6.5
5	3550	340	5.7	377	6.3
6	4225	411	6.3	430	6.6
7	4120	377	5.9	314	4.9
8	3870	391	6.3	367	5.9
9	3360	311	5.4	412	7.1
10	3835	357	5.8	518	8.4
11	3610	390	6.5	458	7.6
Avg.	3790	374	6.1	411	6.7
COV	10.2	10.6	7.3	16.4	17.1

Tensile strength of concrete was approximated as proportional to the square root of the compressive strength. Based on a large number of tests (*Mirza, et al. 1979*), the mean split cylinder strength over the square root of the compressive stress was 6.4 and the mean modulus of rupture over the square root of the compressive stress was 8.3. As shown in Table 3.4 for this research, the mean split cylinder strength over the square root of the compressive stress was 6.1, and the mean modulus of rupture over the square root of the compressive stress was 6.7. The relationship between the tensile strength and the compressive strength of the concrete obtained from the split cylinder tests was relatively similar to that described by Mirza *et al*. (*1979*) However, the relationship obtained from the modulus of rupture tests was lower.

All reinforcing steel was fabricated by a local rebar fabricator per OSU approved shop drawings. Selected stirrups were instrumented in the laboratory and then shipped to the precaster for construction of reinforcing cages. Reinforcing steel in the beams consisted of ASTM A615 Grade 40 and Grade 60 steel and flexural bars above size #6 were of ASTM A706 Grade 60. Stirrups used for all specimens were from a single heat of ASTM A615 Grade 40 reinforcing steel. The Grade 40 #4 reinforcing bars had a yield stress of 51 ksi. The bars were taken from the lowest yield-stress heat of steel produced by Cascade Steel Rolling Mills during a production run. Miscellaneous remaining #4 reinforcing steel used for the beams was ASTM A-615 Grade 60 and varied for each cast.

Table 3.4: Concrete and steel properties for each specimen on the day of test

Specimen	Concrete			Reinforcing Steel											
	Stem		Deck	#4 Grade 40			#11 Grade 60			#6 Grade 60			#4 Grade 60		
	f'_c (psi)	ε'_c	f'_c (psi)	σ_y (ksi)	σ_u (ksi)	σ_f (ksi)/ ε_f	σ_y (ksi)	σ_u (ksi)	σ_f (ksi)/ ε_f	σ_y (ksi)	σ_u (ksi)	σ_f (ksi)/ ε_f	σ_y (ksi)	σ_u (ksi)	σ_f (ksi)/ ε_f
1T6	4700	NA	4370	50.7	78.9	71.1/ 0.286	67.2	99.5	82.2/ 0.218	66.3	93.6	78.2/ 0.308	63.3	105.5	NA
1IT6	4775	NA	4515												
1T18	4925	0.0035	4360												
1IT18	4550	0.0035	4410												
2T10	3550	0.0039	3360				75.8	111.7	89.5/ 0.224	66.9	98.4	78.3/ 0.320	64.8	104.3	95.7/ 0.222
2IT10	3290	NA	3105												
2T12	3520	0.0038	3440												
2IT12	3575	0.0032	3005												
3T12	3990	0.0034	3660				69.7	103.7	82.0/ 0.220	60.7	88.1	70.8/ 0.325	67.3	107.1	NA
3IT12	4180	NA	3455												
3T18	3970	0.0044	3440												
3IT18	3915	0.0036	3220												
4IT6-10	3790	NA	3410				68.3	103.5	82.0/ 0.223	59.7	84.9	69.3/ 0.268	61.0	96.9	82.4/ 0.232
4IT8-12	3710	0.0030	3595												
4T10-12	3945	NA	2995												
4T12-18	4060	NA	3000												
5IT12-B1	3700	0.0037	4610				69.2	103.3	81.3/ 0.215	59.5	83.8	69.5/ 0.220	59.8	100.3	77.7/ 0.262
5IT12-B2	4160	0.0037	4640												
5IT12-B3	4310	0.0044	4530												
5IT12-B4	4130	NA	4130												
6T6	4590	0.0051	4260				71.6	106.4	83.0/ 0.221	62.9	89.1	70.4/ 0.223	NA	NA	NA
6IT6	5110	0.0042	3920												
6T10	4595	0.0048	4195												
6IT10	5495	0.0051	3875												

Table 3.4 (continued): Concrete and steel properties for each specimen on the day of test

Specimen	Concrete			Reinforcing Steel											
	Stem		Deck	#4 Grade 40			#11 Grade 60			#6 Grade 60			#4 Grade 60		
	f'_c (psi)	ε'_c	f'_c (psi)	σ_y (ksi)	σ_u (ksi)	σ_f (ksi)/ ε_f	σ_y (ksi)	σ_u (ksi)	σ_f (ksi)/ ε_f	σ_y (ksi)	σ_u (ksi)	σ_f (ksi)/ ε_f	σ_y (ksi)	σ_u (ksi)	σ_f (ksi)/ ε_f
7T6	4405	0.0044	4215	50.7	78.9	71.1/ 0.286	74.8	101.0	79.5/ 0.274	65.5	93.2	82.0/ 0.282	67.2	110.2	98.5/ 0.207
7IT6	4350	0.0043	3740												
7T12	4280	0.0044	4310												
7IT12	4165	0.0038	3995												
8IT10	4750	0.0041	4090				74.9	98.9	74.0/ 0.265	63.6	91.1	85.0/ 0.298	67.1	110.8	NA
8IT12	4840	0.0038	4045												
8T12-B3	5070	0.0043	4570												
8T12-B4	4995	0.0040	4725												
9IT12-B1	4285	0.0042	5405				70.8	96.1	68.5/ 0.271	62.6	90.0	89.0/ 0.287	NA	NA	NA
9IT12-B2	4605	0.0044	5465												
9T12-B3	4645	0.0045	4890												
9T12-B4	4705	0.0049	4910												
10T0	4610	0.0043	4445				69.3	107.3	88.7/ 0.217	69.4	98.9	76.3/ 0.273	64.5	94.1	78.0/ 0.263
10T12	4655	NA	4405												
10T24-B3	3450	0.0031	3995												
10T24-B4	3420	0.0027	3740												
11IT16	4635	0.0040	4430												
11T16.5	4970	0.0041	4170												
11T22-B3	4470	0.0032	3510												
11T22-B4	4750	0.0042	4010												
Avg.	4332	0.0040	4052				71.2	103.1	81.1/ 0.235	63.7	91.1	76.9/ 0.280	64.4	103.7	86.5/ 0.237
COV	12.4	14.7	15.6				4.3	4.4	7.7/ 10.4	5.2	5.6	9.0/ 12.9	4.5	5.9	11.5/ 10.4

Steel samples cut from the steel reinforcement in each specimen were tested to determine tensile properties. Yield stress (σ_y), ultimate stress (σ_u), fracture stress (σ_f), and fracture strain (ε_f) were obtained and are shown in Table 3.4. The #4 Grade-40, #4 Grade-60, and #6 Grade-60 steel were tested using the actual reinforcing bar cut to a length of 18 in. The #11 Grade-60 bar was machined in accordance with ASTM E8 for the 505 specimen size. The specimens were tested in a 110 kip capacity universal testing machine using a 2 in. gage length extensometer to measure strain. Tensile stress-strain curves for the steel are shown in Appendix A2.

Average yield stresses for #11 Grade-60, #6 Grade-60, #4 Grade-60, and #4 Grade-40 were 71.2, 63.7, 64.4, and 50.7 ksi, respectively. The average ultimate stresses for #11 Grade-60, #6 Grade-60, #4 Grade-60, and #4 Grade-40 were 103.1, 91.1, 103.7, and 78.9 ksi, respectively. The average fracture strains for #11 Grade-60, #6 Grade-60, #4 Grade-60, and #4 Grade-40 were 23.5%, 28.0%, 23.7%, and 28.6%, respectively.

After curing a minimum of 28 days at the precasting yard, specimens were shipped to the structural testing laboratory at OSU. Inverted-T beams were rolled into the inverted position before shipment. After arrival at the laboratory, specimens were placed in a reaction frame, instruments were installed, and the specimens were tested.

3.2 CONTROL TESTS

3.2.1 Test Method

The majority of tests were performed with a four-point loading configuration. Force was applied at midspan through a spreader beam to load points on the specimen spaced 24 in. apart. Applied load was measured with a 500 kip capacity load-cell mounted to the hydraulic actuator. The typical test setup is shown in Figures 3.2a and 3.2b. Instruments were applied to the specimen to capture both local and global behaviors; measurements were monitored during tests; and data were stored using a 16-bit PC-based data acquisition system.

For each test, data from approximately 42 sensors were collected. Sensors included load cells, strain gages, concrete clip gages, as well as displacement and tilt sensors. Sensors and their typical locations are illustrated in Figure 3.3. Specimen displacement at the load point was determined by subtracting support deformations from the load point deflection measurement taken relative to the strong floor. End rotations were measured using tilt sensors located on the specimen beyond the end supports. Strain gages were bonded to selected stirrups and installed prior to casting of concrete. For some tests, strain gages were installed on stirrups or flexural reinforcing bars at diagonal crack locations by chipping into the concrete to expose the embedded steel.

Crack widths were measured three ways: displacement transducers were placed on diagonals within the test span; individual displacement transducers were mounted across diagonal cracks; and at each load step a visual crack comparator was used to determine crack widths at selected locations on the specimen. Support locations were varied for different tests to permit testing of different shear-to-moment ratios. However, the typical center-to-center spacing of supports was 21.6 ft for the inverted-T and 24 ft for the T specimens.

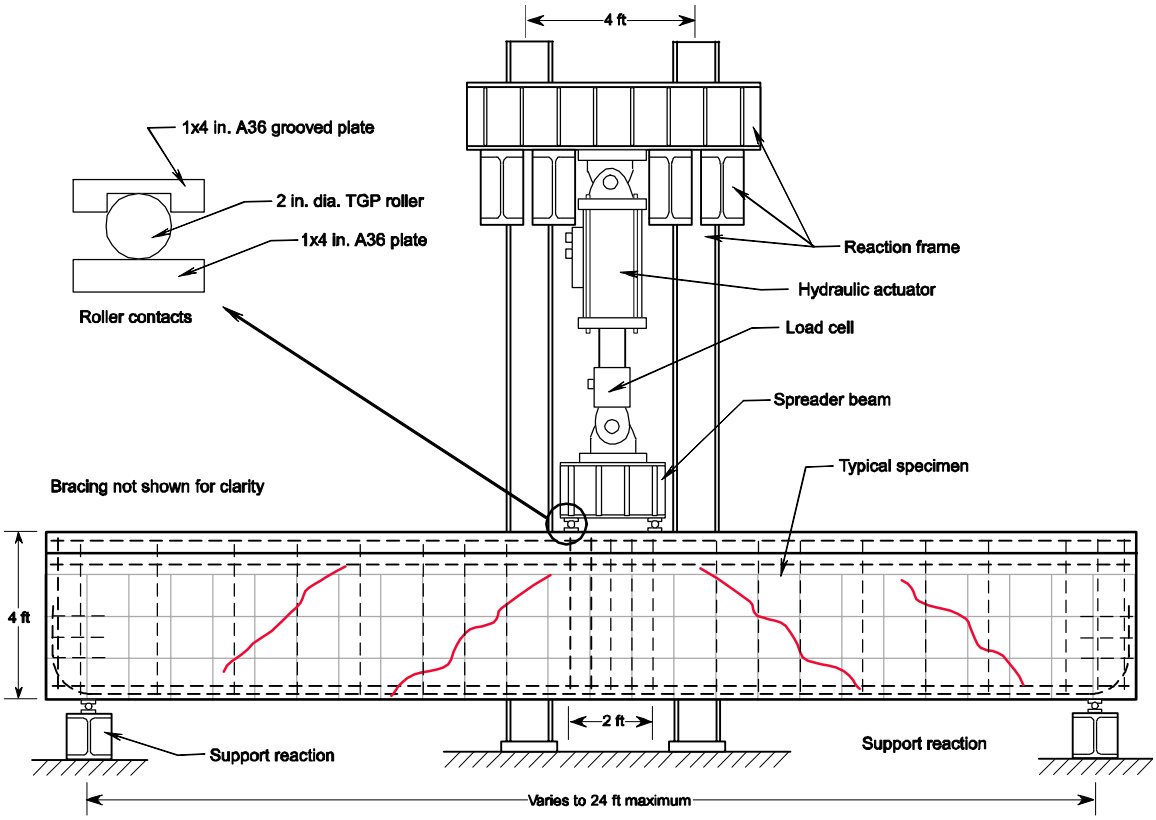

Figure 3.2a: Schematic of test frame with specimen for typical test

Figure 3.2b: Test frame with specimen for typical test

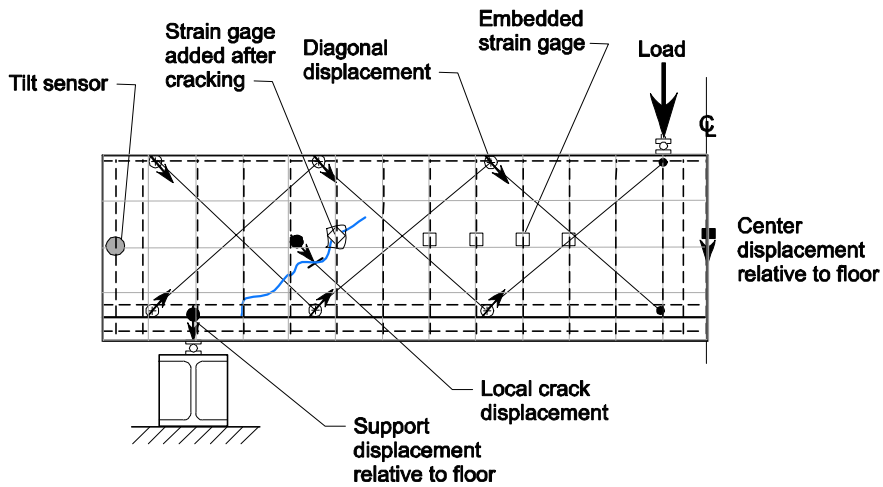

Figure 3.3: Typical instrumentation on test specimen

3.2.2 Support Condition Evaluation

Support conditions were idealized as roller supports permitting rotation with vertical force and minimal horizontal thrust. Actual support behavior was assessed in the lateral direction and the axial thrust generated was estimated. Support conditions used for testing all stationary loaded specimens consisted of a 2 in. diameter turned-ground-and-polished (TGP) roller captive in a grooved plate that was bolted to a W12x120 floor reaction beam. The specimens were supported on 1 in. thick x 4 in. x 16 in. mild steel plates that rested on the roller. The long dimension of the plate was oriented transverse to the span of the specimen.

To assess these boundary conditions, a specimen was placed on the support bearings and a horizontal force was applied at the base of the web by a hydraulic cylinder with load cell, as shown in Figure 3.4. The reaction at the opposite end of the beam consisted of a true roller, as shown in Figure 3.5. Horizontal force was increased and lateral displacement of the beam, bearing plate, and steel reaction beam (shown in Figure 3.6) were measured.

To assess the role of the vertical support reaction magnitude, different applied loads were considered. These were 1) self-weight of the beam and 2) 50 kips of applied vertical load at midspan of the beam. For these conditions, the vertical reaction at the support was 10.875 kips for the self-weight and 35.875 kips for the combined self-weight with 50 kips of applied load at midspan.

Figure 3.4: Setup for support condition evaluation

Figure 3.5: Roller conditions at opposite end of specimen for support condition evaluation

Figure 3.6: Displacement sensors to measure support component motions under lateral load applied to the base of the beam web

The support responses for these two cases are shown in Figure 3.7. As seen in this figure, when small vertical reactions are on the supports, the beam slips on the reaction plate at relatively low lateral load (static friction ~700 lbs). At the larger reaction, the beam slips on the bearing plate at 2900 lbs. The average friction coefficient corresponding to the slip force was 0.073 for the two cases.

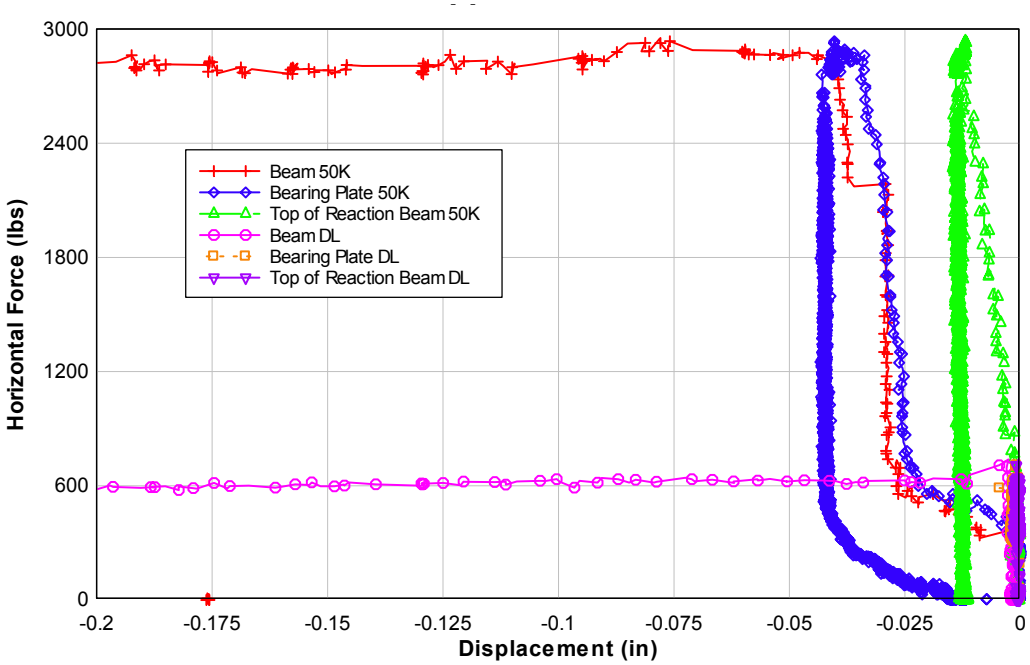

Figure 3.7: Horizontal displacements at supports for applied lateral force at base of beam web

For the case with larger vertical reaction, other support deformations occur before slip of the beam on the bearing plate. These included bearing plate movement relative to the reaction beam due to a gap between the roller and groove on the reaction beam (approximately 0.025 in.), as well as movement of the reaction beam relative to the laboratory floor. The friction force between the concrete beam and bearing plate develops approximately 7.3% of the shear at the support before slip occurs.

The secant stiffness of the support prior to slip was determined from the reaction beam displacement as 247 kips/in with an additional constant deformation component of 0.025 in. associated with the roller gap that occurs at low load. Combining the gap displacement and reaction beam stiffness components of the support conditions, an equivalent secant support stiffness was determined for the lateral force magnitude required to produce slip between the beam and bearing plate. Estimated equivalent support stiffness for different magnitudes of support reaction (shear force) is shown in Figure 3.8.

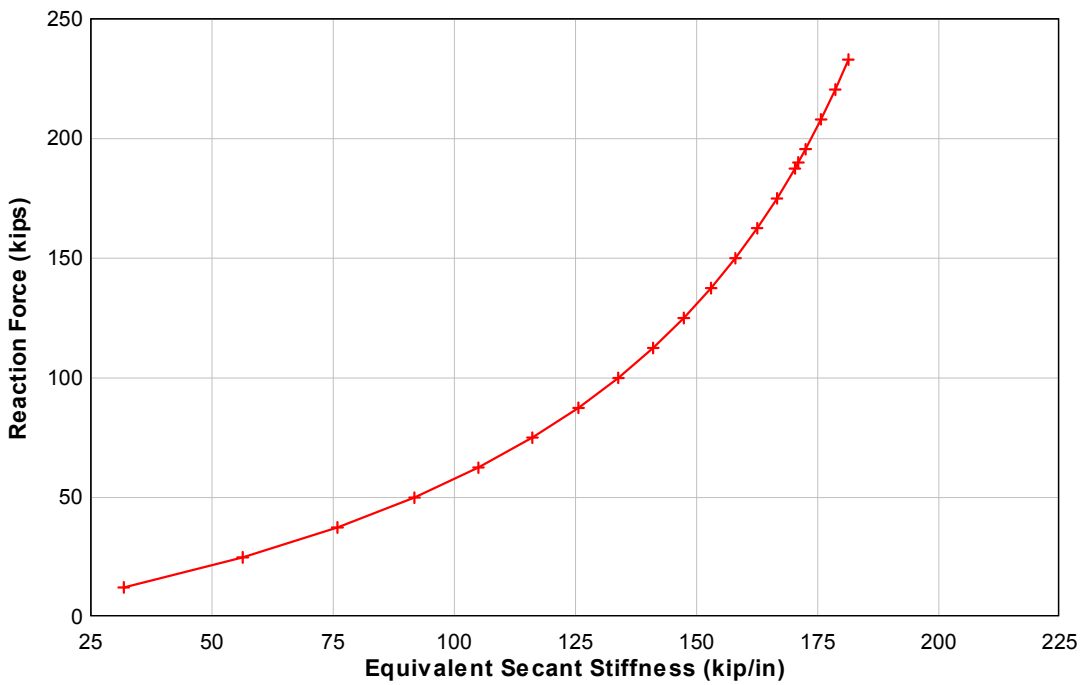

Figure 3.8: Equivalent lateral stiffness of support for different amounts of vertical reaction

Horizontal support displacement demands produced from flexure on a typical specimen were estimated by integrating longitudinal strains at the bottom of the beam over the length of the span. For this analysis, flexural tensile strains were taken at the level of the reinforcing steel. Strains were determined from moment-curvature analysis of the section with the Todeschini concrete constitutive rule for concrete f'_c=4000 psi and elasto-plastic material model for rebar with f_y=68 ksi (*Todeschini, et al. 1964*).

For a typical T-specimen with six #11 bars, the amount of longitudinal elongation of the beam at the level of the support was estimated at 0.015 in. just prior to yielding of the flexural rebar and 0.03 in. at ultimate (concrete crushing with the flexural steel yielding) as show in Figure 3.9.

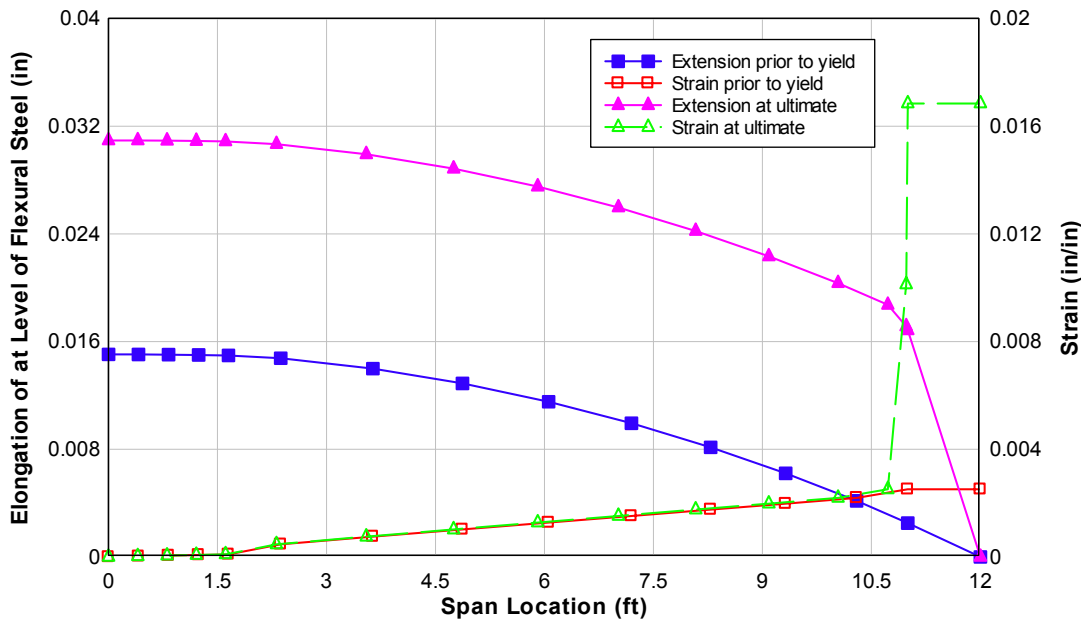

Figure 3.9: Estimated amount of free horizontal displacement required at supports for typical specimen with yielding flexural reinforcing steel

Substituting these lateral support displacements into the support stiffnesses determined previously (with V=190 kips for the flexural bars just prior to yielding and V=195.5 kips for the specimen at ultimate flexural capacity), the lateral force produced at the reactions was estimated at 2.6 kips just prior to flexural rebar yielding and 5.2 kips at ultimate. These values are below the slip force magnitude.

Slip between the plate and beam was not observed during control testing. Applying the support forces as external axial loads (approximated as applied to the centroid of the section), analysis of the section was performed using analysis program *Response 2000*™ (described further in the Analysis section) to determine the impact of these forces on the capacity prediction. Results indicated that for this relatively small magnitude of axial force, there was negligible impact on the resulting strength prediction for the typical beam specimen.

3.2.3 Loading Protocol

The imposed loading history consisted of loading and unloading cycles with each subsequent increment applied at a higher load magnitude. Typical tests were performed in displacement control using a closed-loop servo-hydraulic system. The loading protocol generally consisted of loading and unloading cycles with increasing load magnitudes in increments of 50 kips, as illustrated in Figure 3.10. When the peak force for each increment was achieved, the

displacement was held and crack widths were measured and crack extents were marked and recorded. The beam was subsequently unloaded and the crack widths were again measured and recorded when the load was near zero. This process was repeated until specimen failure.

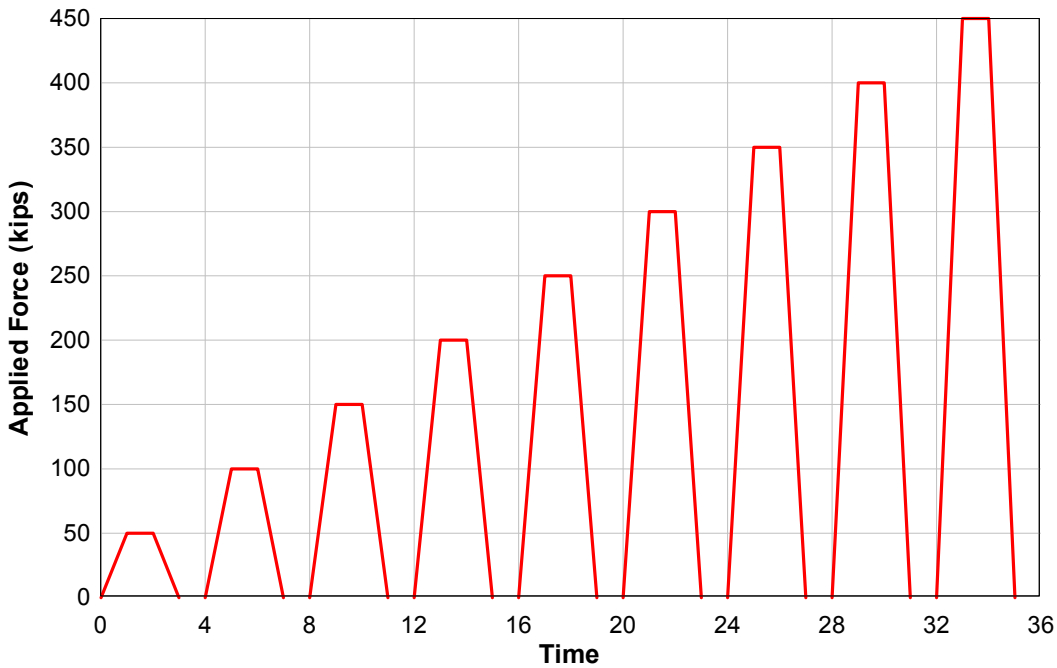

Figure 3.10: Control loading protocol (horizontal lines represent holding of load to mark and measure cracks)

3.2.4 Experimental Results

Overall load-deformation behavior of specimens is shown in Figures 3.11a-l. Digital photographs of specimens at failure are shown in Figures 3.12a-k. Instrument locations and crack patterns are contained in Appendix A3, and instrument data for specimens are contained in Appendix A4.

Key structural response quantities for each of the specimens are summarized in Table 3.5. Deflection reported in this table is taken from the specimen under the loading point and is corrected for support deformations. The largest diagonal crack width observed in the stem, w_{cr}, was measured with an ODOT crack comparator card or by a micrometer and occurred at the peak load in the cycle prior to failure.

Failure modes for most specimens were shear-compression failures (reported as Shear in Table 3.5), although flexural-tension and flexural-compression failures (reported as Flexural in Table 3.5) were observed for the specimens with 6 in. stirrup spacing. The IT specimen with 6 in. stirrup spacing failed in flexural compression while the T specimens with 6 in. stirrup spacing failed in flexural tension. Inverted-T beams with only 12 in. of flexural steel anchorage beyond the centerline of the support exhibited shear-tension failures (reported as Anchorage in Table 3.5) for widely spaced stirrups.

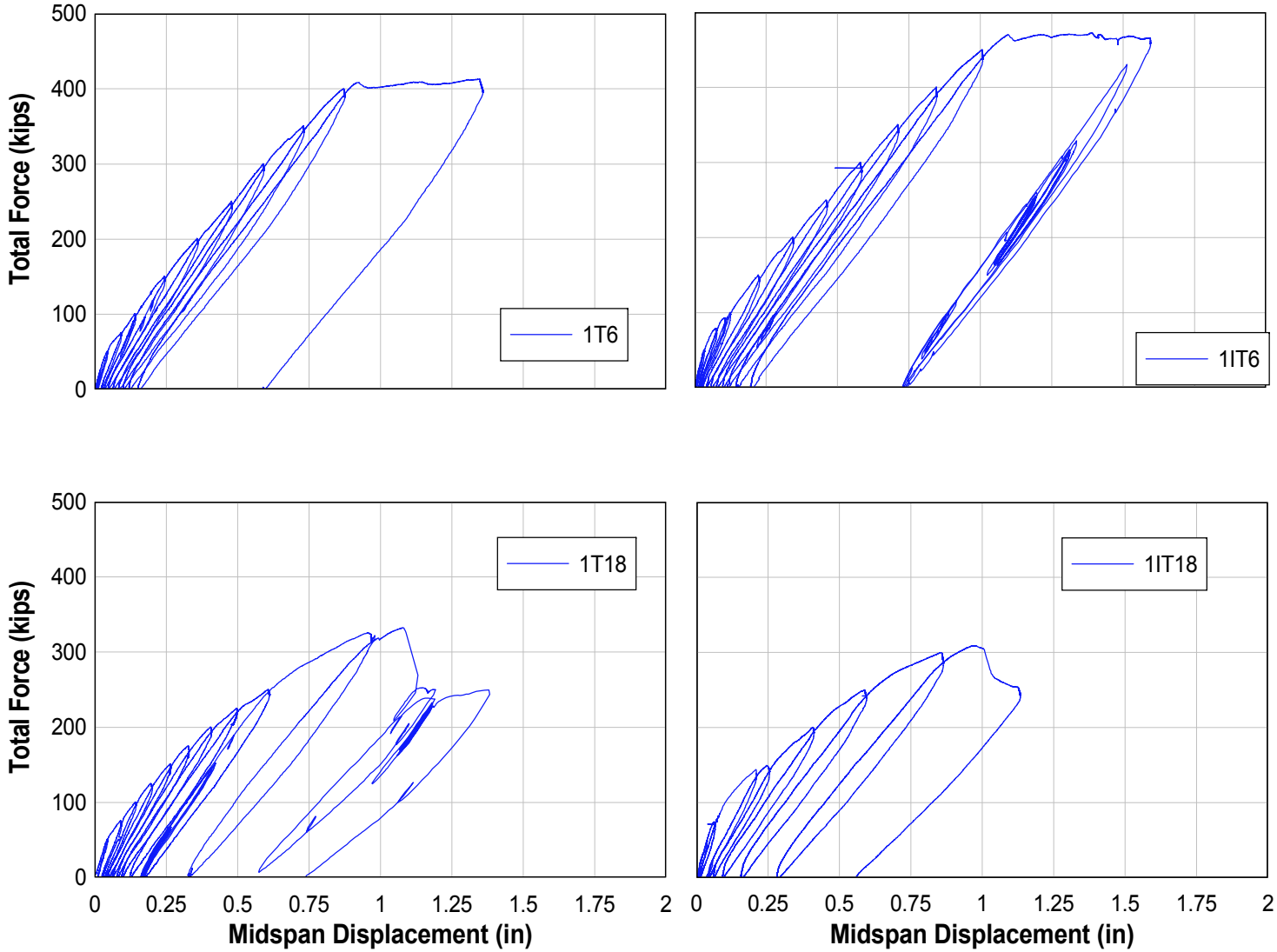

Figure 3.11a: Load-displacement plot at midspan for Group 1 specimens

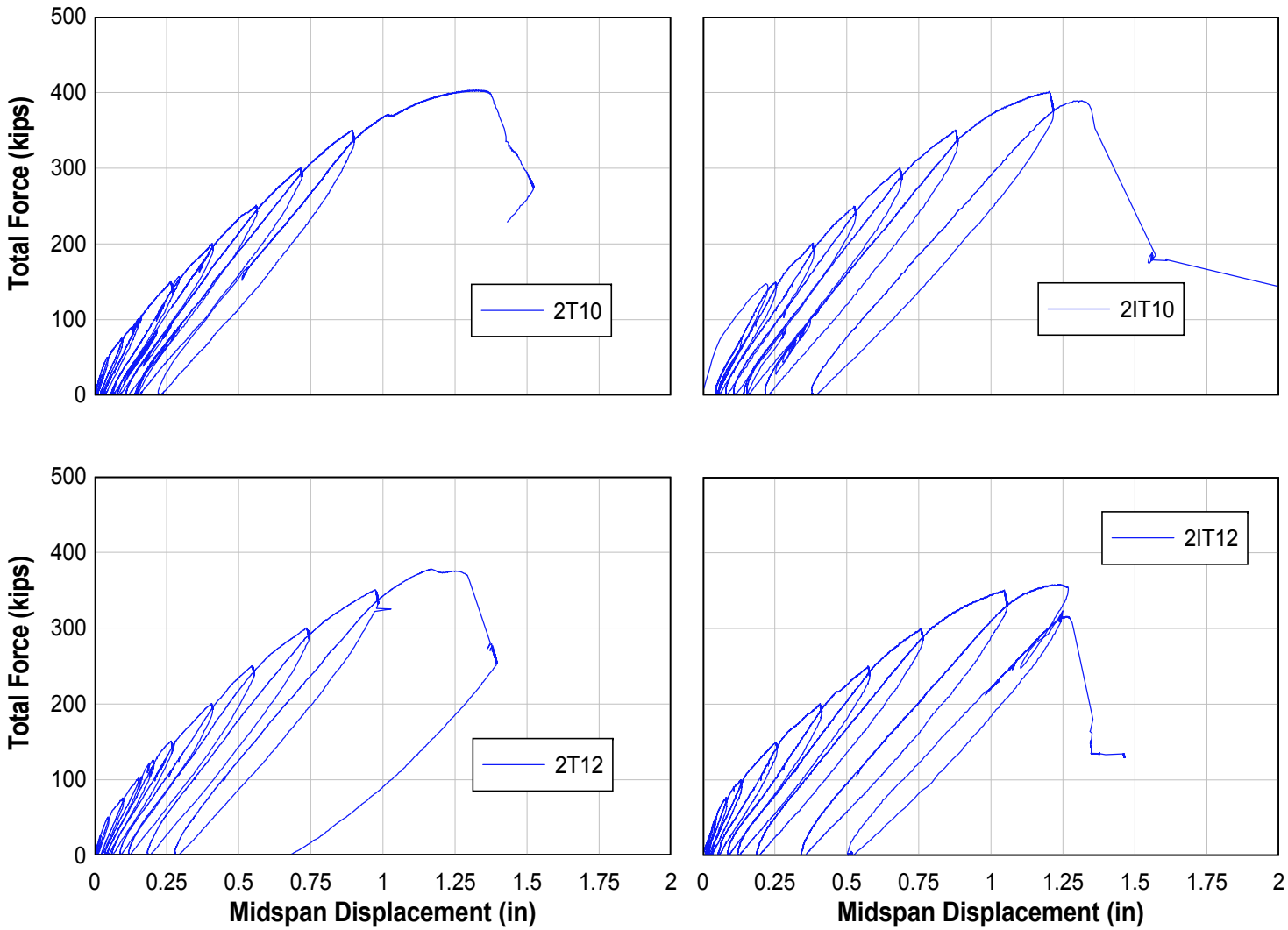

Figure 3.11b: Load-displacement plot at midspan for Group 2 specimens

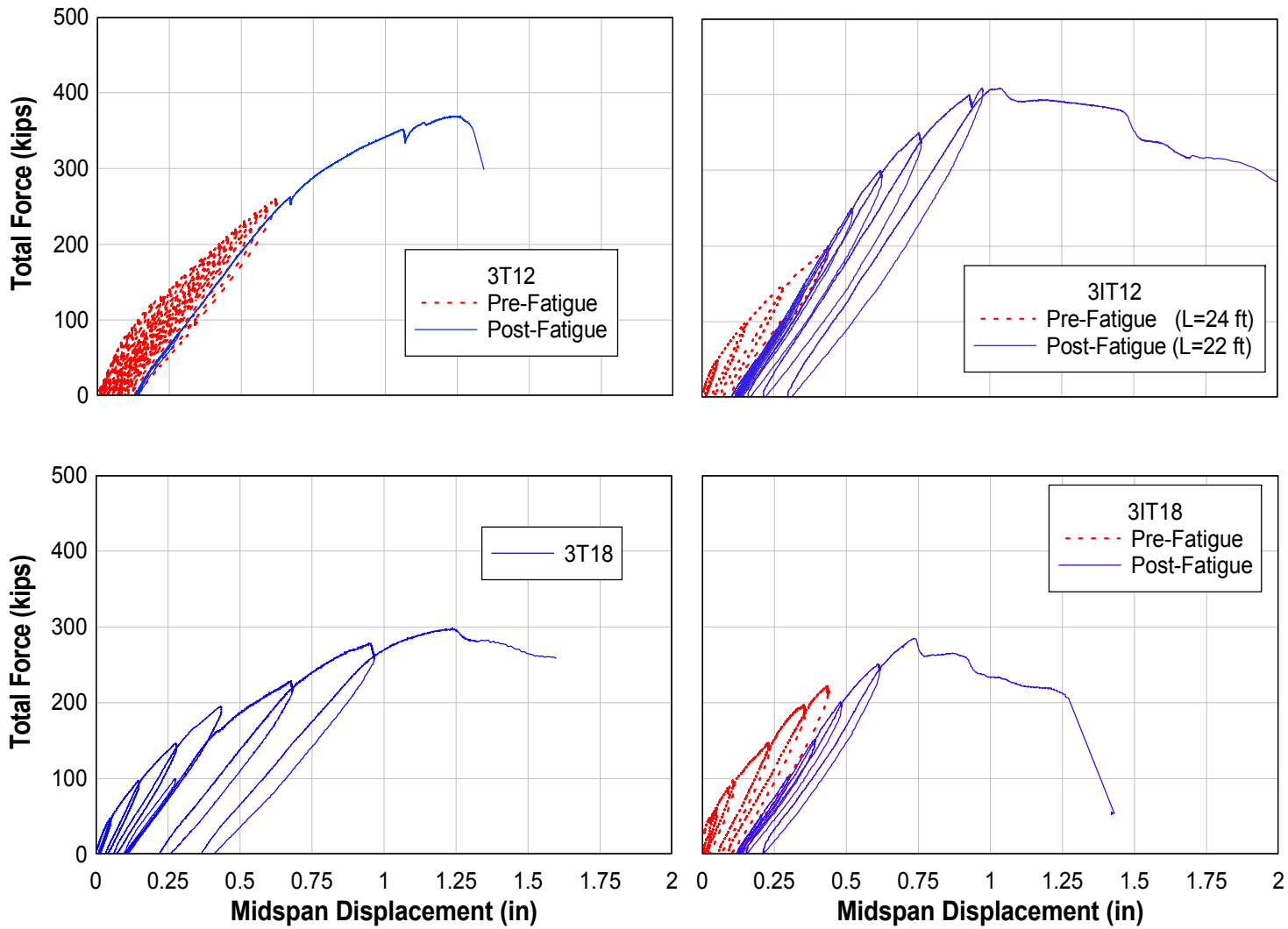

Figure 3.11c: Load-displacement plot at midspan for Group 3 specimens

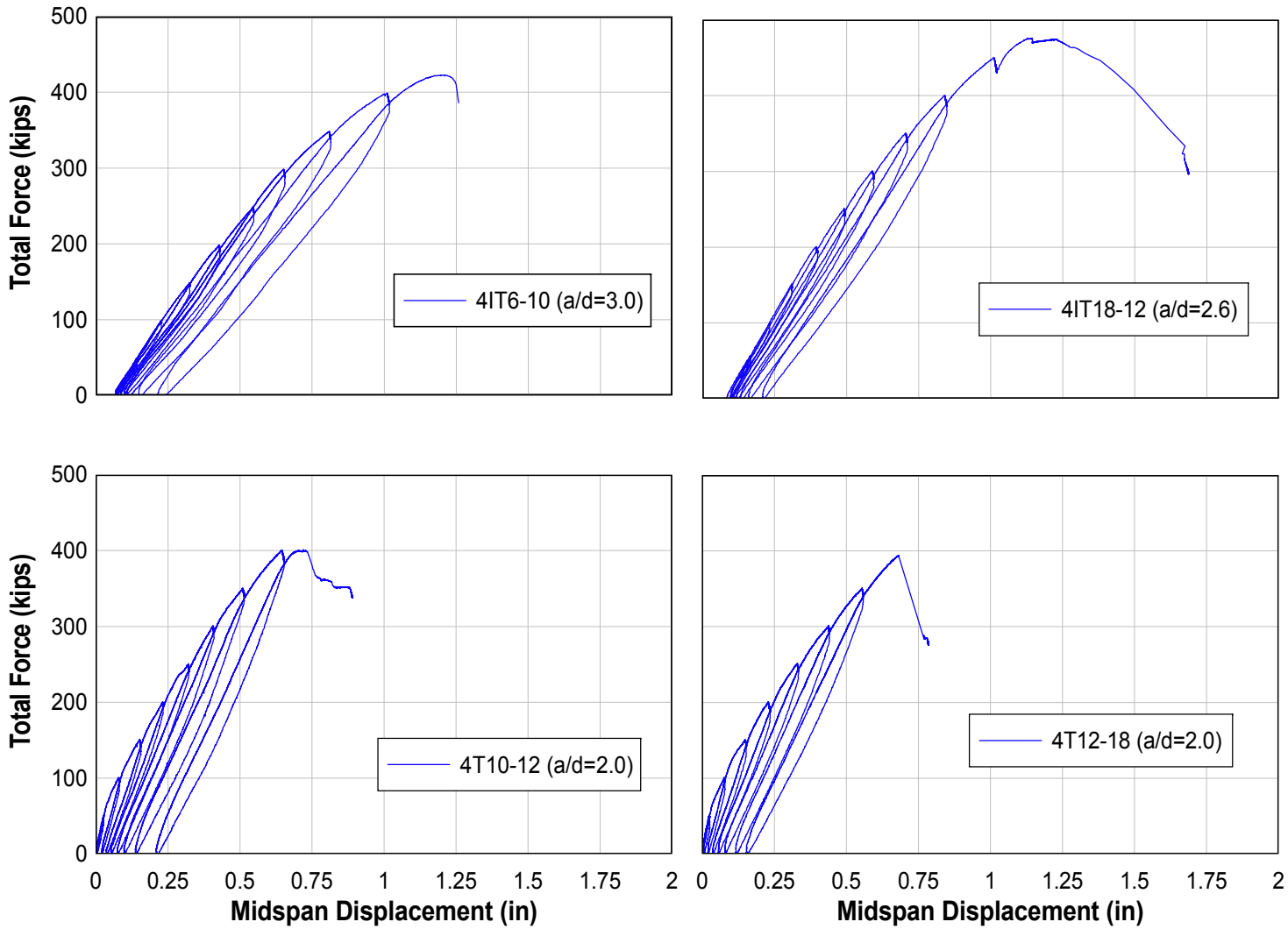

Figure 3.11d: Load-displacement plot at midspan for Group 4 specimens

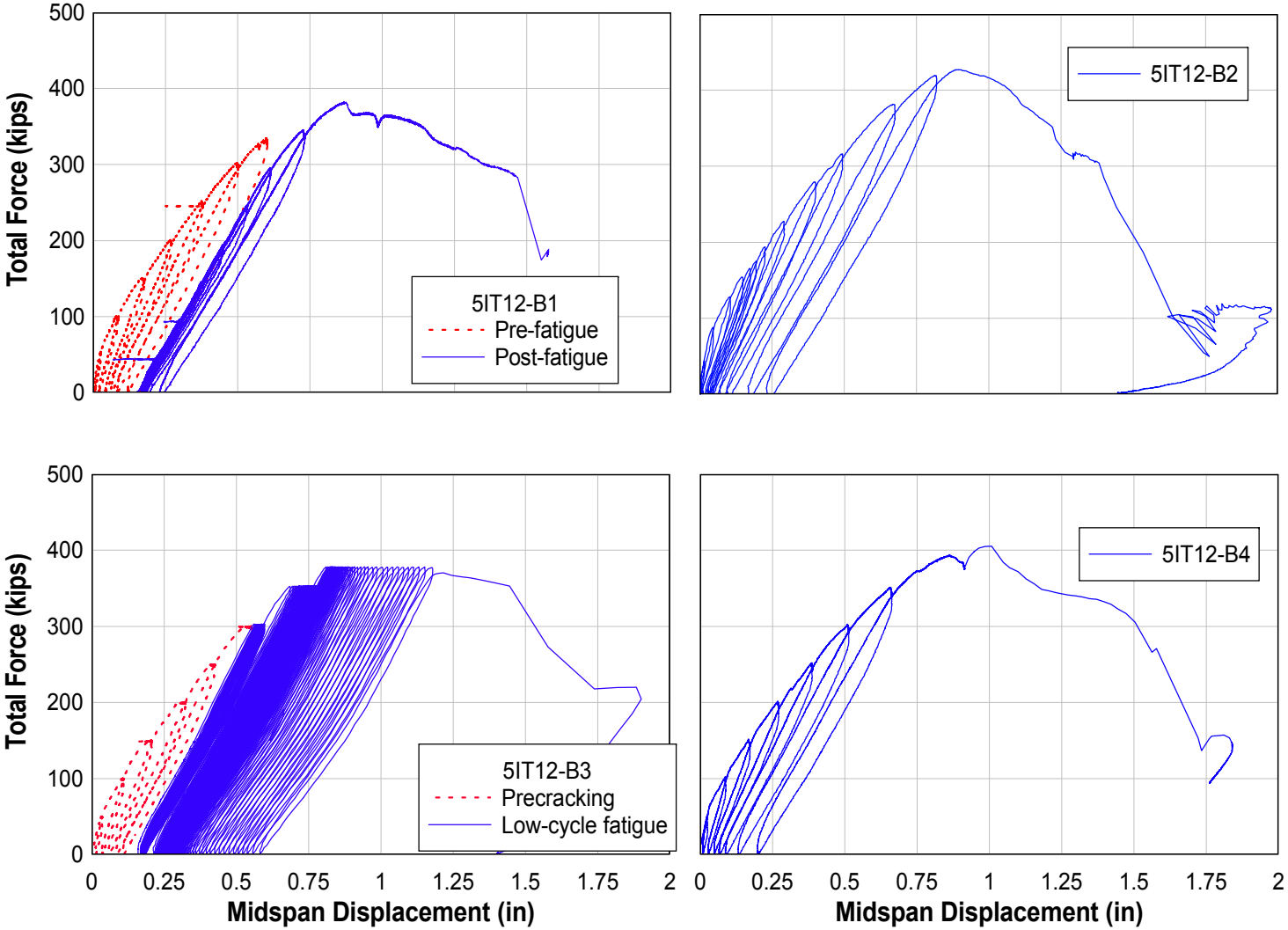

Figure 3.11e: Load-displacement plot at midspan for Group 5 specimens

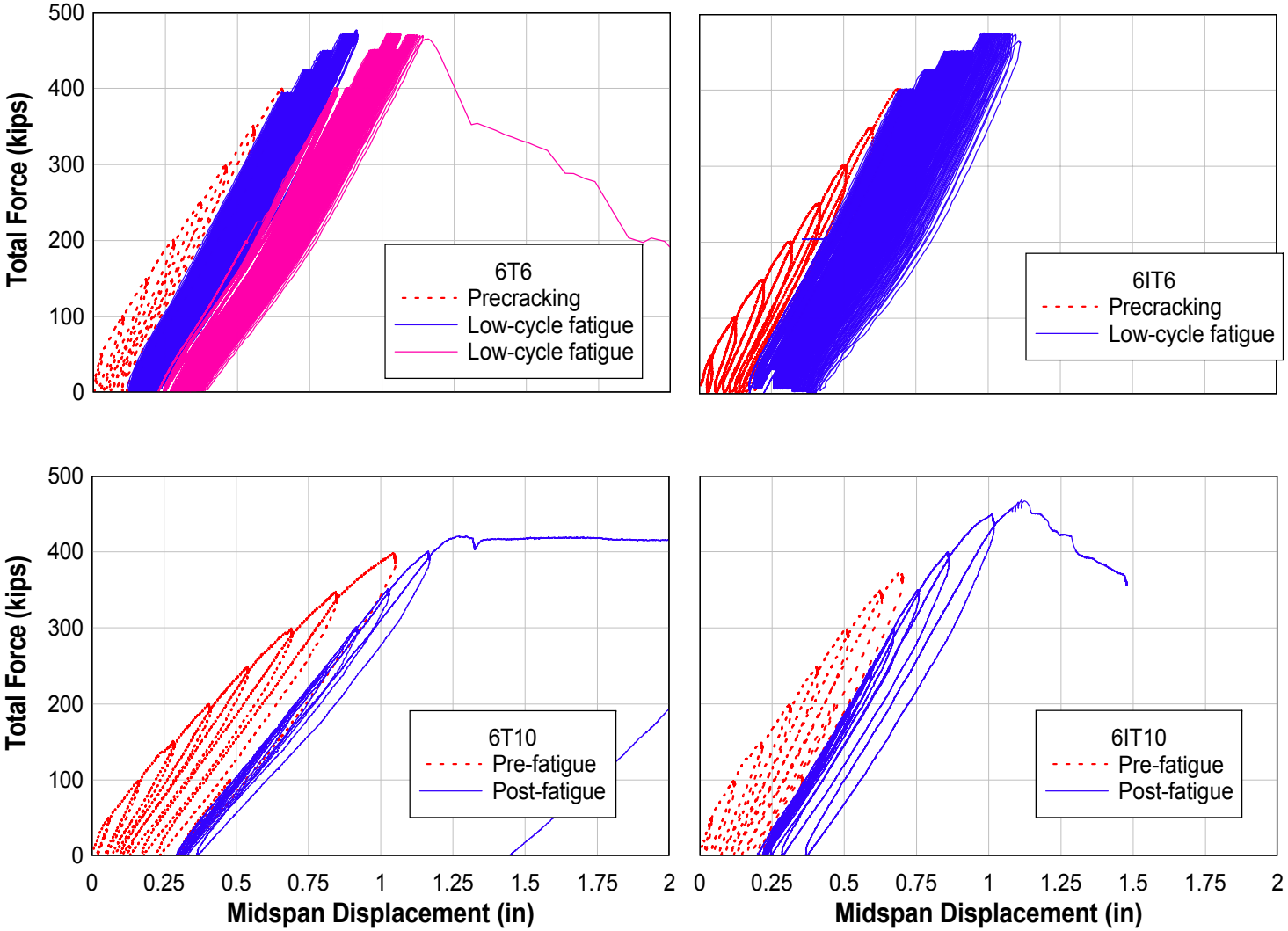

Figure 3.11f: Load-displacement plot at midspan for Group 6 specimens

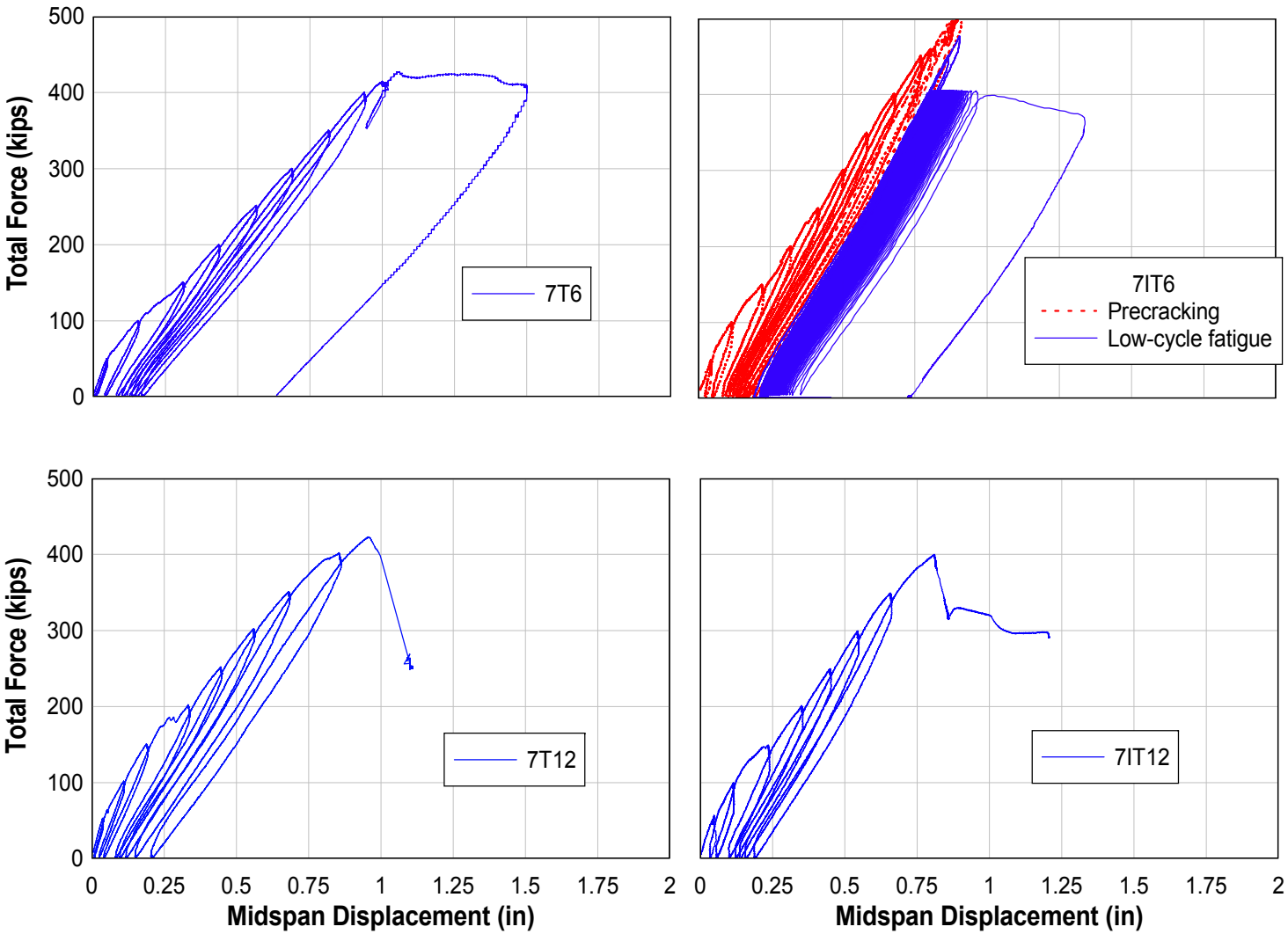

Figure 3.11g: Load-displacement plot at midspan for Group 7 specimens

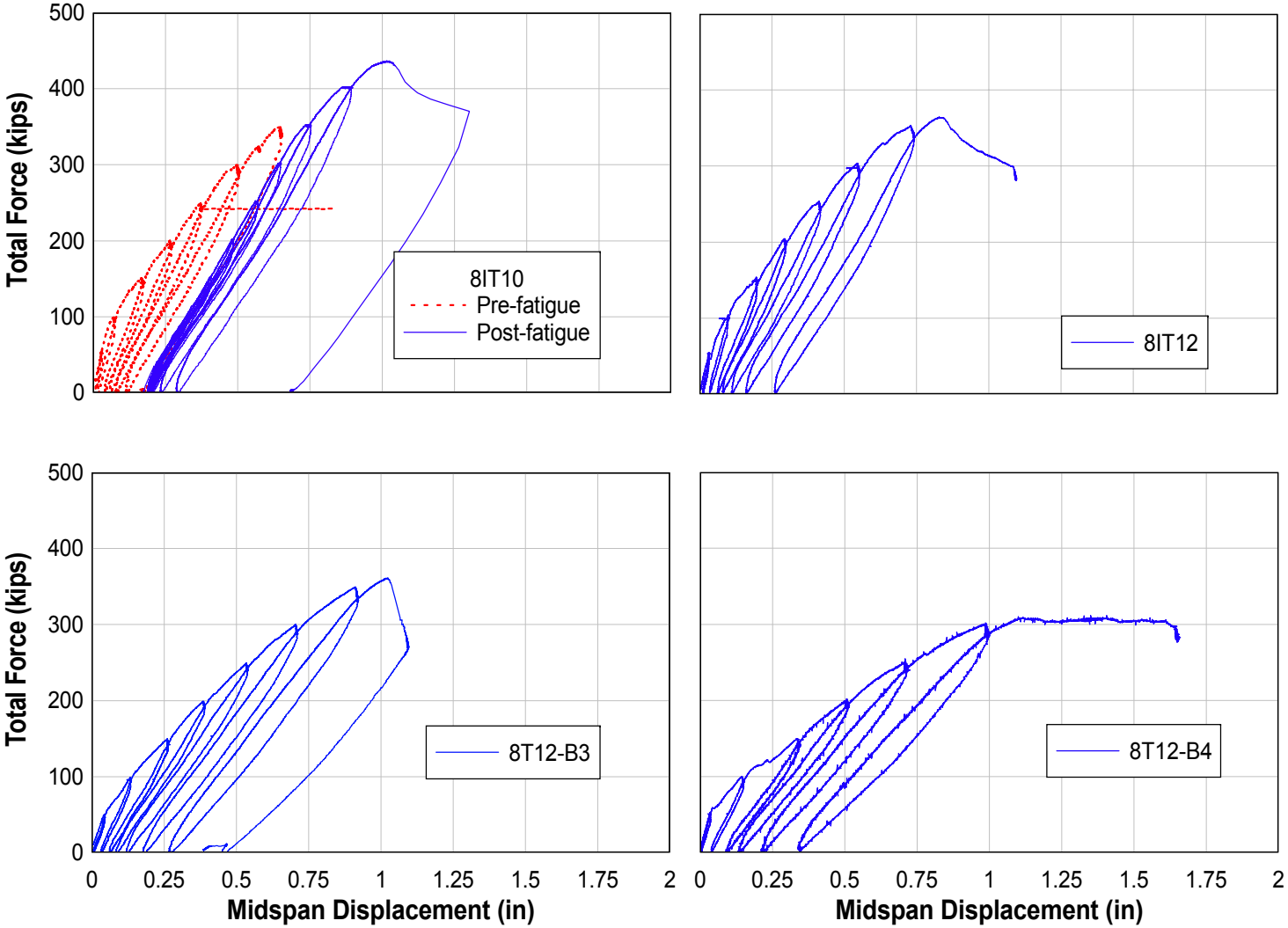

Figure 3.11h: Load-displacement plot at midspan for Group 8 specimens

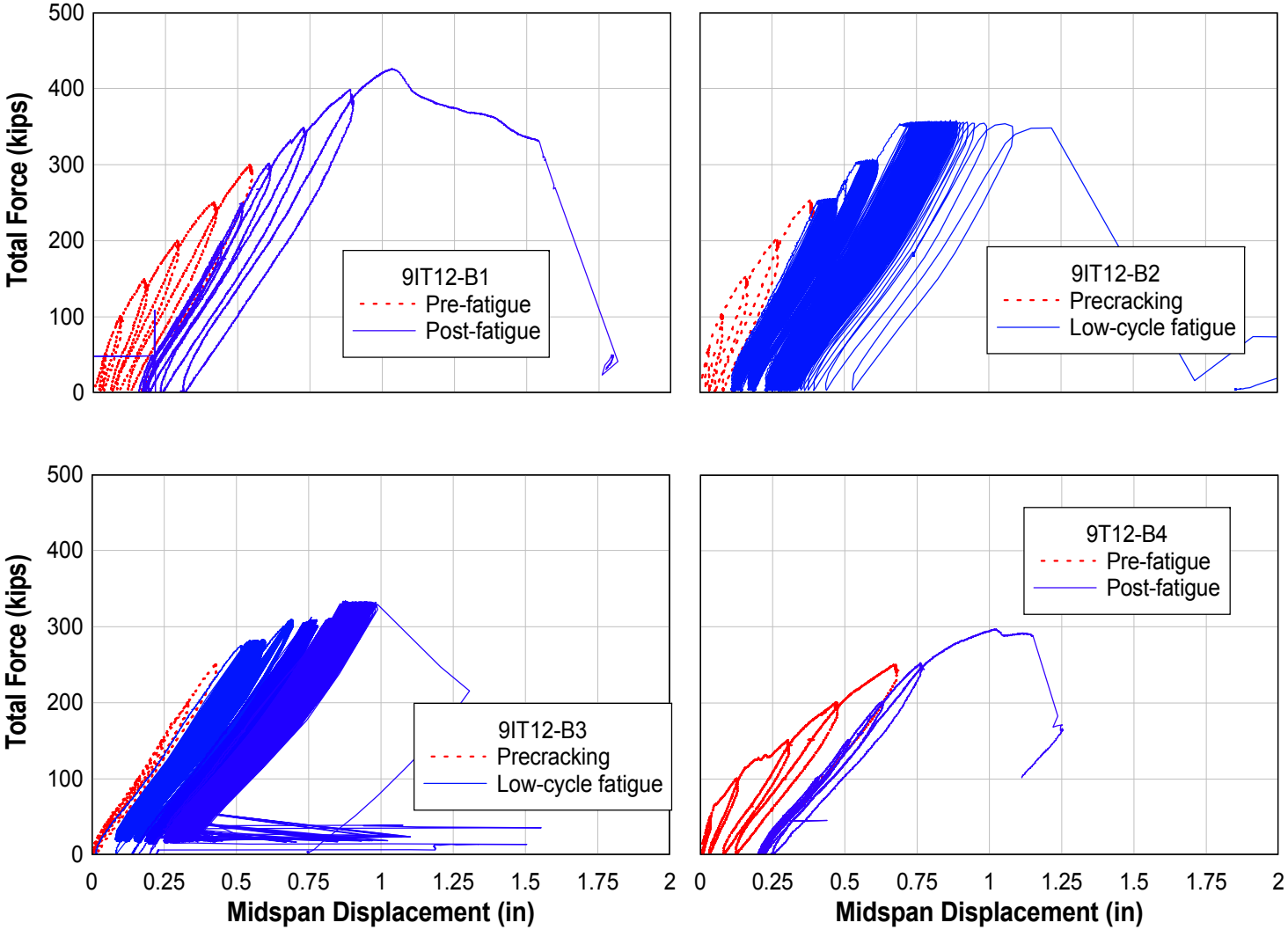

Figure 3.11i: Load-displacement plot at midspan for Group 9 specimens

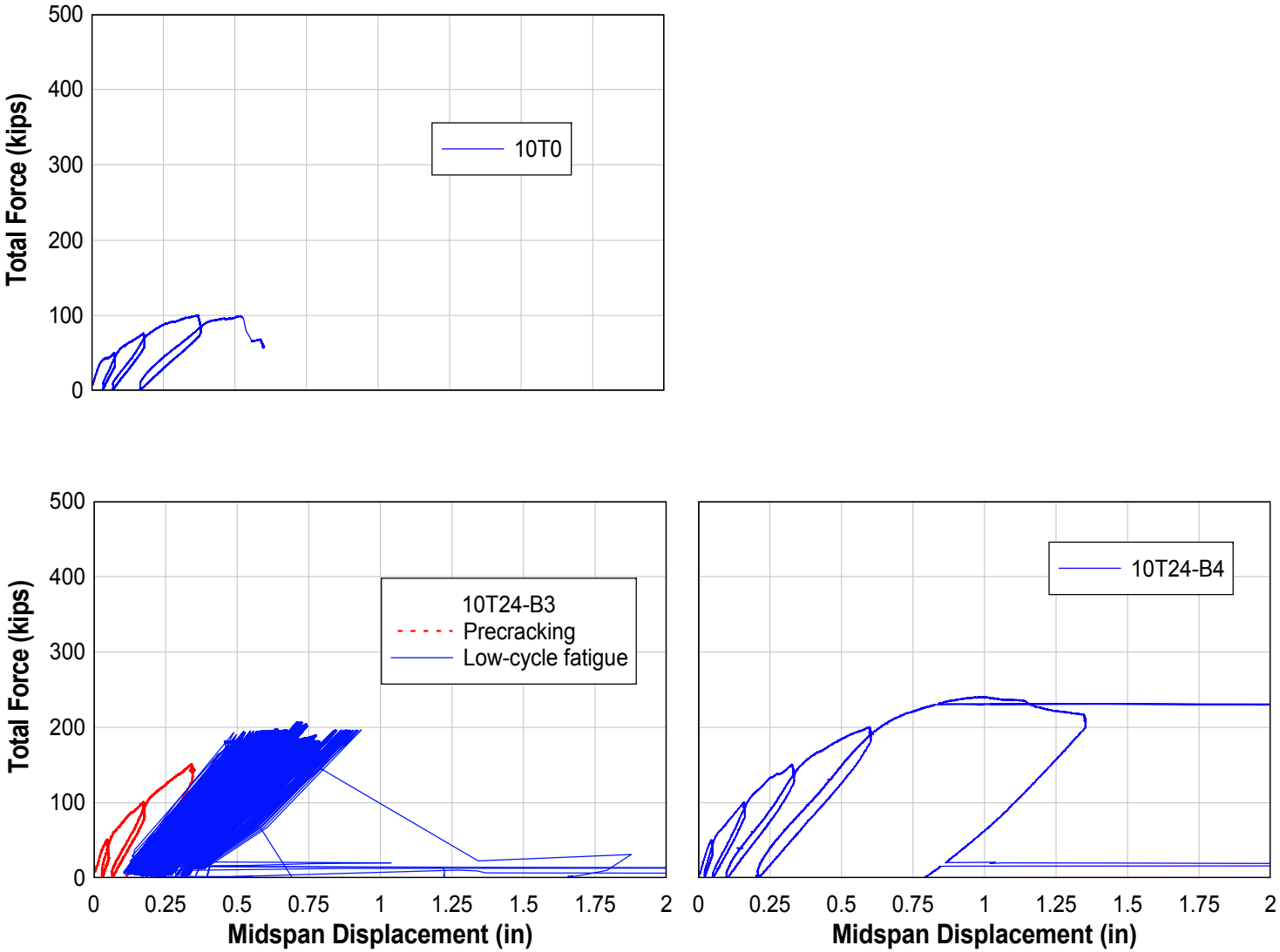

Figure 3.11j: Load-displacement plot at midspan for Group 10 specimens

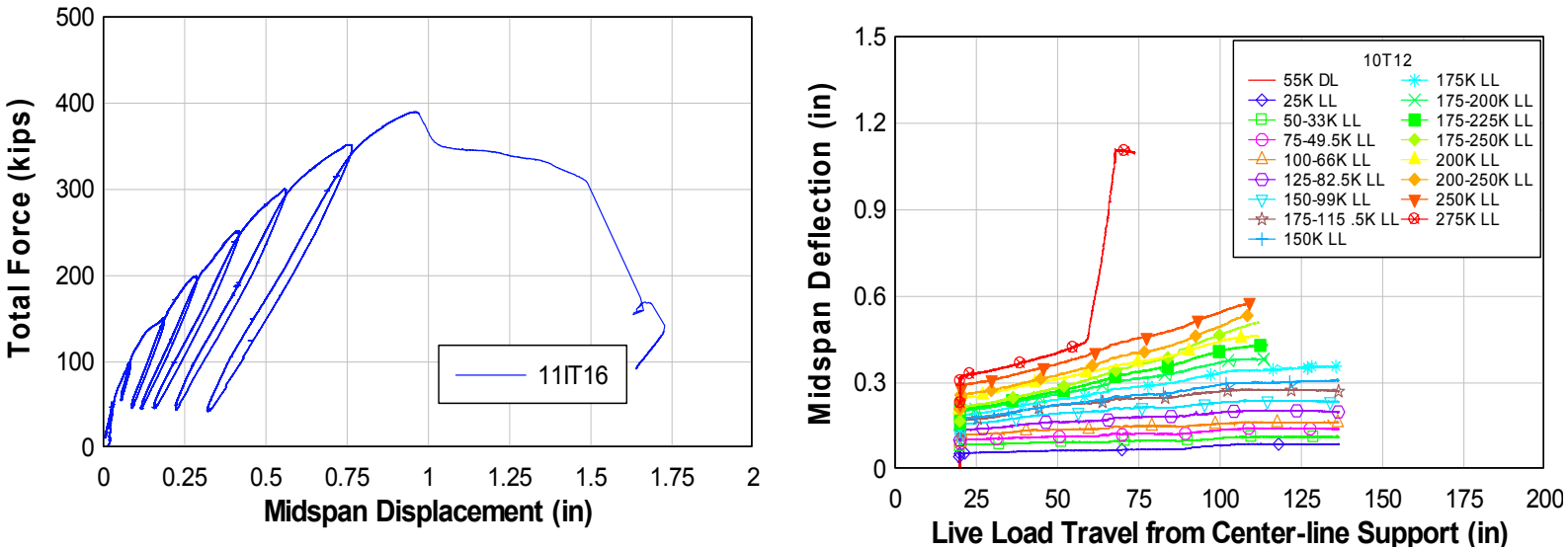

Figure 3.11k: Load-displacement plot at midspan for Group 10 and 11 moving-load specimens

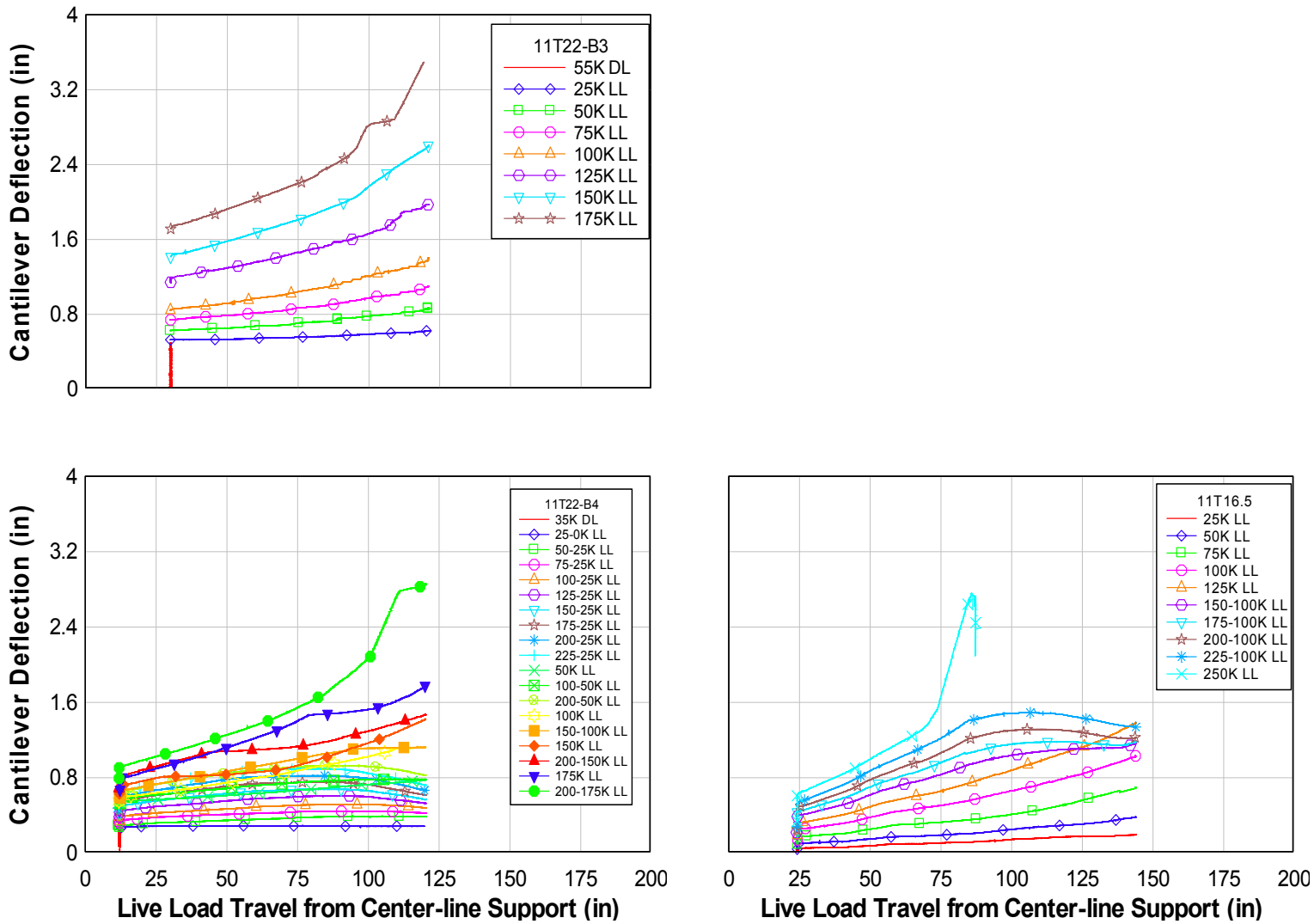

Figure 3.11l: Load-displacement plot at midspan for Group 11 moving-load specimens

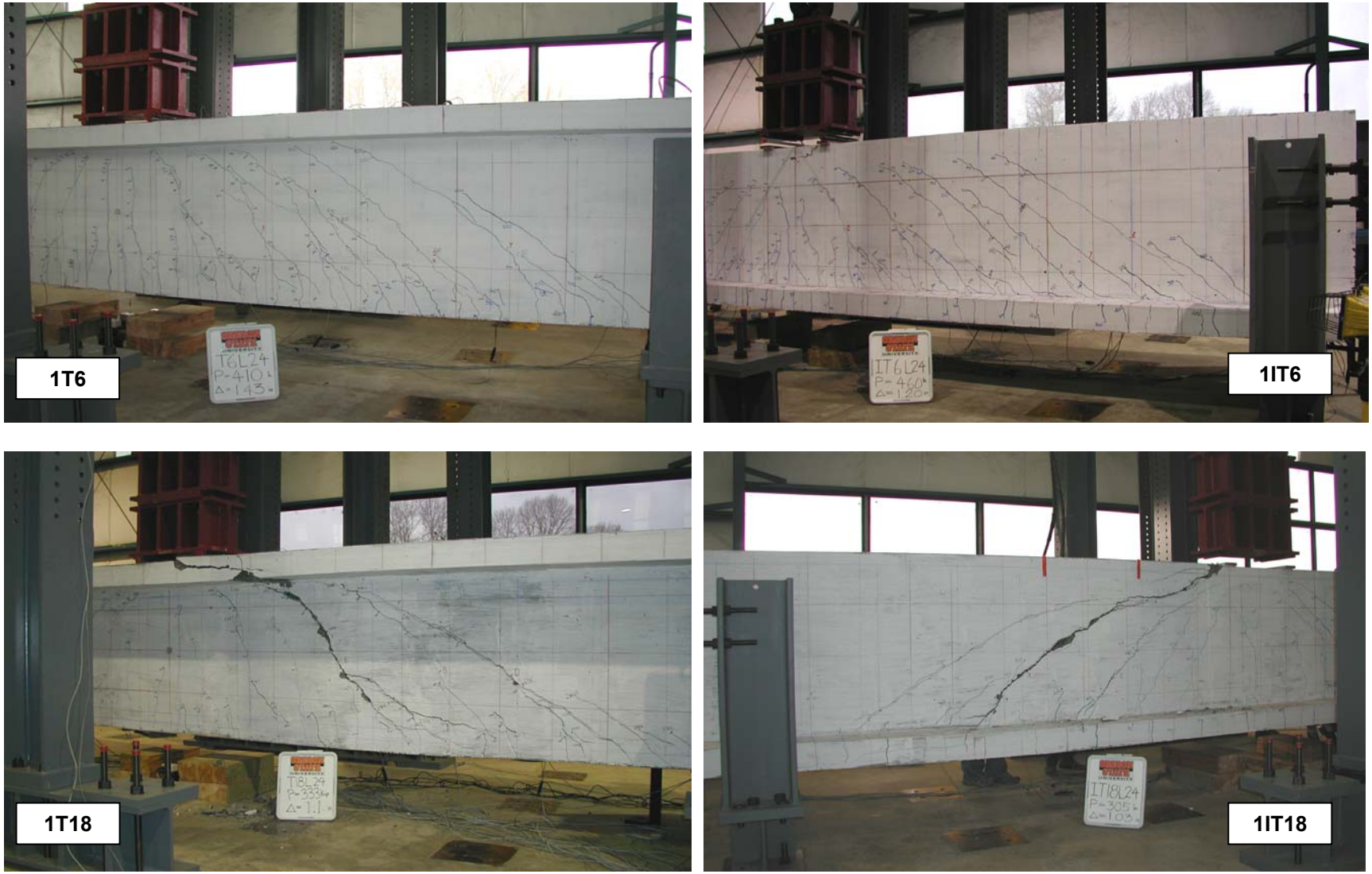

Figure 3.12a: Digital photographs at failure for Group 1 specimens

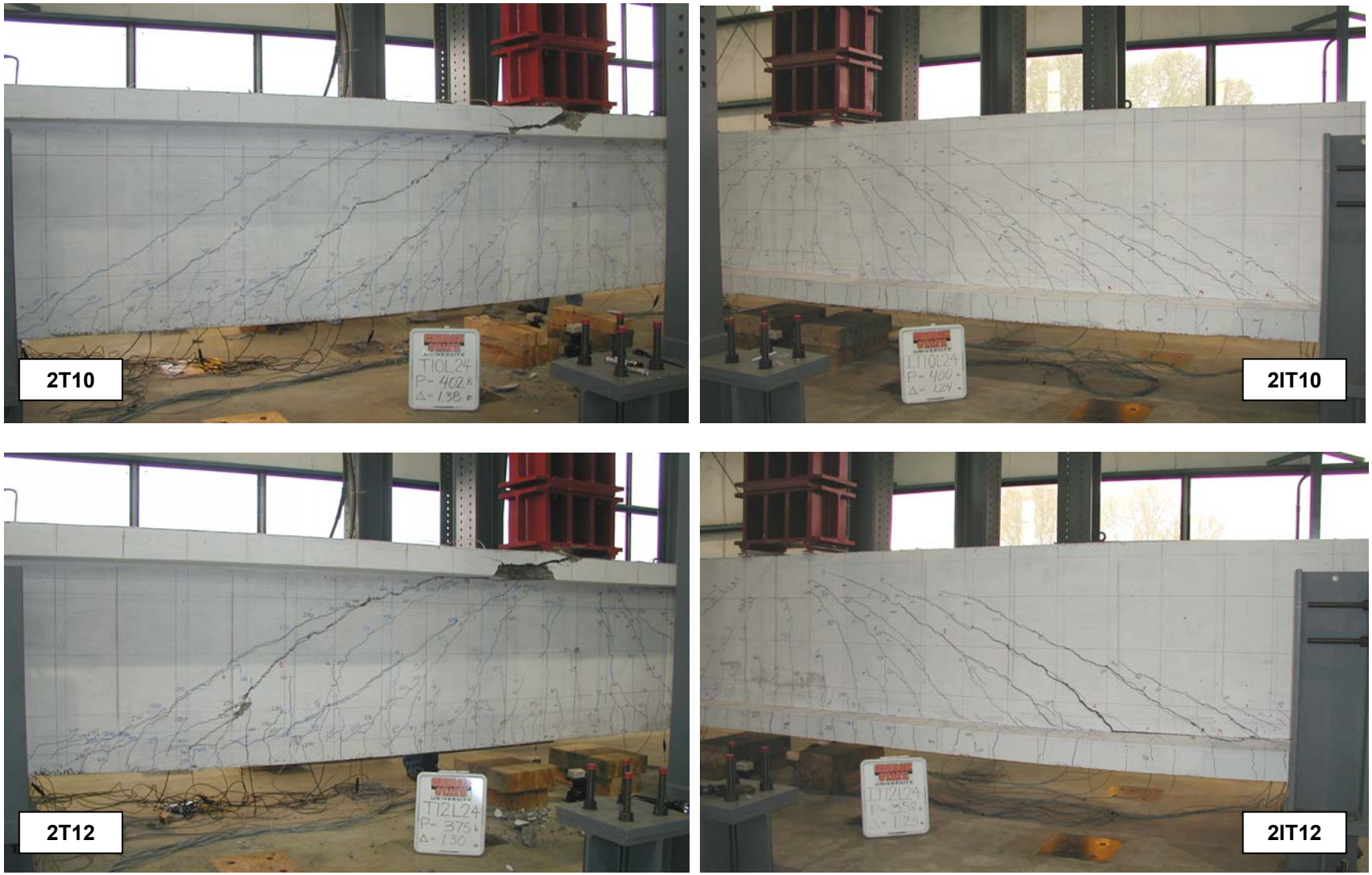

Figure 3.12b: Digital photographs at failure for Group 2 specimens

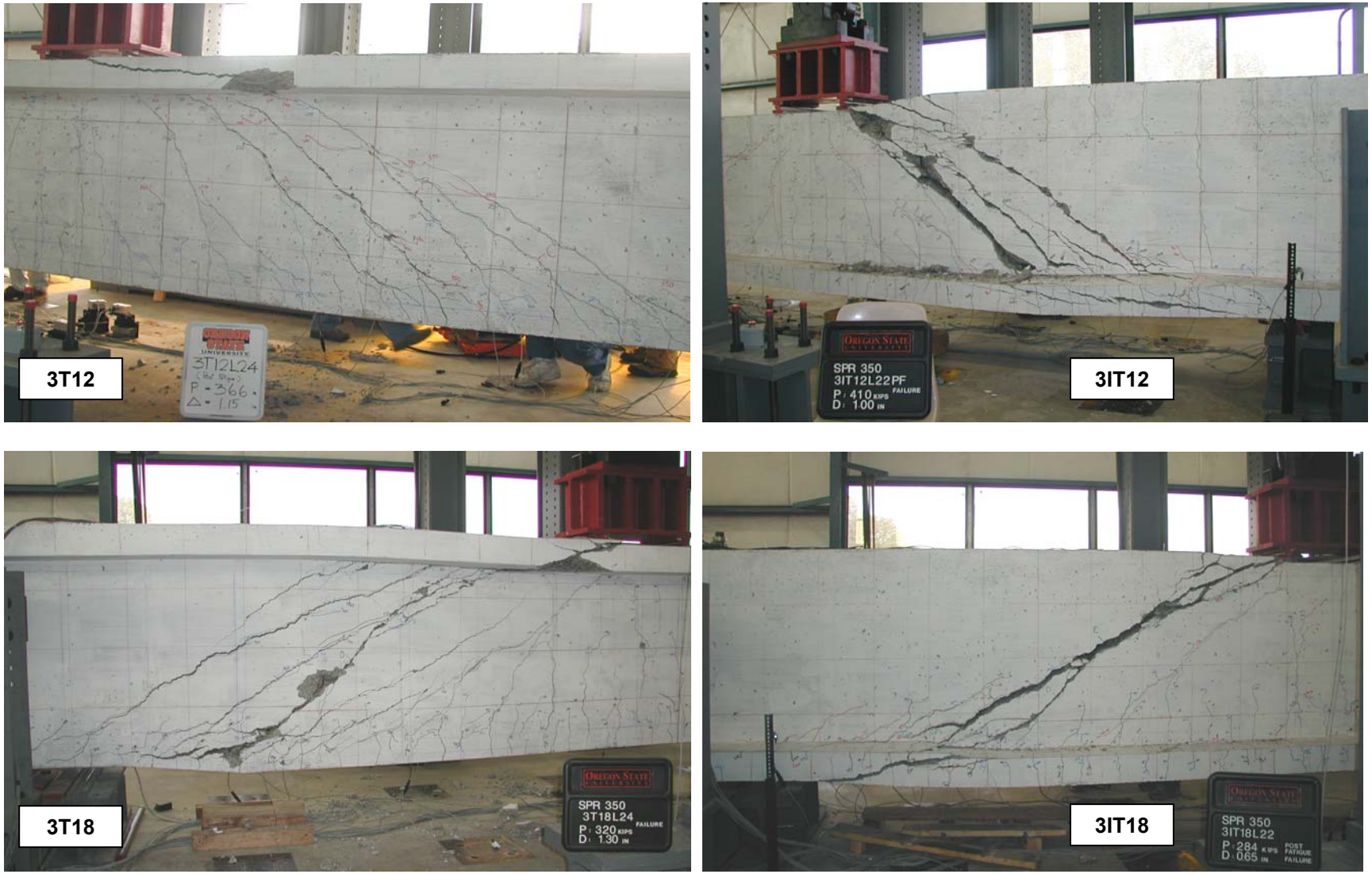

Figure 3.12c: Digital photographs at failure for Group 3 specimens

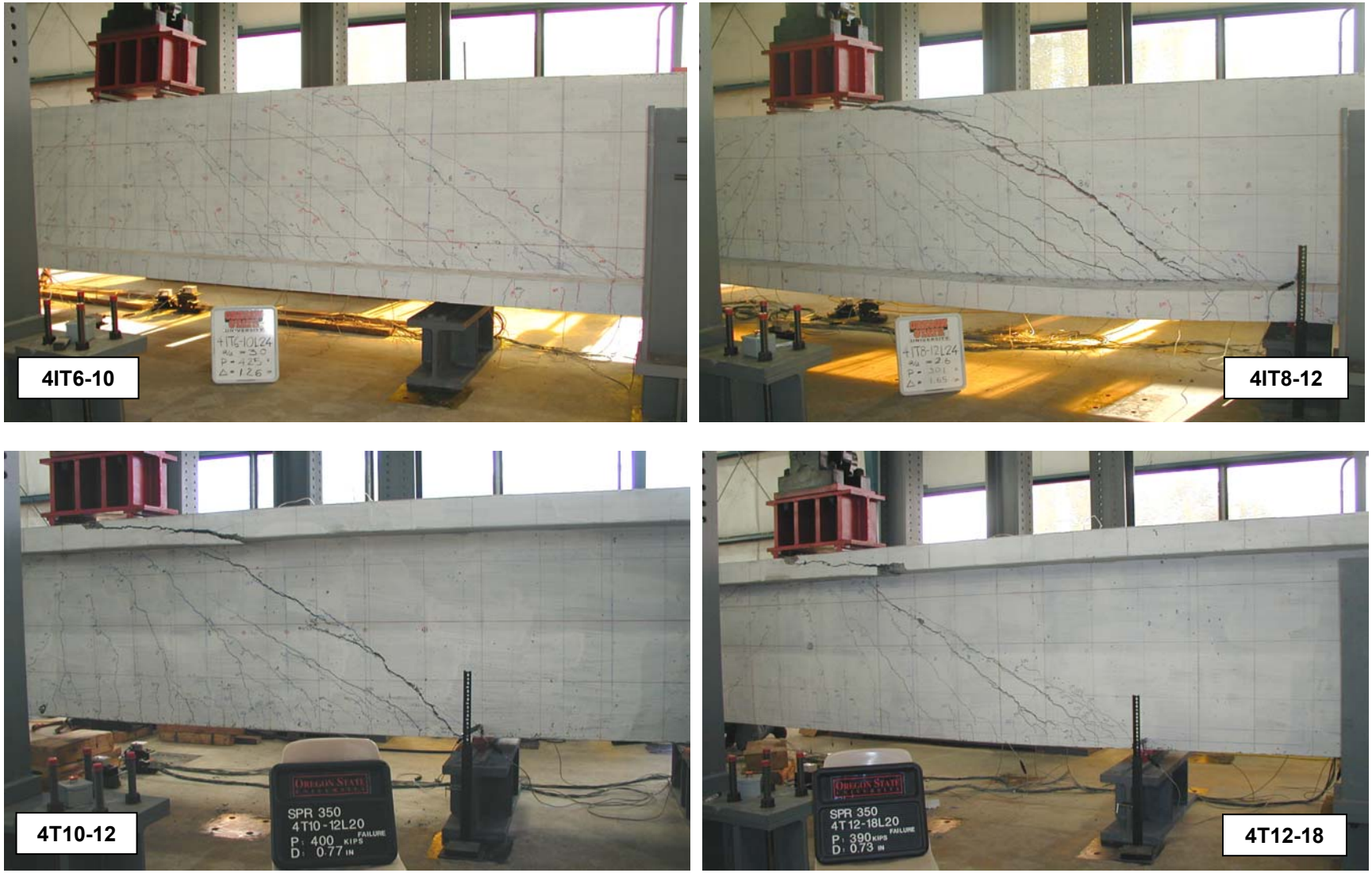

Figure 3.12d: Digital photographs at failure for Group 4 specimens

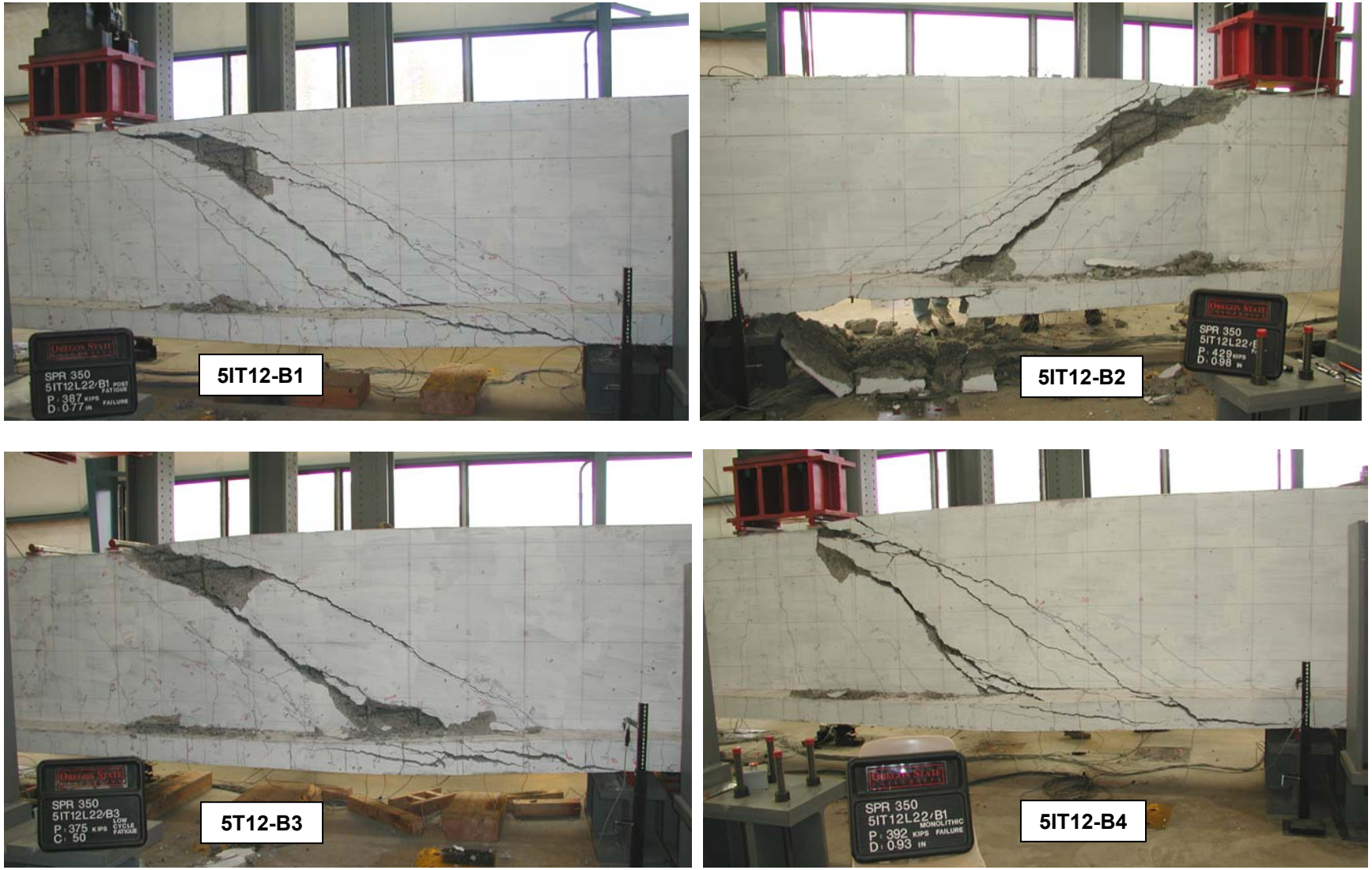

Figure 3.12e: Digital photographs at failure for Group 5 specimens

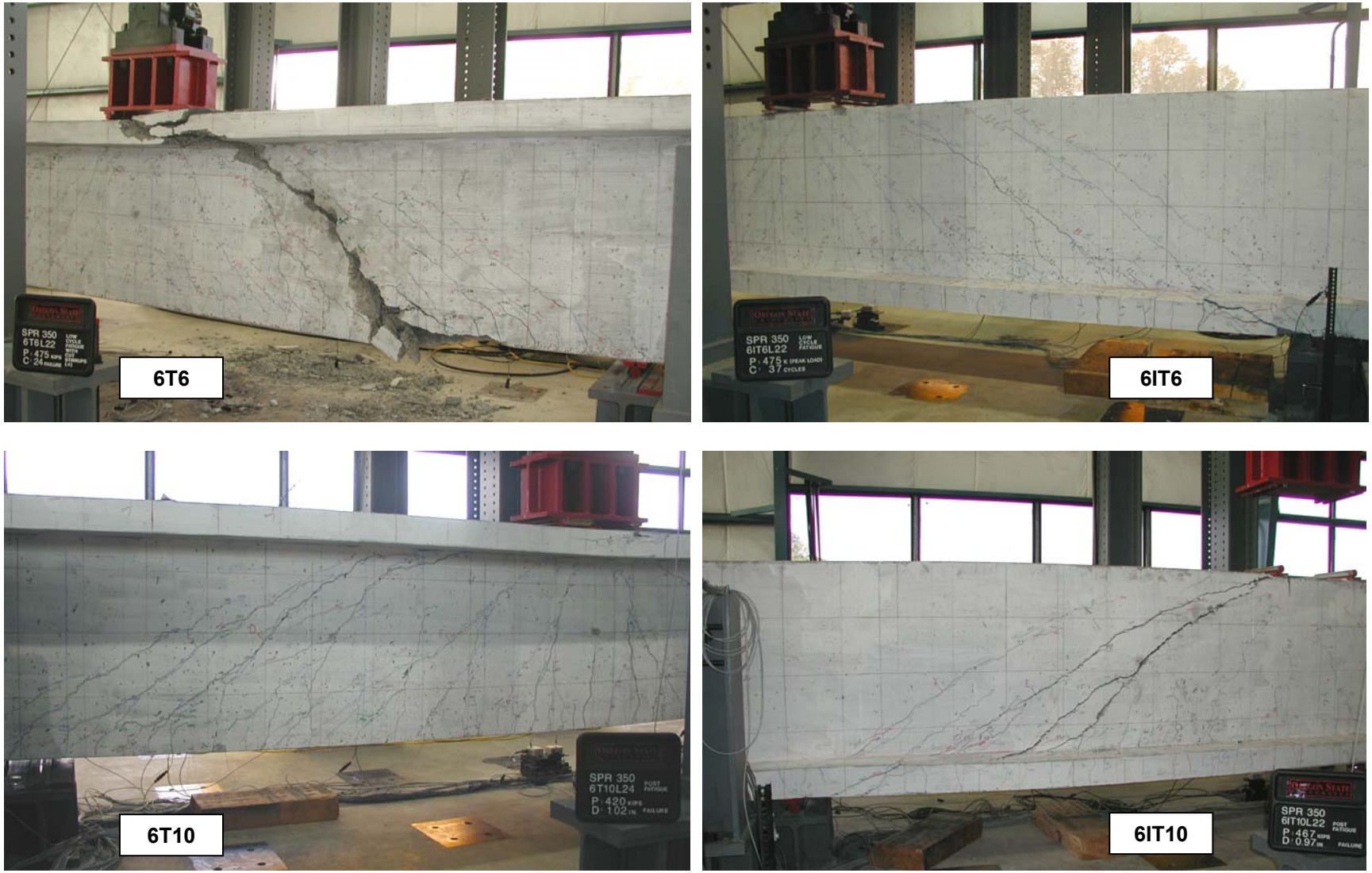

Figure 3.12f: Digital photographs at failure for Group 6 specimens

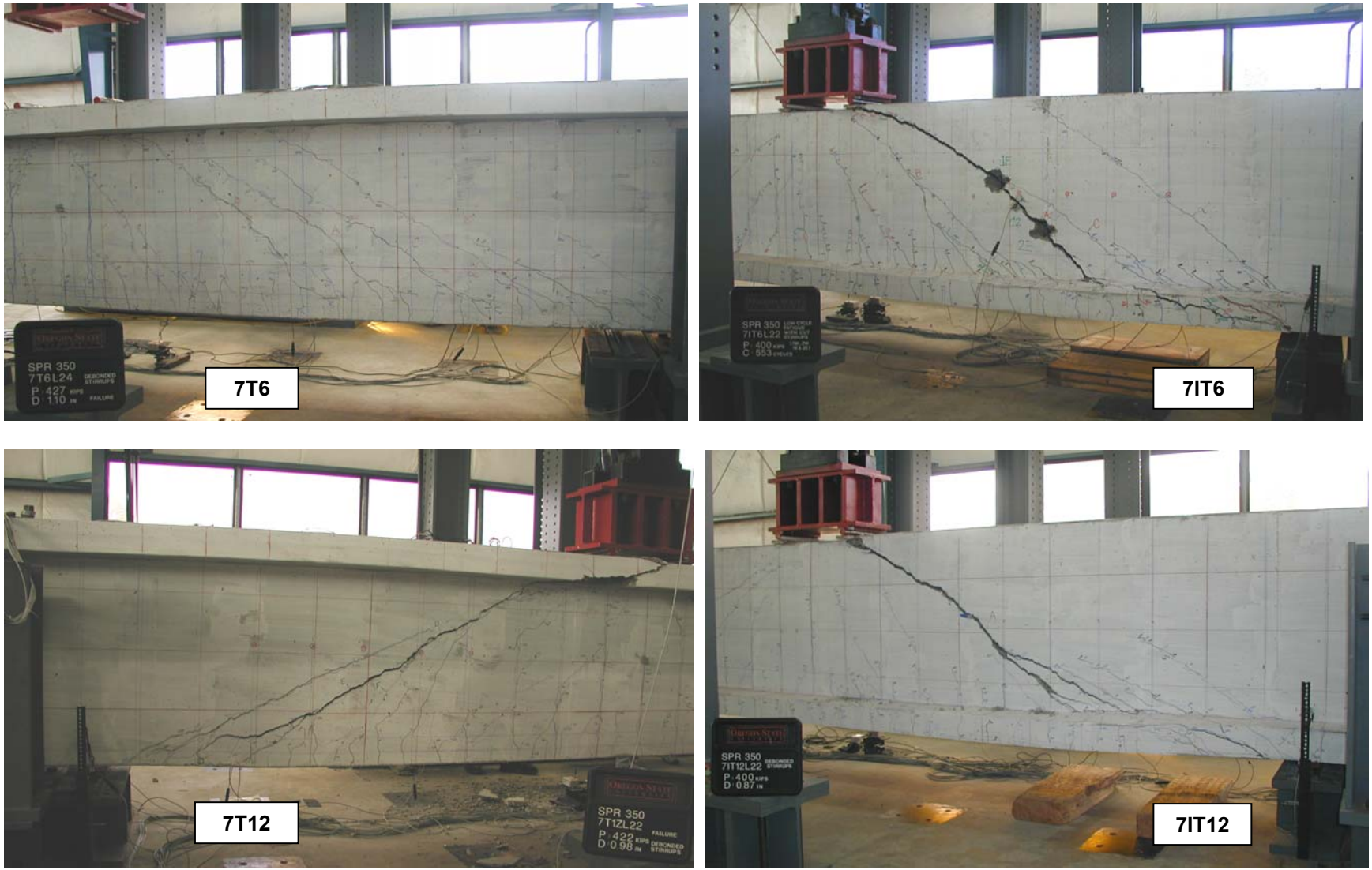

Figure 3.12g: Digital photographs at failure for Group 7 specimens

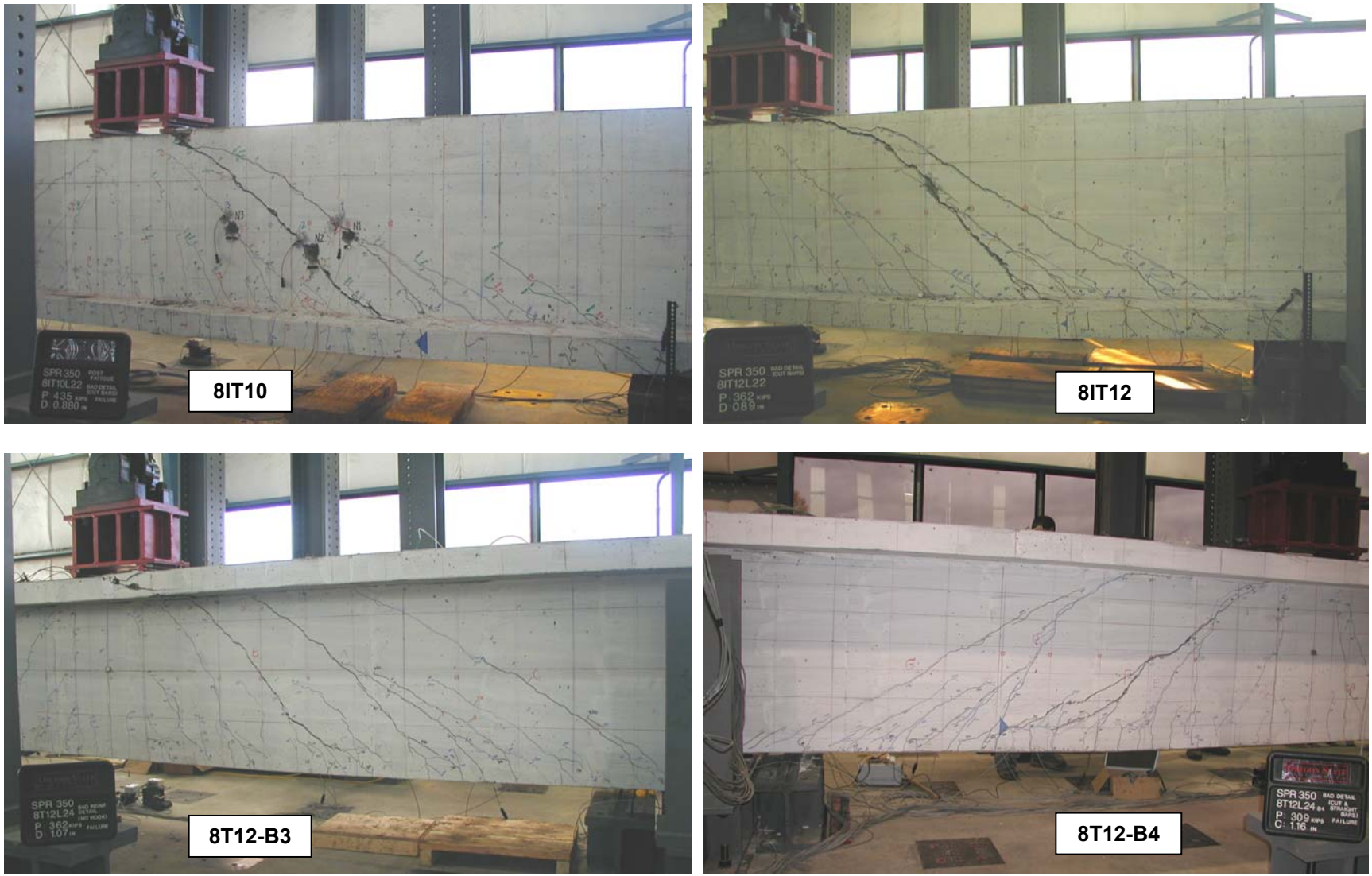

Figure 3.12h: Digital photographs at failure for Group 8 specimens

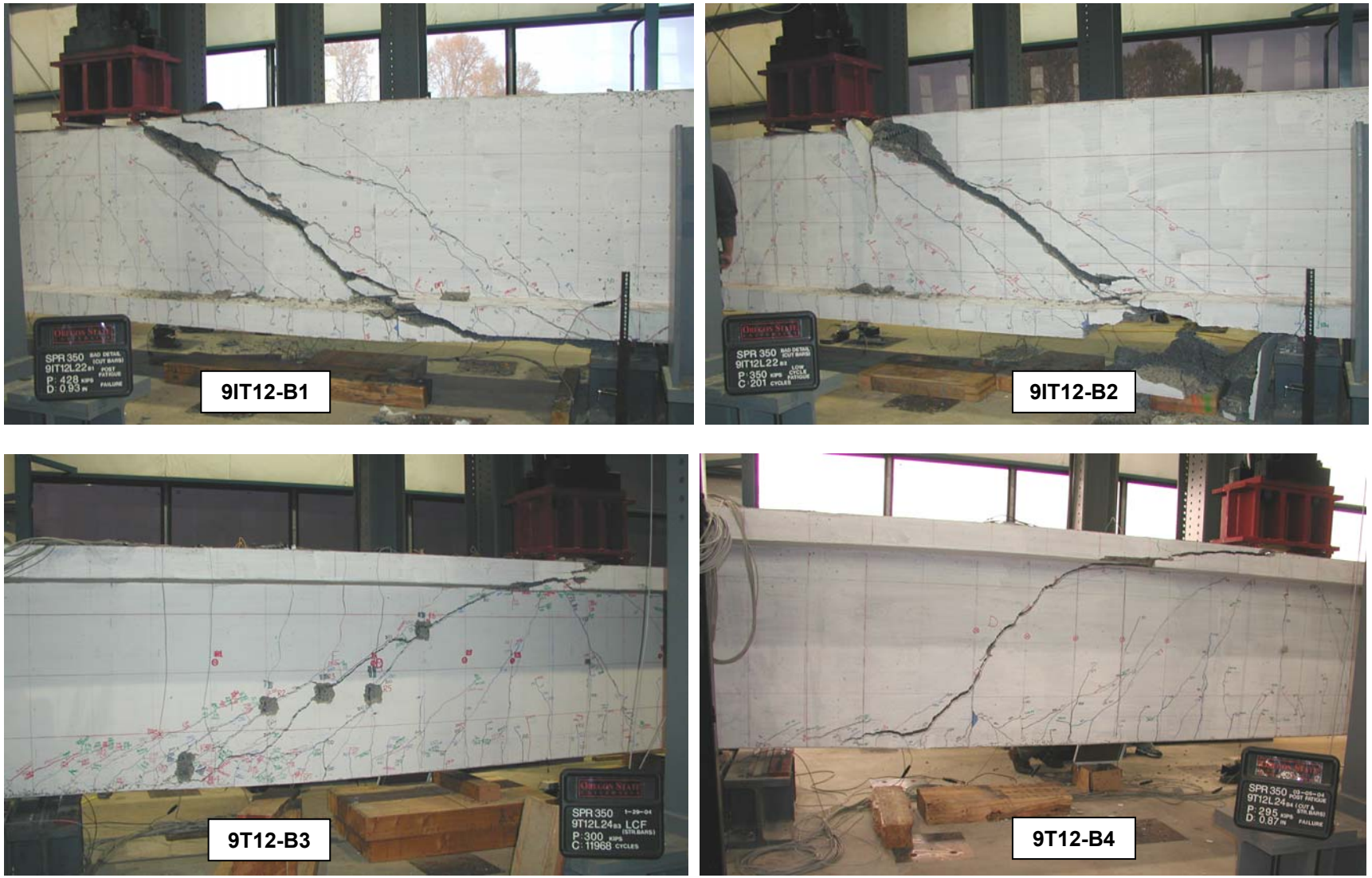

Figure 3.12i: Digital photographs at failure for Group 9 specimens

Figure 3.12j: Digital photographs at failure for Group 10 specimens

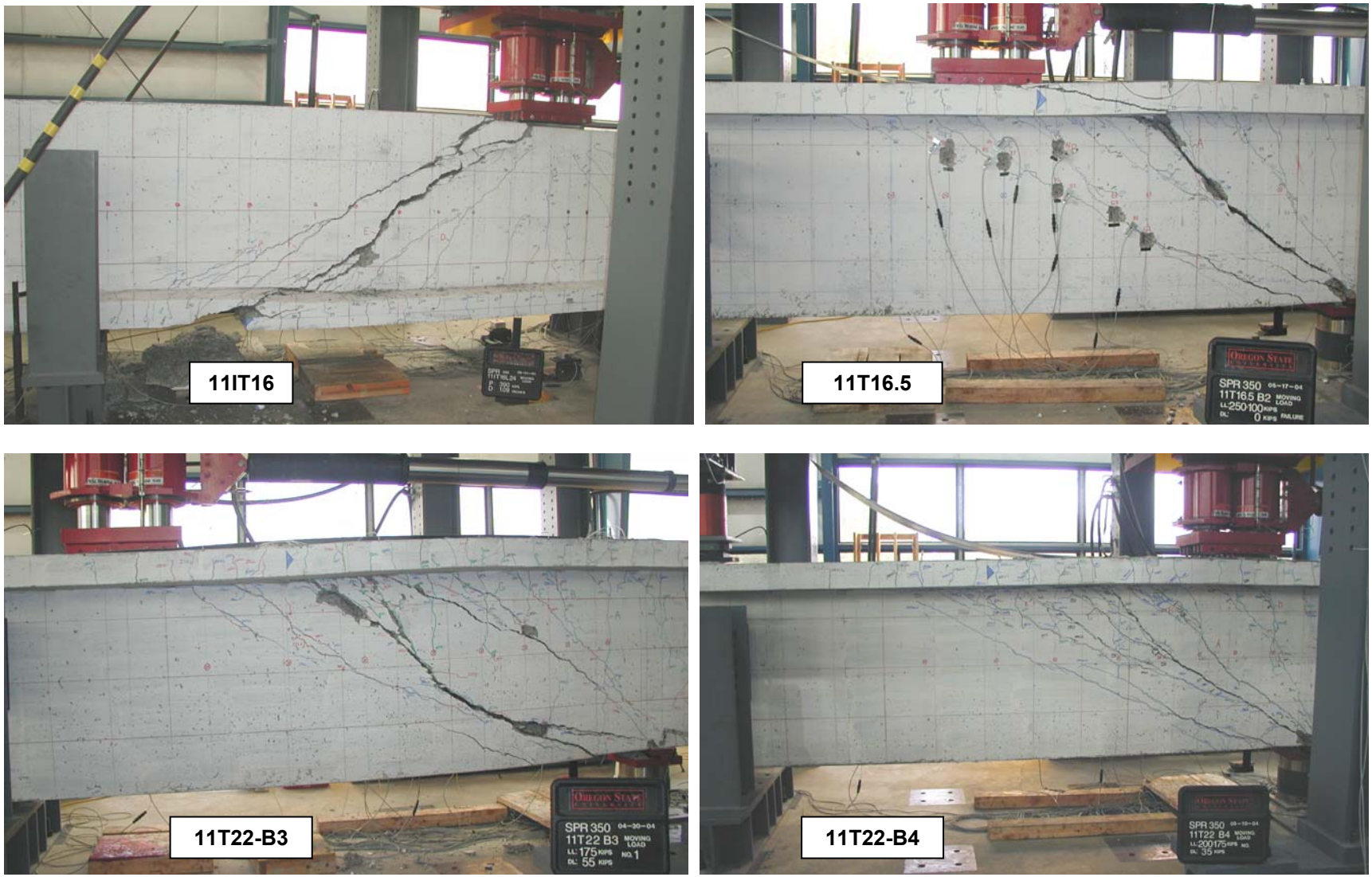

Figure 3.12k: Digital photographs at failure for Group 11 specimens

Table 3.5: Salient test results for laboratory specimens

No.	Specimen	Loading Protocol	Failure Mode	S (in)	f'_c (psi)		L (ft)	V_{EXP} (kips)	V_{DL} (kips)	V_{APP} (kips)	V_{cr} (kips)	Δ (in)	Δ_{Diag} (in)	w_{cr} (in)
					Stem	Deck								
1	1T6	Control	Flexural	6	4700	4370	24.0	206.5	0.0	206.5	37.0	1.35	0.32	0.030
2	1IT6	Control	Flexural	6	4775	4515	24.0	236.0	0.0	236.0	60.0	1.60	0.18	0.040
3	1T18	Control	Shear	18	4925	4360	24.0	166.1	3.7	169.8	34.0	1.08	0.34	0.165
4	1IT18	Control	Shear	18	4550	4410	24.0	154.5	4.3	158.8	36.5	0.97	0.38	0.188
5	2T10	Control	Shear	10	3550	3360	24.0	201.8	3.5	205.3	33.5	1.32	0.39	0.080
6	2IT10	Control	Anchorage	10	3290	3105	24.0	200.7	4.6	205.3	67.5	1.20	0.28	0.125
7	2T12	Control	Shear	12	3520	3440	24.0	188.9	4.0	192.9	11.0	1.17	0.28	0.109
8	2IT12	Control	Anchorage	12	3575	3005	24.0	179.2	4.6	183.8	45.0	1.24	0.34	0.104
9	3T12	HC Fatigue	Shear	12	3990	3660	24.0	184.8	3.9	188.7	40.0	1.22	0.41	0.109
10	3IT12	HC Fatigue	Shear	12	4180	3455	21.6	204.3	3.2	207.5	47.5	1.03	0.29	0.143
11	3T18	Control	Shear	18	3970	3440	24.0	149.5	3.8	153.3	27.0	1.24	0.50	0.210
12	3IT18	HC Fatigue	Shear	18	3915	3220	21.6	142.5	4.6	147.1	49.5	0.74	0.25	0.171
13	4IT6-10	Control	Anchorage	6 , 10	3790	3410	16, 24	211.4	5.1	216.5	88.5	1.13	0.24	0.080
14	4IT8-12	Control	Shear	8 , 12	3710	3595	16, 21.6	237.8	5.1	242.9	62.0	1.06	0.20	0.172
15	4T10-12	Control	Shear	10 , 12	3945	2995	20.0	240.9	3.5	244.4	49.0	0.72	0.20	0.081
16	4T12-18	Control	Shear	12 , 18	4060	3000	20.0	236.6	3.2	239.8	36.0	0.68	0.17	0.095
17	5IT12-B1	HC Fatigue	Shear	12	3700	4610	21.6	191.1	4.0	195.1	60.5	0.87	0.29	0.094
18	5IT12-B2	Control‡	Shear	12	4160	4640	21.6	213.5	4.0	217.5	76.5	0.89	0.28	0.101‡‡
19	5IT12-B3	LC Fatigue	Shear	12	4310	4530	21.6	189.3	4.0	193.3	69.5	1.18	0.65	0.240
20	5IT12-B4	Control	Shear	12	4130	4130	21.6	202.7	3.8	206.5	73.5	1.01	0.42	0.124
21	6T6	LC Fatigue	Shear	6*	4590	4260	21.6	236.6	3.4	240.0	NA	1.14	0.33	0.149
22	6IT6	LC Fatigue	Not Failed	6	5110	3920	21.6	237.6	0.0	237.6	NA	1.10	0.08	0.096
23	6T10	HC Fatigue	Flexural	10	4595	4195	24.0	210.4	0.0	210.4	NA	2.34	0.38	0.120
24	6IT10	HC Fatigue	Shear	10	5495	3875	21.6	234.0	3.8	237.8	NA	1.11	0.35	0.131
25	7T6	Control	Flexural	6	4405	4215	24.0	213.7	0.0	213.7	43.5	1.50	0.17	0.080
26	7IT6	LC Fatigue	Shear	6*	4350	3740	21.6	203.0	4.0	207.0	48.5	0.97	0.23	0.200
27	7T12	Control	Shear	12	4280	4310	21.6	211.5	4.1	215.6	65.0	0.96	0.27	0.216
28	7IT12	Control	Shear	12	4165	3995	21.6	200.1	4.3	204.4	55.5	0.81	0.20	0.132

Table 3.5 (continued): Salient test results for laboratory specimens

No.	Specimen	Loading Protocol	Failure Mode	S (in)	f'c (psi)		L (ft)	V_{EXP} (kips)	V_{DL} (kips)	V_{APP} (kips)	V_{cr} (kips)	Δ (in)	Δ_{Diag} (in)	w_{cr} (in)
					Stem	Deck								
29	8IT10	HC Fatigue	Shear	10	4750	4090	22	218.3	3.5	221.8	63.5	1.02	0.24	0.090
30	8IT12	Control	Shear	12	4840	4045	22	182.3	3.8	186.1	59.5	0.83	0.20	0.113
31	8T12-B3	Control	Shear	12	5070	4570	24	180.7	3.2	183.9	37.5	1.02	0.24	0.080
32	8T12-B4	Control	Shear	12	4995	4725	24	156.0	2.9	158.9	50.0	1.12	0.25	0.170
33	9IT12-B1	HC Fatigue	Shear	12	4285	5405	22	213.0	3.8	216.8	57.0	1.03	0.26	0.147
34	9IT12-B2	LC Fatigue	Shear	12	4605	5465	22	179.3	4.0	183.3	73.5	1.06	0.60	0.110
35	9T12-B3	LC Fatigue	Shear	12	4645	4890	24	166.8	3.5	170.3	34.5	0.98	0.33	0.138
36	9T12-B4	HC Fatigue	Shear	12	4705	4910	24	148.7	4.8	153.5	47.0	1.02	0.32	0.167
37	10T0	Control	Shear	0	4610	4445	24	50.4	4.4	54.8	NA	0.37	0.03	0.080
38	10T12	Moving Load	Shear	12	4655	4405	21	217.4	6.7	224.1	NA	0.45	NA	0.137
39	10T24-B3	LC Fatigue	Shear	24	3450	3995	24	103.7	4.2	107.9	41.0	0.93	0.55	0.284
40	10T24-B4	Control	Shear	24	3420	3740	24	120.7	4.6	125.3	49.5	1.00	0.48	0.097
41	11IT16	Moving Load	Shear	10.5	4635	4430	21	185	4.6	189.6	NA	0.95	NA	0.084
42	11T16.5	Moving Load	Shear	8	4970	4170	13.5†	244	8.9	252.9	NA	1.60	NA	0.04
43	11T22-B3	Moving Load	Shear	10.5-16	4470	3510	13.5†	208.2	7.6	215.8	NA	2.57	NA	0.229
44	11T22-B4	Moving Load	Shear	10.5	4750	4010	13.5†	194.4	8.4	202.8	NA	2.16	NA	0.07

* Cut-stirrup testing performed
‡ Using force control and faster loading rate
‡‡ Taken at 0 kip
† Length of cantilever

S is the stirrup spacing;
L is the span distance between supports;
V_{EXP} is the applied actuator shear force;
V_{DL} is the specimen self-weight shear force at the failure section;
V_{APP} is the total shear force from the actuator load and dead load shear at the failure section;
V_{cr} is the shear force at first diagonal cracking;
Δ is the midspan displacement at failure;
Δ_{Diag} is the maximum displacement measured on one of the web diagonal displacement sensors (crossing multiple cracks); and
w_{cr} is the maximum crack width measured at peak load prior to failure.

Shear forces reported in Table 3.5 include the applied shear on the specimen from the actuator, V_{EXP}, the shear force from the beam self-weight acting at the failure plane, V_{DL}, and the total shear force, V_{APP}. The shear force from specimen self-weight was estimated by computing the weight of concrete acting on the diagonally cracked failure plane as illustrated in Figure 3.13. A unit weight of reinforced concrete equal to 150 lb/ft^3 was used to estimate the additional specimen self-weight at the cracked section.

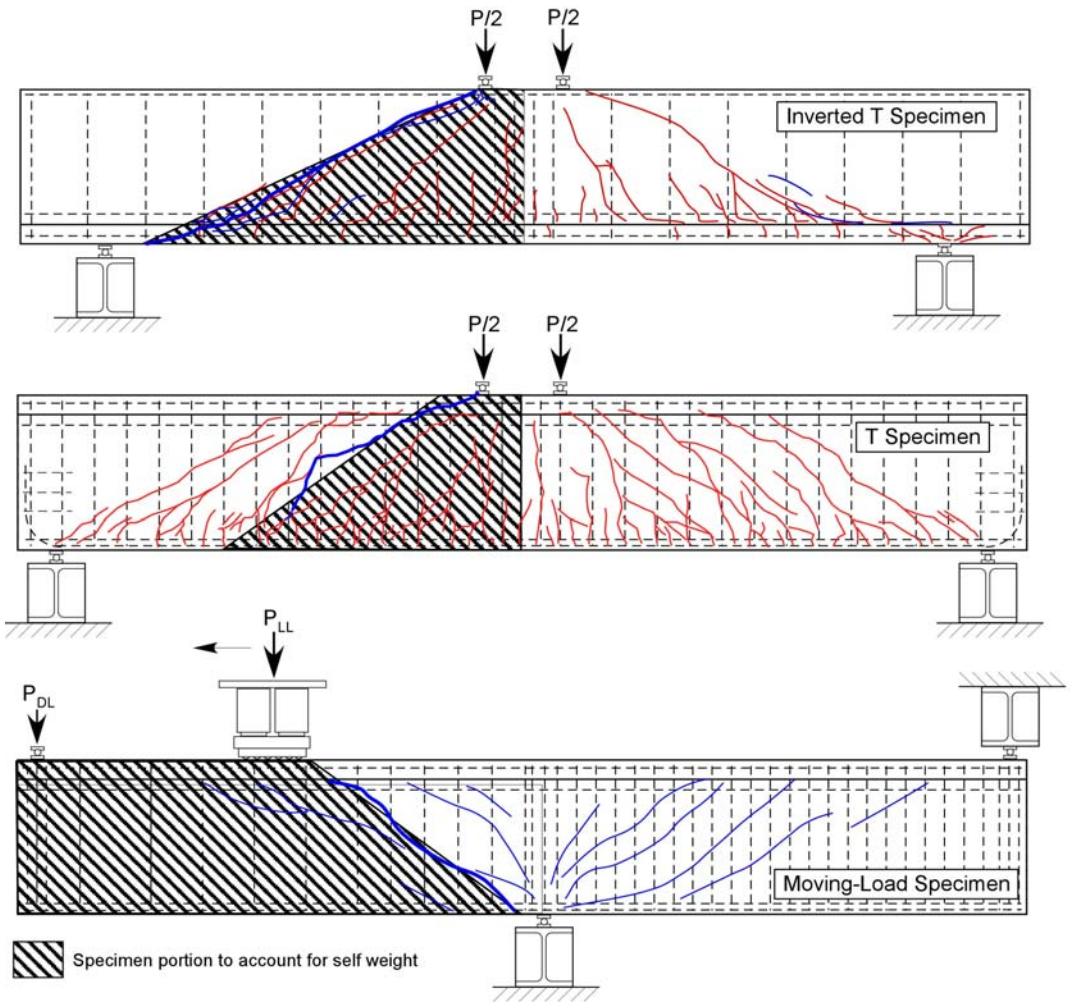

Figure 3.13: Approach used to determine self-weight at the failure location for different specimens

The average shear stress at the onset of diagonal cracking was estimated from the applied shear force based on observation of the first significant strain deviation for the instrumented stirrups. An estimated self-weight contribution (using the weight from a quarter span length) was added to the applied shear to estimate the total shear force at the onset of diagonal cracking. The combined shear force was divided by the web width and the effective depth to the flexural reinforcing steel (43.4 in. for T and 45 in. for IT specimens) to determine the diagonal cracking shear stress.

Maximum diagonal deformation was determined from one of the 12 displacement sensors mounted diagonally on the stem of the beam in one of the six segments along the span. Crack motions were monitored for selected specimens to determine the amount of deformation occurring in the parallel and transverse directions. This was performed by marking a grid of reference points on the specimen web across a diagonal crack. Digital photographs taken of the grid points prior to and during loading were superimposed to determine the crack motions. Two crack motion studies are shown in Figures 3.14a and 3.14b.

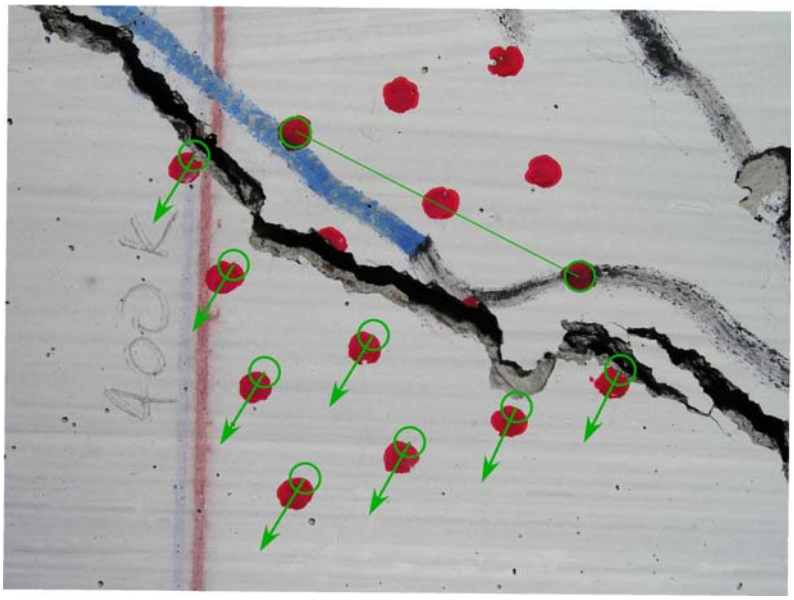

Figure 3.14a: Crack motion for specimen C4T12 (unbonded stirrups)

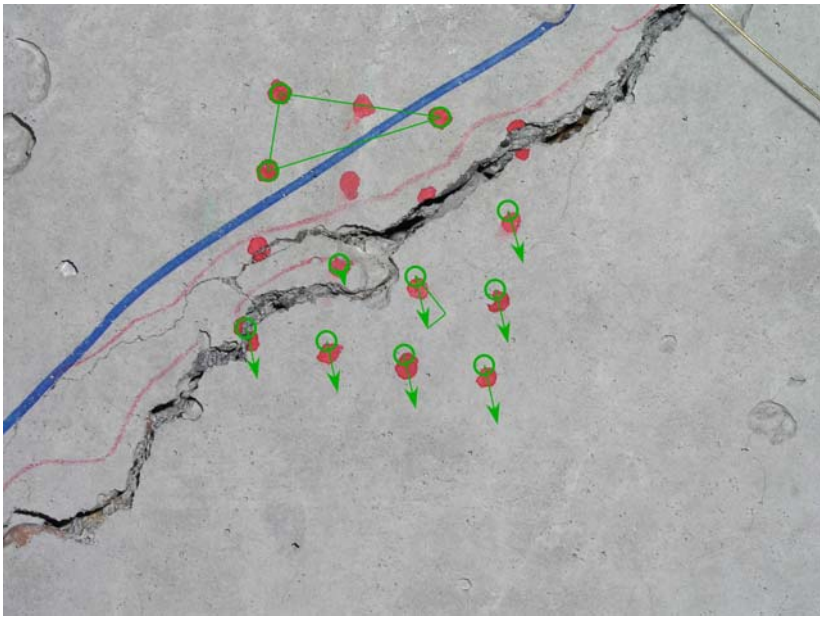

Figure 3.14b: Crack motion for specimen IT18

The specimen with debonded stirrups exhibited crack motions principally in the direction perpendicular to the crack (crack opening) (Figure 3.14a). Specimens with bonded stirrups typically exhibited crack motions with transverse deformations (crack opening) approximately three times that observed parallel to the crack (crack slipping) (Figure 3.14b). The observed crack motions and crack widths indicate that force transfer across the widest portions of the diagonal cracks near midheight is unlikely for the stationary loading considered.

3.3 INCREASED LOADING RATE TEST

3.3.1 Test Method

Typical capacity tests were performed near static conditions, with a slowly applied loading rate. To simulate the effect of a more realistic loading rate possible on a vintage RCDG bridge, a specimen (5IT12-B2) was tested under load control with variable load rates. A typical RCDG span length for a bridge identified as containing a high density of diagonal cracks was determined as 55 ft from a database of the ODOT bridge inventory (*Higgins, et al. 2004*). For a truck traveling over the bridge at the posted speed of 55 mph, a bent cap would reach peak load in approximately 0.7 sec and then unload in the same time period. Table 3.6a indicates typical time to reach peak load in a bent cap for various span lengths and vehicle speeds. Girders may be loaded much more rapidly, particularly at locations near supports where the load comes on suddenly. This was observed in the field test data presented in a previous section.

Table 3.6a: Time to peak load at a bent cap for different span lengths and vehicle speeds

Truck Speed (mph)	Span Length (ft)	Time to Peak (sec)
50	45	0.614
50	50	0.682
50	55	0.750
50	60	0.818
55	45	0.558
55	50	0.620
55	55	0.682
55	60	0.744
65	45	0.472
65	50	0.524
65	55	0.577
65	60	0.629

The test specimen was subjected to the conventional loading protocol of increasing loads followed by unloading, but instead of using displacement feedback for the servo-hydraulic control system, load control was used. Force was applied to the specimen using a ramp function to achieve the target load amplitude and was followed by unloading at the same rate. Loading rates were initially selected to be in the range of that observed in the field. However, once cracking occurred and the specimen stiffness reduced, the hydraulic flow available to the large

force actuator was not sufficient to permit achievement of the target loading rates. Thus the loading rate was reduced as higher load levels were imposed. The loading histories are shown in Figure 3.15 and are summarized in Table 3.6b. The highest loading rate achieved was 369 kips/sec. The specimen failed at a load of approximately 429 kips with a loading rate of 124 kips/sec.

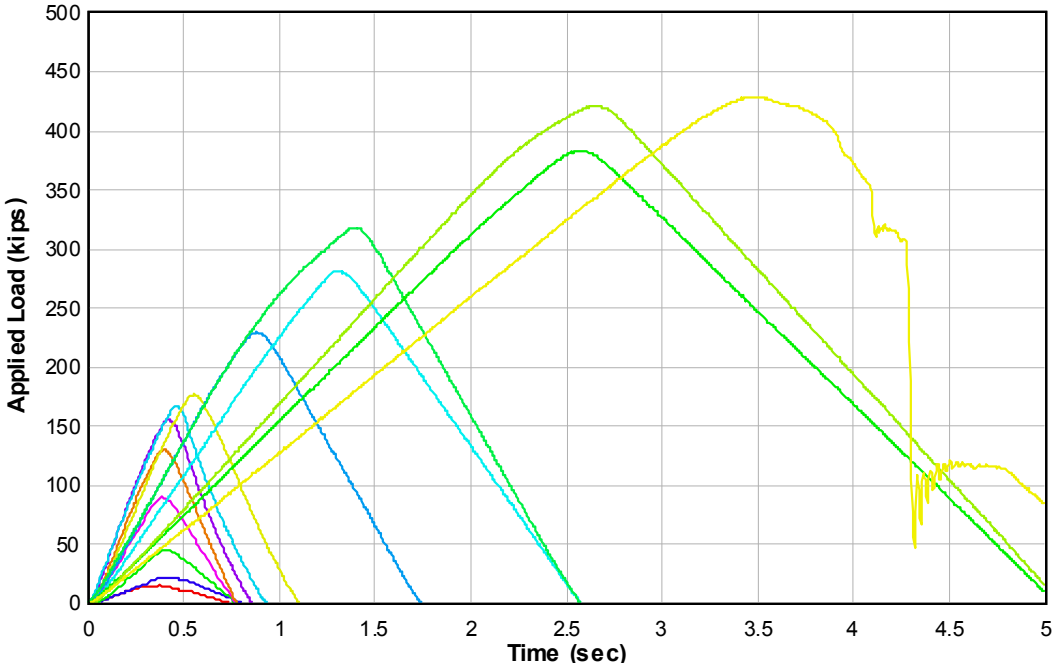

Figure 3.15: Loading histories for specimen tested at higher loading rates

Table 3.6b: Loading rates for different test load increments

Increment Number	Time to Peak (sec)	Peak Force (kips)	Loading Rate (kips/sec)
1	0.276	15.7	57
2	0.392	22.6	57
3	0.368	45.6	124
4	0.376	90.1	240
5	0.393	130.6	332
6	0.424	156.5	369
7	0.463	167.5	362
8	0.551	177.2	322
9	0.882	229.6	260
10	1.298	281.3	217
11	1.403	318.2	227
12	2.555	383.2	150
13	2.630	421.0	160
14	3.450	428.9	124

3.3.2 Experimental Results

During this test it was not possible to measure and mark cracks at the maximum load, as the specimen was fully unloaded after application of the loading ramp. The cracks were marked and measured with no force on the specimen. At this unloaded condition, flexural cracks were not easy to distinguish, but the diagonal cracks were quite evident. Diagonal cracks were visible after the peak force of 156 kips was achieved; however flexural cracks in the flange were not visible until the applied force increased to 178 kips. The specimen tested at the higher loading rate exhibited slightly higher capacity (5.3%) and lower overall displacement (11.9%) than a similar specimen cast within the same group (specimen 5IT12-B4) tested under the control loading protocol.

The reduced deflection observed with this specimen can be partially attributed to reduced creep deformations, as the load was never held at a large magnitude during crack mapping and inspection. The observed failure mode was similar to other specimens and the overall behavior was not markedly different. The slight increase in capacity at the higher loading rate may slightly offset some of the amplified force effects due to dynamic and impact response on actual bridge members due to vehicles traveling at highway speeds.

3.4 MOVING SUPPORT TESTS

3.4.1 Test Method

A series of two tests was performed by placing specimens on relatively closely spaced supports and loading using the conventional loading protocol until formation of significant diagonal cracks and achievement of a prescribed force level of 400 kips. After achieving the prescribed load magnitude, loading was halted and the supports were moved to new locations, thereby providing a longer test span.

The specimens had two different stirrup spacings, 6 in. near midspan and 10 in. near beam ends for 4IT6-10 specimen; and 8 in. near midspan and 12 in. near beam ends for 4IT8-12 specimen. Transverse reinforcement details of these specimens reflected reinforcement details near the mid-bent region of a girder in a continuous span bridge to the dead load points of inflection, where stirrup spacing becomes incrementally larger toward the midspan region.

The specimens were precracked using the control loading protocol with a span length equal to 16 ft. The precracking load was 400 kips for both specimens. Then the supports were pushed out to produce a span length of 24 ft for 4IT6-10 specimen and a span length of 21.6 ft for 4IT8-12 specimen before being loaded to failure. This testing procedure attempted to simulate load effects within a girder near the bent cap region. A vehicle could produce diagonal cracking within the region with tighter stirrup spacing and then produce a subsequent diagonal crack at a location further out on the span, where the stirrup spacing is larger.

3.4.2 Experimental Observation

Crack widths measured using a crack comparator card during the precracking stage were fairly narrow, 0.025 in. at 400 kips applied load for 4IT6-10 specimen and 0.04 in. at 400 kips applied load for 4IT8-12 specimen. During failure testing, new cracks formed outside the 16 ft span length and developed quickly. The largest crack widths measured at the loadstep prior to failure were 0.08 in. for specimen 4IT6-10 and 0.172 in. for specimen 4IT8-12.

The diagonal-tension crack widths previously formed in the precracking stage were fairly constant during the failure testing. Specimen 4IT6-10 failed due to an anchorage failure at the north-end support with a total applied load of 423 kips. Specimen 4IT8-12 exhibited a shear-compression failure in the north side with an applied load of 476 kips. The failure crack spanned from the support plate to the loading plate crossing both the 8 in. and 12 in. stirrup spacing regions.

3.5 INFLUENCE OF FLEXURAL BAR DETAILS

3.5.1 Test Method

Specimens from groups 8 and 9 were designed and fabricated with different anchorage and flexural bar cutoff details as shown in Appendix A1. Specimens 8IT10, 8IT12, 8T12-B4, 9IT12-B1, 9IT12-B2, and 9T12-B4 contained straight end bar anchorages and flexural bar cutoff details. Specimens 8T12-B3 and 9T12-B3 were reinforced with continuous reinforcing bars, except they used straight bar anchorages at the ends instead of 90° hooked anchorages.

For specimens with cutoff details, the flexural reinforcing steel (six #11 bars for Inverted-T specimens and five #11 bars for T specimens) provided adequate flexural capacity at the midspan region. The number of flexural bars was reduced toward the ends of the specimens. These cutoff locations, in the flexural tension region, combined with no additional stirrups, represent typical 1950s vintage construction details. For Inverted-T specimens, four #11 bars and for T specimens three #11 bars, were extended into the supports at the beam end regions.

The specimens were loaded with various loading protocols. Specimens 8IT12, 8T12-B3, and 8T12-B4 were tested with the control loading protocol. High-cycle fatigue loads were applied to specimens 8IT10, 9IT12-B1, and 9T12-B4; and specimens 9IT12-B2 and 9T12-B3 were subjected to low-cycle fatigue loading.

3.5.2 Experimental Results

Wide flexural cracks formed at the location of cut flexural bars, when the specimens were loaded with about 60% of the ultimate load. Flexural cracks at these locations propagated diagonally up toward the loading plate and eventually led to specimen failure. The specimens with straight end anchorages and cutoff details had smaller failure loads and displacements at the peak load than those of similar control specimens. For specimens in Groups 8 and 9, angles of the failure diagonal cracks were steeper than those of the control specimens. The failure load of specimen 8T12-B3 with straight end details was 361 kips and lower than that of 2T12 specimen (378 kips),

even though concrete strength of 8T12-B3 (5070 psi) was much higher than that of specimen 2T12 (3520 psi) and the same amount of flexural steel area was provided. This indicated that straight end flexural bar details caused the reduced specimen capacity.

3.6 SUMMARY OBSERVATIONS FROM CONTROL LABORATORY TESTS:

- Initial diagonal-tension cracking was observed at an average concrete shear stress approximately corresponding to $v_c = 1.4\sqrt{f'_c}$, with a coefficient of variation of 0.29.

- Anchorage of flexural steel was key to developing higher ultimate capacity, particularly for inverted-T specimens with straight bar development lengths.

- In regions of relatively high shear containing flexural reinforcing steel cutoffs, flexural cracks are likely to form into diagonal cracks near bar cutoffs due to the stress concentration at these locations. Diagonal cracks may not be as well constrained at the level of the flexural steel at these regions.

- Diagonal-tension crack widths measured above hairline were sufficiently wide to permit the stirrup to reach yield (at the crack location).

- Diagonal-tension cracks were quite wide at mid-depth of the beam, tapered to zero in the compression zone and were fine at the level of the flexural steel. This condition was also observed in the field.

- Offset of the concrete surface was observed locally at stirrup locations due to incipient spalling at diagonal crack locations and was attributed to localized stirrup debonding.

- Offset of the entire cross-section was observed for a test with widely spaced stirrups (18 in. spacing) and occurred near ultimate load.

- Stem cracking at the deck interface was observed in tests for both T and IT specimens. The stem/deck cracking at the interface exhibited lengths of approximately only 12 in. before intersecting another diagonal web crack.

- Initial cracking damage may not necessarily contribute to the final failure mode, as observed for specimens 4IT6-10 and 4IT8-12. Thus, if loading conditions change so as to create a new critical region in a beam, the beam may fail at a section that did not previously exhibit cracking.

- Crack width alone may not indicate the level of previous damage to the beam. Tightly spaced stirrups exhibited small crack widths at failure while widely spaced stirrups exhibited large and wider cracks at failure. Crack width for a given stirrup spacing may provide a better relative measure of damage.

- Observed crack motions indicated relatively little motion parallel to diagonal cracks, with more motion in the direction transverse to the crack. As a result, little or no aggregate interlock may be available. Further, little dowel action from the flexural steel may exist from these deformations. However, as seen in later analysis, methods to predict capacity of specimens that account for force transfer across cracks reasonably predicted capacity of the specimens, even with the wide cracks.

- Angle of diagonal crack was dependent on the interaction of moment and shear at the section. It was also influenced by the flexural reinforcing details.

- Diagonal-tension failure of the beam was generally attributed to failure at a particular section due to anchorage failure of flexural steel in tension zone or failure of compression zone, precipitated by the diagonal cracks. In all cases, diagonal cracks were sufficiently wide to permit yielding of stirrups.

- A specimen tested at a higher loading rate exhibited slightly higher capacity and lower overall displacement. The reduced displacement was likely due to reduced creep deformations.

3.7 LOW-CYCLE FATIGUE TESTS

Repeated loading effects can be divided into two phenomena: low-cycle fatigue and high-cycle fatigue. High-cycle fatigue (HCF) is generally characterized by millions of load cycles. Low-cycle fatigue (LCF), however, is less well defined. Low cycle fatigue generally consists of fewer than 10,000 cycles, but is defined as fatigue caused by repeated plastic deformations (*Bannantine, et al. 1990*). In reinforced concrete girders with diagonal cracks, LCF occurs when the girder is repeatedly subjected to load effects that produce stresses above yield in stirrups at diagonal crack locations.

The phenomenon of LCF has been studied previously, but earlier work has focused on flexural response during seismic events (*Manfredi and Pecce 1997*). During seismic loading, structures are exposed to a low number of cycles, but experience stress reversals that cause compression in the reinforcing steel. In bridges, stirrups are exposed primarily to tensile stresses without reversals causing compression. This is due to the self-weight of the structure acting at the diagonal crack location, so that even small live load induced unloading caused by continuous span effects may not produce compressive stress in the stirrups.

A series of tests was performed to evaluate the life of girders under repeated overloads that cause yielding of stirrups. The load ranges were selected to simulate different overload events. Specimen variables included: T and inverted-T configurations, stirrup spacing, and flexural reinforcing details. Test specimens were subjected to the conventional control loading protocol up to prescribed force levels between 72% and 85% of the nominal shear capacity. Nominal shear capacity was determined using AASHTO-MCFT (*AASHTO-LRFD 2003*). The specimen was then subjected to repeated applications of a prescribed force amplitude. Constant force amplitude loading was continued until the observed increment of deformation became linear or until a given number of cycles was achieved. Subsequently, load amplitudes were increased and

again a number of constant force amplitude cycles was applied until the eventual failure of the specimen.

3.7.1 Test Method

The loading frame for the low-cycle fatigue tests was the same as that used for the control tests, as described previously. The specimen was loaded until the desired force magnitude was reached and then additional strain gages and crack displacement sensors were added to the specimens at diagonal crack locations. After instruments were placed, testing was continued under load control, with force feedback to the servo-hydraulic control system provided by a load cell in series with the hydraulic actuator.

Two 15 GPM servovalves were used to facilitate application of the repeated load at frequencies between 0.1 and 0.25 Hz. This relatively low loading rate required several days to complete testing for some specimens. The fluctuating fatigue load was applied to the specimens at midspan through a spreader beam with reaction points on the specimen spaced 24 in. on-center.

During testing, the fatigue loading was suspended and the crack widths and extents were measured and recorded. These inspection intervals varied for the different specimens but were performed before a higher load range was applied or after a certain number of cycles was achieved. Crack widths were measured using an ODOT crack comparator with the actuator load magnitude held constant at applied forces between 150 and 200 kips. The observed crack extensions during low-cycle fatigue testing are shown in Appendix A5 for each of specimens.

3.7.2 Experimental Results

Seven specimens were subjected to low-cycle fatigue testing. These included specimens 5IT12-B3, 6T6, 6IT6, 7IT6, 9IT12, 9T12, and 10T24. The specimens tested were both T and inverted-T configurations, and contained stirrups spaced between 6 and 24 in. as well as different flexural reinforcing bar details. Specimen details are shown in Appendix A1. Initial force amplitudes were varied for the different specimens and are summarized in Table 3.7 with the number of cycles for each force amplitude.

Measured stirrup stress ranges varied between specimens due to the different specimen configurations and loading levels imposed during fatigue testing. However, strain gages on stirrup legs crossing diagonal crack locations indicated strains at or above the yield strain for the load amplitudes investigated. The measured stirrup strain ranges for the instrumented stirrups applied after diagonal cracking, are summarized in Table 3.8. These data were taken from the response histories near the end of the particular cycle load range.

Table 3.7: Loading levels and number of cycles for low-cycle fatigue tests

Specimen	Load Level (kips)	Vn (kips)	V/Vn	Vs/Vn	Vs/Vc	N
5IT12	303	186	0.836	0.436	1.091	50
	353	186	0.970	0.436	0.816	10
	303	186	0.836	0.436	1.091	10
	353	186	0.970	0.436	0.816	190
	378	186	1.038	0.436	0.725	49
					Total Cycles	309
Specimen	Load Level (kips)	Vn (kips)	V/Vn	Vs/Vn	Vs/Vc	N
6T6	394	235	0.853			200
	425	235	0.919			200
	450	235	0.972			200
	472	235	1.019			100
	400	235	0.866			600
	450	235	0.972			200
	472	235	1.019			200
	400	235	0.866			150
	450	235	0.972			150
	472	235	1.019			24
					Total Cycles	2024
Specimen	Load Level (kips)	Vn (kips)	V/Vn	Vs/Vn	Vs/Vc	N
6IT6	401	256	0.783	0.634	4.240	150
	426	256	0.832	0.634	3.196	200
	451	256	0.881	0.634	2.565	200
	474	256	0.926	0.634	2.170	37
					Total Cycles	587
Specimen	Load Level (kips)	Vn (kips)	V/Vn	Vs/V	Vs/Vc	N
7IT6	404	253	0.814			553
					Total Cycles	553
Specimen	Load Level (kips)	Vn (kips)	V/Vn	Vs/Vn	Vs/Vc	N
9T12	282	173	0.835	0.586	2.353	1000
	301	173	0.890	0.586	1.928	365
	309	173	0.913	0.586	1.792	10500
	332	173	0.980	0.586	1.489	1468
					Total Cycles	13333
Specimen	Load Level (kips)	Vn (kips)	V/Vn	Vs/V	Vs/Vc	N
9IT12	255	182	0.723	0.446	1.610	200
	305	182	0.860	0.446	1.076	100
	357	182	1.003	0.446	0.800	201
					Total Cycles	501
Specimen	Load Level (kips)	Vn (kips)	V/Vn	Vs/V	Vs/Vc	N
10T24	195	123	0.827	0.330	0.663	10000
	207	123	0.876	0.330	0.604	4057
					Total Cycles	14057

Table 3.8: Average strain range for low-cycle fatigue tests (strain is microstrain)

10T24

	V/Vn=.823	ε range	Yield?
Internal	Green 1	1294	No
	Green 4	753	No
External	Green 5	3254	Yes
	Green 6	2089	Yes
	Green 7	832	Yes
Internal	Grey 2	3935	Yes
	Grey 3	-480	Yes
External	Grey 4	244	No
	Grey 5	3467	Yes
	Grey 7	2170	Yes

	V/Vn=.875	ε range	Yield?
Internal	Green 1	1443	No
External	Green 4	852	No
	Green 5	3447	Yes
	Green 6	2316	Yes
	Green 7	820	Yes
Internal	Grey 3	-3	Yes
External	Grey 4	434	No
	Grey 5	3878	Yes
	Grey 7	2249	Yes

9T12

	V/Vn=.835	ε range	Yield?
External	Yellow 2	1815	Yes
Internal	Yellow 5	1248	No
External	Red 6	2336	Yes

	V/Vn=.890	ε range	Yield?
Internal	Yellow 5	1464	No

	V/Vn=.913	ε range	Yield?
External	Yellow 1	2877	Yes
	Yellow 2	2284	Yes
	Yellow 3	2306	Yes
	Yellow 4	2488	Yes
Internal	Yellow 5	1428	No
External	Yellow 6	1906	Yes
External	Red 2	2129	Yes
	Red 3	3190	Yes
External	Red 5	3099	Yes
	Red 6	2619	Yes

	V/Vn=.980	ε range	Yield?
External	Yellow 1	3465	Yes
	Yellow 3	2654	Yes
External	Yellow 4	2701	Yes
	Yellow 6	2139	Yes
External	Red 2	2851	Yes
	Red 3	3414	Yes
	Red 5	3575	Yes
	Red 6	3808	Yes

9IT12

	V/Vn=.723	ε range	Yield?
Internal	Yellow 1	1348	No
	Yellow 3	1312	No
	Yellow 4	903	No
	Yellow 5	1528	No
Internal	Red 1	552	No
	Red 2	4346	Yes
	Red 3	863	Yes
	Red 4	1670	Yes
	Red 5	32	No

	V/Vn=.860	ε range	Yield?
Internal	Yellow 1	1746	No
	Yellow 3	1875	Yes
	Yellow 4	1253	No
	Yellow 5	1558	Yes
Internal	Red 1	890	No
	Red 2	481	Yes
	Red 3	3144	Yes
	Red 4	1728	Yes
	Red 5	17	No

	V/Vn=1	ε range	Yield?
Internal	Yellow 1	2012	Yes
	Yellow 3	2664	Yes
	Yellow 4	1386	Yes
	Yellow 5	1622	Yes
Internal	Red 2	826	Yes
	Red 4	1730	Yes
	Red 5	14	No

6T6

	V/Vn=.866	ε range	Yield?
External	Green 1	2176	Yes
	Green 2	2014	Yes
	Green 3	1788	Yes
	Green 4	1896	Yes

	V/Vn=.972	ε range	Yield?
External	Green 1	Cut	Yes
	Green 2	Cut	Yes
	Green 3	3352	Yes
	Green 4	Cut	Yes

6IT6

No Strain Gages Used

5IT12

	V/Vn=.836	ε range	Yield?
Internal	Red 1	-57	No
	Red 2	30	No
	Red 3	244	No
	Red 4	979	No
	Red 5	1145	Yes
Internal	Yellow 1	-7	No
	Yellow 2	52	No
	Yellow 3	-3151	Yes Comp
	Yellow 4	2145	Yes
	Yellow 5	581	No
	Yellow 6	1547	Yes

	V/Vn=.970	ε range	Yield?
Internal	Red 1	-63	No
	Red 2	57	No
	Red 3	421	No
	Red 4	1516	Yes
	Red 5	1639	Yes
Internal	Yellow 1	-8	No
	Yellow 2	66	No
	Yellow 3	-428.3	Yes Comp
	Yellow 4	2144	Yes
	Yellow 5	869	No
	Yellow 6	1816	Yes

	V/Vn=1.04	ε range	Yield?
Internal	Red 1	-61	No
	Red 2	68	No
	Red 3	500	No
	Red 5	1701	Yes
Internal	Yellow 1	-5	No
	Yellow 2	69	No
	Yellow 3	-399	Yes Comp
	Yellow 4	869	Yes
	Yellow 5	1583	No

7IT6

	V/Vn=.836	ε range	Yield?
Internal	Grey 2	1324	Yes
	Grey 4	1191	Yes
	Grey 5	1343	Yes
External	Grey 6	1208	Yes
	Grey 8	1689	Yes
Internal	Green 1	587	No
	Green 2	1199	No
	Green 3	173	No
	Green 4	2168	Yes
Internal	Green 6	1796	Yes
External	Green 7	1595	Yes

Example stirrup strain response during a typical low-cycle fatigue test is shown in Figures 3.16. The strain range remains consistent even as the mean value tends to increase. The mean strain increase occurred rapidly after the initial load cycle was applied and then diminished to a steady increment during subsequent cycles.

Example crack displacement response during a typical low-cycle fatigue test is shown in Figure 3.17. This exhibits similar behavior to that observed for the stirrup strains. Complete histories of

stirrup strain and diagonal crack motions during fatigue tests as well as other sensor data are contained in Appendix A5 and individual test descriptions are summarized below.

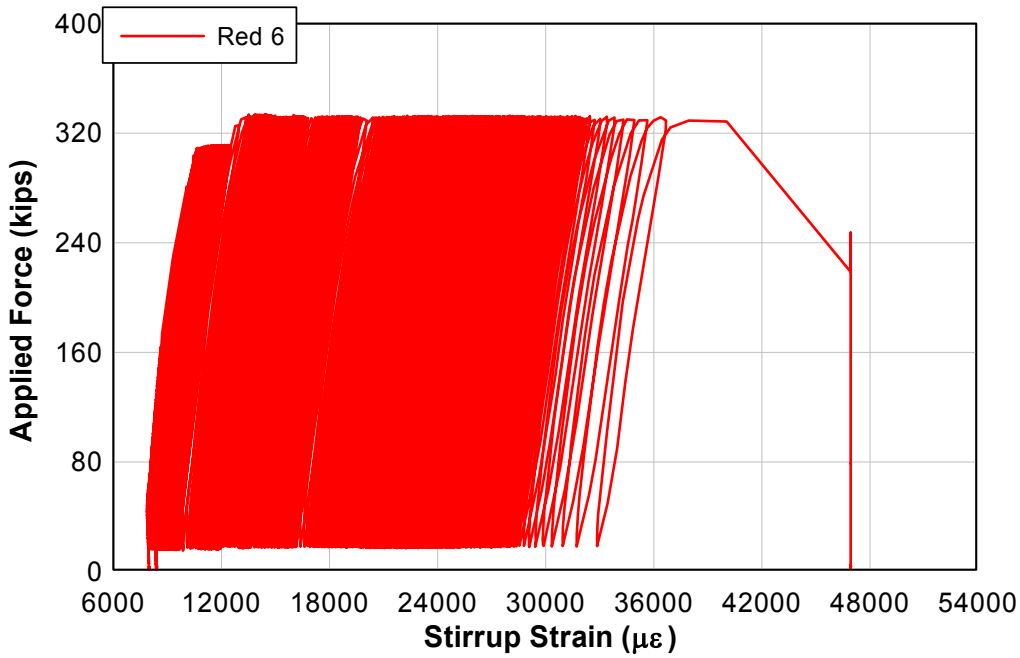

Figure 3.16: Typical applied force - stirrup strain response from low cycle fatigue specimen 9T12, part 4

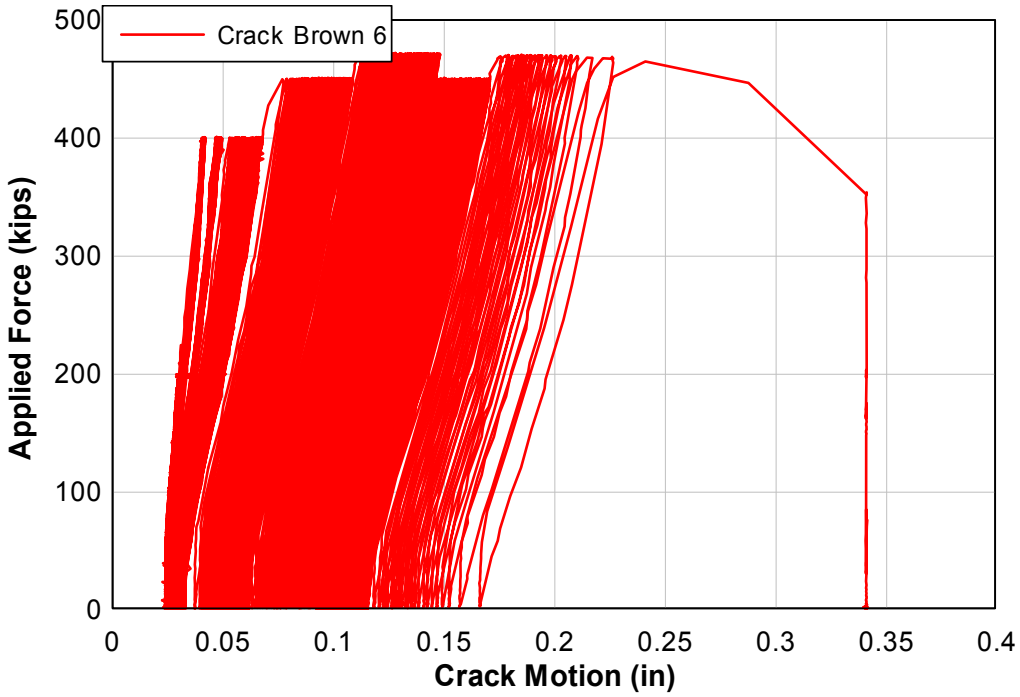

Figure 3.17: Typical applied force - crack motion response from low cycle fatigue specimen 9T12, part 2

3.7.2.1 Low-Cycle Fatigue Specimen 5IT12L22

The specimen was initially loaded using the control testing protocol up to a load level of 303 kips, which corresponds to a V/V_n ratio of 0.84. Four additional strain gages and five additional crack displacement sensors were added to the specimen and a low-cycle fatigue loading protocol was applied to the specimen. The loading sequence for the low-cycle fatigue test consisted of 50 cycles with force amplitudes ranging from 4 to 303 kips (V/V_n=0.84), 10 cycles from 4 to 353 kips (V/V_n=0.97), 10 cycles from 4 to 303 kips (V/V_n=0.84), 190 cycles from 4 to 353 kips (V/V_n=0.97), and 49 cycles from 4 to 378 kips (V/V_n=1.04). Low-cycle fatigue loads were applied at a frequency of 0.10 Hz. Before moving to a higher load range, crack measurements were made while holding the actuator force at 150 kips, except after achieving the first 60 cycles, where measurements were made at a force of 179 kips.

Centerline beam deflections for the initial 303 and 353 kip loadings increased in a nonlinear fashion in the cycles that immediately followed application of the new load range. After initial cycles, the rate of change of the deflections decreased and eventually became steady with linearly increasing displacements with each cycle. There was a small increase in crack width during the initial 303 kip loading cycles with all measured cracks along the length of the beam increasing during the first 50 cycles. Some cracks also coalesced after the first 10 cycles at the 303 kip peak force.

The peak force was increased to 353 kips and applied to the specimen. After 10 cycles at 353 kips were completed, the beam was then subjected to 10 cycles at the original force level of 303 kips. During these 10 cycles at the reduced load level, the centerline displacement and crack widths did not measurably increase. The loading was then increased back to the 353 kip level for an additional 190 cycles. A crack sensor indicated continued growth at the higher load level, however crack measurements taken at a stationary load of 179 kips were not measurably different from those previously recorded at 150 kips. The peak load was then increased to 378 kips. At this load level several crack sensors and visual observation indicated significant crack width increase. Eventually, the specimen failed in shear-compression after 49 cycles at the peak force level of 378 kips.

3.7.2.2 Low-Cycle Fatigue Specimen 6T6L22

The specimen was initially loaded using the control testing protocol up to a load level of 400 kips, which corresponded to a V/V_n ratio of 0.87. Four additional strain gages and five additional crack displacement sensors were added to the specimen and a low-cycle fatigue loading protocol was applied to the specimen. The loading sequence for the low-cycle fatigue test consisted of 200 cycles with force amplitudes ranging from 4 to 400 kips (V/V_n=0.87), 200 cycles from 4 to 425 kips (V/V_n=0.92), 200 cycles from 4 to 450 kips (V/V_n=0.97), and 100 cycles from 4 to 472 kips (V/V_n=1.02). Low-cycle fatigue loads were applied at a frequency of 0.10 Hz. Before moving to a higher load range, crack measurements were made while holding the actuator force at 200 kips.

During the first several cycles of each new load increment, increasing beam deflections were observed. However, deflections did not change after approximately 100 cycles. The

test was eventually halted after 100 cycles with a peak load range of 472 kips, because there was no sign of damage (crack widths and deformations did not change). It was not possible to increase the load above this level due to the force capacity of the hydraulic actuator.

Because failure of the specimen was not possible, it was used to study the effects of sequential stirrup fracture occurring along a diagonal crack. A diagonal crack on the north end of the specimen was selected as a critical location based on the observed crack width of 0.04 in. and location (approximately the effective depth away from the loading point). At the crack location, strain gages were bonded on the stirrups crossing the crack. The four gages were identified as Gr1, Gr2, and Gr3 on the east face and Gr4 on the west face. Two crack gages, identified as Br3 and Br6, were attached on the east face of the specimen across the crack near the instrumented stirrup locations. The specimen and instrumentation are shown in Figure 3.18.

Figure 3.18: Instrumentation for damage sequencing of stirrups for specimen 6T6L22

The specimen was loaded to 200 kips and crack measurements were taken for reference. Subsequently, 150 cycles at a peak load of 400 kips were applied. Strains of approximately 1200 με (at maximum) were observed at Gr1, Gr2, and Gr4, while 900 με was seen at location Gr3. The specimen deflection and crack widths did not exhibit significant changes.

The load was reduced to zero and the stirrup instrumented with strain gage Gr2 was cut with an angle grinder. An additional 150 cycles at a peak load of 400 kips were applied to the specimen. The maximum strain was 2000 με at Gr1 and about 1200 με at Gr3 and Gr4. No significant change in specimen deflection or crack widths was observed.

Next, the load was again reduced to zero and the stirrup instrumented with strain gage Gr1 was cut with an angle grinder. The specimen was subjected to 150 cycles with a 400 kip peak load. Instrumented stirrups Gr3 and Gr4 indicated 1200 με at maximum load. At this stage, crack widths began to increase with a maximum crack width measured at 0.07 in. compared to 0.05 in. at the beginning of this test.

Next, the stirrup instrumented with strain gage Gr4 was cut with an angle grinder. A sequence of low-cycle fatigue loads was applied as follows: 150 cycles with a 400 kip peak load; 200 cycles with a 450 kip peak load; and 200 cycles with a 472 kip peak load. The maximum strain in the remaining instrumented stirrup (Gr3) exceeded 2800 με. The maximum crack width increased to 0.177 in. However, the increasing deflection of the specimen exhibited the same trend as previously observed; relatively large increases in deflections during the first several cycles gradually decreasing rates of change and then becoming steady.

Finally, a stirrup leg was cut on the opposite face of that for the instrumented stirrup Gr1 (final cut stirrup located on the west face). A sequence of low-cycle fatigue loads was applied as follows: 150 cycles with a 400 kip peak load; 150 cycles with a 450 kip peak load; and 24 cycles with a 472 kip peak load which eventually produced a shear-compression failure of the specimen. A maximum crack width of 0.222 in. was measured after the final 200 cycles at the 450 kip peak load amplitude.

3.7.2.3 Low-Cycle Fatigue Specimen 6IT6L22

The specimen was initially loaded using the control testing protocol up to a load level of 401 kips, which corresponded to a V/V_n ratio of 0.78. Subsequently, low-cycle fatigue loading was applied to the specimen. The sequence of the low-cycle fatigue was: 150 cycles with a peak load of 401 kips (V/V_n=0.78), 200 cycles with a peak load of 425 kips (V/V_n=0.83), 200 cycles with a peak load of 450 kips (V/V_n=0.88), and 37 cycles at a peak load of 475 kips (V/V_n=0.93), at which point the test was terminated for safety reasons. Diagonal crack measurements were made at intervals when the applied load was held constant at 200 kips.

Five displacement sensors were attached to the beam after monotonic loading to monitor crack motions. Instruments designated Br1 and Br2 were attached on the east face of the

north side of the specimen. Instruments designated Br4, Br5, and Br6 were attached on the east face of the south side of the specimen. Diagonal crack measurements were made after each set of cycles was completed and with the applied load held constant at 200 kips.

Upon achieving peak force amplitude for the first time, beam displacements incrementally increased with successive cycles. The rate of change in the beam deflection slowed on subsequent cycles and tended to fit a limiting exponential curve. After 150 cycles at the peak load of 400 kips, no significant changes in either crack width or centerline displacement were observed.

The cyclic load amplitude was then increased to a peak load of 425 kips. Noise appearing to be associated with the flexural rebar anchorage was noted in the vicinity of the supports. Crack Br6 closed rapidly after 25 cycles from 0.023 in. to only 0.011 in. After 50 cycles, the support plate at the south end had almost slipped off the roller and testing was suspended while the plate was repositioned. This required that support deformation sensors be removed while the support plates were repositioned. Data acquisition was restarted and the specimen was loaded to 205 kips to measure crack widths. Crack widths and centerline displacements increased slightly during the 425 kip loading cycles.

The load was increased to 450 kips. Crack sensors Br6 and Br5 indicated the instrumented diagonal cracks were closing. Crack sensors Br1, Br2, and Br4 indicated diagonal crack opening as the number of cycles increased. Centerline displacement continued to increase. The load was further increased to 475 kips. After 37 cycles, the specimen began to tilt toward the east. Testing was halted and specimen was loaded to 205 kips to permit measurement of the diagonal cracks. Cracks at sensor locations Br1 and Br4 opened sharply during this portion of the testing, while crack location Br5 closed sharply due to twisting of the cross-section. Testing was stopped due to safety concerns.

3.7.2.4 Low-Cycle Fatigue Specimen 7IT6L22

Specimen 7IT6L22 was initially loaded using the control testing protocol up to a load level of 2193kN (493 kips), which corresponded to a V/V_n ratio of 0.97, without specimen failure. This was the maximum load that could be applied with the testing system. However, to develop additional data on specimen response under stirrup damage progression, the specimen was further tested after instrumentation and subsequent cutting of stirrup legs at diagonal crack locations. The tests were performed under a low-cycle fatigue tested protocol.

A crack (identified as Crack A) located on the north side of the specimen was selected to be a critical crack based on the observed crack width and location (0.070 in. at 493 kips prior to low-cycle loading). Additional strain gages (identified as 1E, 2E, 1W, 2W) were applied to both the east and west legs of the two stirrups that crossed diagonal crack A. The 2E strain gage failed after initial installation. Two crack gages (identified as C1 and C2) were also added near the middle of the crack, one on the west face (C1) and one on the east face (C2). Crack displacement sensors Br2 and Br6 were removed to permit the additional sensor channels.

The specimen was loaded statically to 475 kips and then unloaded. After unloading, stirrup 1W was cut with an angle grinder and low-cycle fatigue loading was applied to the specimen with 50 cycles ranging from 5 kips to a peak load of 404 kips (V/V_n=0.81). After the cycles were complete, stirrup 2E was cut with an angle grinder and an additional 100 cycles from 5 kips to a peak load of 404 kips was applied to the specimen. After this sequence, stirrup 1E was cut with an angle grinder and 200 cycles from 5 kips to a peak load of 400 kips was applied. Finally, stirrup 2W was cut with an angle grinder and 203 additional cycles from 5 kips to 400 kips was applied until the specimen failed in shear-compression. All low-cycle loadings were applied at a frequency of 0.10 Hz and diagonal crack measurements were made at an applied 200 kips.

After stirrup cutting 1W, the stirrup strain in 2W increased at a higher rate than 1E, which was the other leg of the cut stirrup. After stirrup 2E was cut and the fatigue load applied, the width of crack A, and the measured stirrup strains across crack A increased sharply upon initial reloading; and then crack widths and strains continued to increase but at a slower rate. Similar behavior was observed after stirrup 1E was cut, where crack widths and strains in crack A increased sharply immediately after the stirrup was cut. The strain in stirrup 2W increased rapidly to a maximum recorded strain of 6252με after 33 cycles and then went out of range. Both diagonal crack measurements continued to increase with location C2 increasing more quickly than location C1. At this point, Stirrup 2W was cut. Crack widths and strains in crack A increased sharply after the stirrup was cut and crack widths at crack A increased rapidly immediately prior to failure.

3.7.2.5 Low-Cycle Fatigue Specimen 9IT12L22

Specimen 9IT12L22 was initially loaded using the control testing protocol up to a load level of 255 kips, which corresponded to a V/V_n ratio of 0.72. Low-cycle fatigue loading (load control) was then applied to the specimen. The sequence of the low-cycle fatigue is described as follows: 200 cycles from 4 kips to a 255 kip peak load (V/V_n=0.72); 100 cycles from 4 kips to a 305 kip peak load (V/V_n=0.86), and 201 cycles from 4 kips to a 357 kip peak load (V/V_n=1.00). The beam exhibited a shear-compression failure. Low-cycle fatigue load was applied at a frequency of 0.1 Hz and diagonal crack measurements were made at a constant applied load of 250 kips.

Centerline displacement response for this specimen closely followed that observed for previous tests, whereby after the peak load was achieved on the first cycle, displacement continued to increase quickly on subsequent cycles, but the rate of change slowly decreased until linear displacement increments were achieved. This was also observed for diagonal crack displacements. Prior to failure, the displacements began to increase rapidly for each subsequent cycle and continued to increase until the specimen failed.

3.7.2.6 Low-Cycle Fatigue Specimen 9T12L24

Specimen 9T12L24 was initially loaded using the control testing protocol up to a load level of 250 kips, which corresponded to a V/V_n ratio of 0.72. Low-cycle fatigue loading (load control) was then applied to the specimen. The sequence of the low-cycle fatigue is described as follows: 1000 cycles from 4 kips to a 282 kip peak load (V/V_n=0.84); 365

cycles from 4 kips to a 301 kip peak load (V/V_n=0.89), 10500 cycles from 4 kips to a 309 kip peak load (V/V_n=0.91), and 1468 cycles from 4 kips to a 332 kip peak load (V/V_n=0.98). The beam exhibited a shear-compression failure. Low-cycle fatigue load was applied at a frequency of 0.25 Hz and diagonal crack measurements were made at a constant applied load of 150 kips.

After 100 cycles at the 275 kip peak load magnitude, strain gages were rebalanced because several of the readings had exceeded the range capability of the data acquisition system. After 1000 cycles at the 275 kip peak load, testing was suspended because the specimen had shifted on the end supports. The beam was adjusted back to its original position and diagonal crack sensor identified as Br1 was moved to an adjacent crack location because the crack that was being monitored closed. The peak load was increased to 301 kips for 365 cycles and was then increased to 309 kips for another 135 cycles before the test was stopped for the day.

Before restarting the test, high-elongation strain gages were bonded to the stirrups crossing selected cracks. These included sensors identified as Rd2, Rd3, Rd5, and Rd6 on the south side and sensors identified as Ye1, Ye2, Ye3, and Ye6 on the north side of the specimen. Residual strains from the data taken the previous day were taken as the initial strains for the new gages. Residual strains for several stirrups were not known precisely because the strain gages on those stirrups had gone out of range. In these cases, the maximum previously recorded strain was used as the residual strain. Strain gages were also added on the flexural reinforcement on both the north and south sides of the beam and two clip gages were bonded to the deck surface, centered over the web, and located 12 in. from the spreader beam contact points on both the north and south sides.

The second day of low-cycle fatigue testing consisted of 2,500 cycles at a peak load of 309 kips. The beam again shifted in the supports after only 22 cycles. Testing was suspended and the beam was readjusted onto the supports. After 1,825 total cycles, there was a sharp pop emitted from the north end of the beam. After 2,140 total cycles another pop was heard in the south end of the beam near the Rd5 gage. Four more pops were heard from the south side of the beam after 2,220 cycles, 2,295 cycles, 2,326 cycles, and 2,436 cycles. After testing, concrete was removed around stirrup locations and revealed three fractured stirrup locations. The other popping sounds were attributed to stirrup slip.

The third day of low-cycle fatigue testing consisted of 5,000 cycles at a peak load of 1374kN (309 kips). After 4,234 total cycles, the beam position was again readjusted. A crack in the deck was observed after 6,900 total cycles. The crack extended from a diagonal crack identified as D in the instrumentation plan.

Before starting tests for the fourth day, the beam was again repositioned on the supports and then 2,762 cycles at a peak load of 309 kips were applied to the specimen. After the first cycle, a loud noise sounding like steel on steel was heard from the south end support, but no evidence of damage was observed. The south end support required adjustment after 9,280 total cycles. After 11,762 total cycles, the peak load was increased to 320 kips. Eventually, failure occurred after 13,333 total cycles with the specimen exhibiting a shear compression failure.

3.7.2.7 Low-Cycle Fatigue Specimen 10T24L24

Specimen 10T24L24 was initially loaded using the control testing protocol up to a load level of 190 kips, which corresponded to a V/V_n ratio of 0.80. Low-cycle fatigue loading (load control) was then applied to the specimen. The sequence of the low-cycle fatigue is described as follows: 10,000 cycles from 4 kips to a 195 kip peak load (V/V_n=0.83) and 4057 cycles from 4 kips to a 207 kip peak load (V/V_n=0.88). The beam exhibited a shear-compression failure. Low-cycle fatigue load was applied at a frequency of 0.22 Hz and diagonal crack measurements were made at a constant applied load of 100 kips.

Before application of the low-cycle loading, five high-elongation strain gages were bonded to stirrups crossing diagonal cracks on the west face of the specimen. Two were applied to the north end and three were applied to the south end. Low-cycle fatigue loading was then applied to the specimen. During loading, raveling of the concrete along the diagonal cracks and crack extension along the deck-stem interface were observed. After 1507 cycles, the loading increased slightly to 198 kips for 495 cycles and then reduced back to 195 kips.

Over the course of the day, the sun angle changed and reflected off the specimen, thereby heating the strain gages and other instruments located on the exposed face. Shading was provided to reduce temperature effects on the sensor measurements. Centerline displacement increased nonlinearly over the first 1000 cycles and then increased in a linear fashion thereafter. Diagonal crack sensor identified as Br1 indicated increased crack movement over the first 1000 cycles and changed linearly after during subsequent cycles. Diagonal crack sensor identified as Br2 indicated increasing crack growth during the first 400 cycles and then became linear after that point. Diagonal crack sensors identified as Br4 and Br5 indicated decreasing crack motions. The test was halted at the end of the day and restarted the following day.

Prior to beginning testing on the second day, the beam was repositioned on the supports and the centerline displacement and support displacement sensors were reset. Strain gages Gy3 and Gy4 jumped slightly from the previous days testing. This was most likely caused by a temperature differential from the end of the previous day. After 3089 cycles, an external strain gage went out of range. The gage was replaced and rebalanced while there was a 100 kip load on the specimen at 4002 cycles. Strains continued to increase slowly during the second day of testing.

At the end of the day, the testing was suspended and restarted on the third day after again repositioning the specimen on the supports. The centerline displacement sensor was also reset. After 10,000 total cycles, the load was increased to 207 kips. At this load level, strain gages identified as Gn5 and Gn6 began to increase more quickly than during the previous load step. The other strain measurements increased at about the same rate as at the previous lower load amplitude. Prior to failure, the centerline displacement began to increase rapidly as did cracks locations identified as Br1 and Br2. The beam eventually failed in a shear-compression failure mode.

3.7.3 Conclusions

Full-size tests of conventionally-reinforced concrete (CRC) girders, designed and constructed to reflect 1950's vintage details and materials, were performed under low-cycle fatigue. Low-cycle fatigue loading was applied after specimens were initially loaded to between 72% and 85% of the nominal shear capacity. Constant force amplitude loading was applied until the observed increment of deformation became linear or until a given number of cycles was achieved. Load amplitudes were increased and loading cycles were applied until the eventual failure of the specimen. Based on these tests, the following conclusions are presented:

- LCF damage occurs at loads sufficient to cause yielding in stirrups across diagonal cracks.
- Damage from LCF was observed from bond deterioration and cumulative plasticity of the stirrups.
- Failure was controlled by progressive fracture of stirrups.
- Damage from LCF was observed to occur in three distinct phases: an initial nonlinear phase, a middle linear phase, and a final nonlinear phase leading to eventual specimen failure.
- Rates at which incremental deformations occurred during LCF in each of the three damage phases increased with higher loading ratios (V/V_n).
- Diagonal deformations across the web increased under LCF and at failure were larger than similar specimens subjected to the control loading protocol. Diagonal deformations based on conventional monotonic loading may be used as an estimate of the cumulative diagonal deformations under LCF.
- Specimens were able to sustain relatively large numbers of cycles of repeated loads at large loading ratios.
- For sequenced loads of varying magnitudes, low magnitude load cycles occurring after a higher amplitude load exhibited incremental deformations associated with the lower magnitude in the middle linear phase accumulation range.

3.8 HIGH-CYCLE FATIGUE TESTS

Diagonal cracks have been identified on reinforced concrete deck-girder (RCDG) bridges, which are exposed to millions of load cycles during service life. The anticipated life of these bridges in the cracked condition under repeated service loads is uncertain. A series of tests was performed to evaluate possible deterioration in load-carrying capacity or reduction in service life. Specimen variables included: T and inverted-T configurations, stirrup spacing, and flexural reinforcing details. Stirrup strain data previously collected during field investigations of four in-service RCDG bridges were used as a reference for the laboratory high-cycle fatigue (HCF) tests.

Test specimens were initially cracked to impose diagonal cracks of the desired width prior to initiation of fatigue testing. Precracking of the specimens was performed in the setup described previously for the tests conducted to failure. The specimens were then moved to a separate test frame to apply the high-cycle fatigue loading protocol. After application of fatigue loads, the specimens were moved back to the original load frame and tested to failure to observe differences in capacity from similar non-fatigued specimens.

3.8.1 Test Method

Test specimens were precracked to produce a desired diagonal crack width as measured by an ODOT crack comparator both with and without applied load. Diagonal crack width conditions at peak load and at zero load for the high-cycle fatigue specimens are shown in Table 3.9. Initial specimens were loaded so as to produce crack widths corresponding to field observations. The diagonal cracks were at least 0.025 in. when the specimens were unloaded. Some cracks were larger because precracking was performed with discrete load increments. Sensor data recorded during precracking is contained in Appendix A4. After pre-cracking, the specimens were moved to a separate load frame for HCF testing.

Table 3.9: Precrack stage crack widths for HCF specimens

Specimen	Precrack Load [kips]	Maximum w_{cr} [in]		
		At precrack load	At 0 kip	At 100 kip Total Load
3T12	260	0.050	0.025	0.030
3IT12	260	0.040	0.025	NA
3IT18	225	0.105	0.070	NA
5IT12-B1	330	0.060	0.050	NA
6T10	400	0.110	0.070	0.080
6IT10	375	0.070	0.040	0.050
8IT10	350	0.060	0.030	0.040
9IT12-B1	300	0.060	0.025	0.040
9T12-B4	250	0.095	0.06+	0.080

The loading frame for high-cycle fatigue tests consisted of a 110 kip capacity fatigue-rated actuator mounted to a large steel reaction frame as shown in Figures 3.19a and b. Fatigue tests were performed in load control, with force feedback to the servo-hydraulic control system provided by a load cell in series with the hydraulic actuator. A 30 GPM servovalve was used to allow application of the repeated load at a frequency of 2.4Hz. This permitted application of approximately 200,000 cycles of repeated loading per day. The alternating fatigue load was applied at midspan through a spreader beam with reaction points spaced 24 in. on-center.

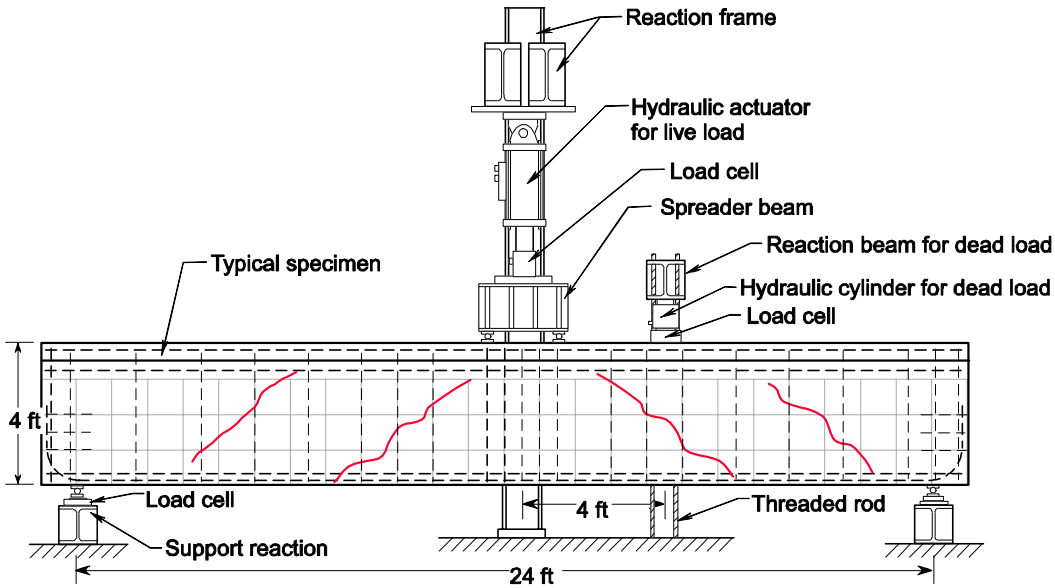

Figure 3.19a: Schematic of high-cycle fatigue test setup

Figure 3.19b: Image of high-cycle fatigue test setup

A simulated dead load of between 80-100 kips was also applied to the specimen, using a complementary loading system. This dead load represents the associated weight of portions of a bridge attributed to a girder, but not reflected in the self-weight of the specimen. The dead load force was applied with a hydraulic cylinder attached to a hydraulic accumulator. The hydraulic pressure in the cylinder and the nitrogen pressure in the hydraulic accumulator were adjusted to provide as consistent a level of dead load force as possible. The accumulator compensated for the pressure drop in the dead load hydraulic cylinder due to deformation of the specimen from the applied fatigue force. Adjustments of the dead load cylinder were required periodically due to hydraulic oil temperature changes and seal leakage.

Applied dead load was measured directly using a load cell in-series with the hydraulic cylinder. The dead load cylinder was located 4 ft from the beam centerline. From static analysis of the simply supported beam specimens, 33% of the dead load is attributed to the support farthest from the applied dead load force, and 66% is attributed to the support closest to the applied dead load. These force distributions were verified by three different load cells located on the fatigue loading actuator, south support reaction, and dead load cylinder.

The magnitude of the fatigue load ranged from 4 to 84 kips to ensure the actuator remained in contact with the specimen. This produced a load range of 80,000 lbs, which corresponds roughly to the gross vehicle weight of a typical 18-wheel container truck. The load range was applied to each of the high-cycle fatigue specimens 2 million times to simulate damage produced during the service life of a bridge girder. Stress ranges and numbers of cycles to represent 50 years of service life were previously determined from instrumentation of field study bridges. These are compared with the laboratory stress ranges imposed on test specimens as described below.

Fatigue loading was suspended at regular intervals and a series of performance tests were conducted for specimens in the latter phases of testing. These tests were performed at intervals of approximately every 100,000 cycles up to 500,000 cumulative cycles and then every 250,000 cycles until 2 million cumulative cycles were achieved. Crack widths were measured with the fatigue load magnitude at approximately 2 kips using the ODOT crack comparator and crack extents were monitored and recorded. The crack extensions during fatigue testing are shown in Appendix A3 for each of specimens.

Displacement sensors were reattached and a sequence of loading tests were performed: 10 cycles ranging from 4 to 84 kips at 0.5 Hz; 5 cycles ranging from 4 to 104 kips at 0.1 Hz; and finally another 10 cycles ranging from 4 to 84 kips at 0.5 Hz. The first 15 cycles of the sequence were used to ensure seating of the reapplied sensors, and data were taken from the final 10 cycles of this sequence to assess changes in response. No specimen failure was observed during fatigue loading and after completion of 2 million load cycles. Specimens were moved back to the original test setup and loaded to failure.

3.8.2 Experimental Results

Nine specimens were subjected to the fatigue testing protocol as listed in Table 3.9. Specimen details are shown in Appendix A1. Measured stirrup stress ranges varied between specimens, even as the applied fatigue load range and peak value were held constant for all tests. This was due to the different specimen configurations and initial cracking levels imposed at the start of

fatigue testing, as well as the applied dead load effects. The average measured stirrup strain ranges and crack displacement ranges, at the beginning of fatigue testing and after completion of 2 million cycles, are summarized in Tables 3.10 and 3.11, respectively.

Table 3.10: Stirrup strain ranges at the beginning and completion of HCF testing

Specimen	Strain Gage	ε Range (με)	
		After precrack	After 2million cycles
3IT12	GS1	10	5
	GS2	170	150
	GS3	250	255
	GS4	230	240
	GS5	430	450
	GS6	130	120
	GS7	390	390
	GS8	420	460
	GN1	10	10
	GN2	15	10
	GN3	*	*
	GN4	280	290
	GN5	860	830
	GN6	*	*
	GN7	610	610
	GN8	*	*
3T12	GS1	360	350
	GS2	50	40
	GS3	320	310
	GS4	230	190
	GS5	5	5
	GS6	*	*
	GS7	500	460
	GS8	460	420
	GN1	*	*
	GN2	280	280
	GN3	330	320
	GN4	640	630
	GN5	270	260
	GN6	*	*
	GN7	400	380
	GN8	750	720
3IT18	GS1	15	20
	GS2	30	15
	GS3	800	0
	GS4	230	360
	GS5	20	30
	GS6	850	1350
	GS7	990	30
	GS8	550	980
	GN1	15	20
	GN2	15	30
	GN3	870	870
	GN4	50	80
	GN5	20	20
	GN6	810	840
	GN7	1520	1480
	GN8	800	600

Specimen	Strain Gage	ε Range (με)	
		After precrack	After 2million cycles
5IT12-B1	GS1	5	10
	GS2	5	10
	GS3	30	20
	GS4	120	110
	GS5	420	400
	GS6	570	630
	GS7	600	650
	GS8	230	740
	GN1	10	10
	GN2	15	20
	GN3	300	240
	GN4	340	300
	GN5	190	90
	GN6	690	650
	GN7	1010	900
	GN8	660	560
6IT10	GS1	720	750
	GS2	600	620
	GS3	*	*
	GS4	290	330
	GS5	410	440
	GS6	460	480
	GN1	490	530
	GN2	560	610
	GN3	540	570
	GN4	590	550
	GN5	630	620
	GN6	180	230
6T10	GS1	650	650
	GS2	650	650
	GS3	350	10
	GS4	440	520
	GS5	410	470
	GS6	470	530
	GS7	360	410
	GS8	110	170
	GN1	440	520
	GN2	460	540
	GN3	360	460
	GN4	320	410
	GN5	420	410
	GN6	640	610
	GN7	920	840
	GN8	720	640

*indicates a broken gage, provided value taken before gage broke if possible

Specimen	Strain Gage	ε Range (με)	
		After precrack	After 2million cycles
8IT10	GS1	440	420
	GS2	350	300
	GS3	10	170
	GS4	410	470
	GS5	30	20
	GS6	570	480
	GS7	590	500
	GS8	550	440
	GN1	400	420
	GN2	510	560
	GN3	420	560
	GN4	260	430
	GN5	*	*
	GN6	820	800
	GN7	1070	1110
	GN8	490	590
9IT12-B1	GS1	400	400
	GS2	440	430
	GS3	*	*
	GS4	50	50
	GS5	2150	220
	GS6	570	550
	GS7	800	760
	GS8	700	690
	GS9	500	480
	GN1	*	*
	GN2	460	490
	GN3	290	250
	GN4	240	250
	GN5	270	250
	GN6	630	570
	GN7	760	720
9T12-B4	GS1	460	600
	GS2	40	30
	GS3	5	2
	GS4	180	190
	GS5	5	4
	GS6	840	890
	GS7	960	980
	GS8	530	460
	GN1	*	*
	GN2	5	5
	GN3	400	410
	GN4	60	20
	GN5	280	310
	GN6	870	630
	GN7	1260	1030
	GN8	790	880

Table 3.11: Crack displacement ranges at the beginning and completion of HCF testing

Specimen	Crack Gage	Crack Range (in.)	
		After precrack	After 2million cycles
3IT12	#1	0.0042	0.0052
	#2	0.0160	0.0193
	#4	0.0068	0.0091
	#5	0.0060	0.0072
3T12	#1	0.0082	0.0084
	#2	0.0030	0.0034
	#4	0.0066	0.0056
	#6	0.0066	0.0059
5IT12-B1	#1	0.0002	0.0069
	#2	0.0050	0.0057
	#5	0.0090	0.0093
3IT18	#2	0.0112	0.0123
	#3	0.0102	0.0120
	#4	0.0085	0.0130
	#5	0.0068	0.0094
	#6	0.0050	0.0078
6IT10	#2	0.0060	0.0148
	#3	0.0063	0.0086
	#4	0.0075	0.0095
	#5	0.0046	0.0062
	#6	0.0033	0.0063
6T10	#1	0.0061	0.0098
	#2	0.0107	0.0134
	#3	0.0091	0.0121
	#4	0.0062	0.0098
	#5	0.0038	0.0070
	#6	0.0076	0.0134
9IT12-B1	#1	0.0082	0.0096
	#4	0.0132	0.0143
	#5	0.0082	0.0088
8IT10	#1	0.0091	0.0096
	#2	0.0068	0.0085
	#3	0.0073	0.0101
	#4	0.0063	0.0072
	#5	0.0044	0.0062
	#6	0.0074	0.0075
9T12-B4	#1	0.0084	0.0054
	#2	0.0115	0.0060
	#3	0.0084	0.0146
	#4	0.0132	0.0124
	#5	0.0081	0.0080

An example of measured stirrup strain ranges and mean strain response during a fatigue test are shown in Figures 3.20 and 3.21, respectively. Example crack displacement range and mean crack width changes during a typical fatigue test are shown in Figures 3.22 and 3.23. Complete histories of stirrup strain and diagonal crack motions during fatigue tests are contained in Appendix A6. Stirrup stress and deformation ranges determined during each of the interval tests are summarized in Table 3.12a and b.

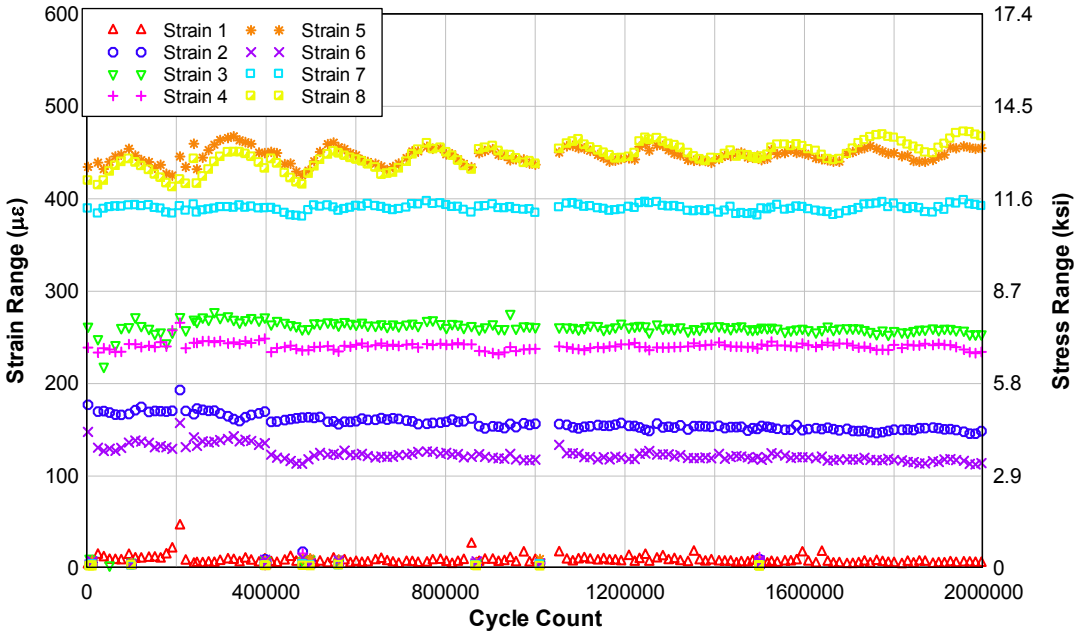

Figure 3.20: Example strain ranges during HCF test (specimen 3IT12 south end)

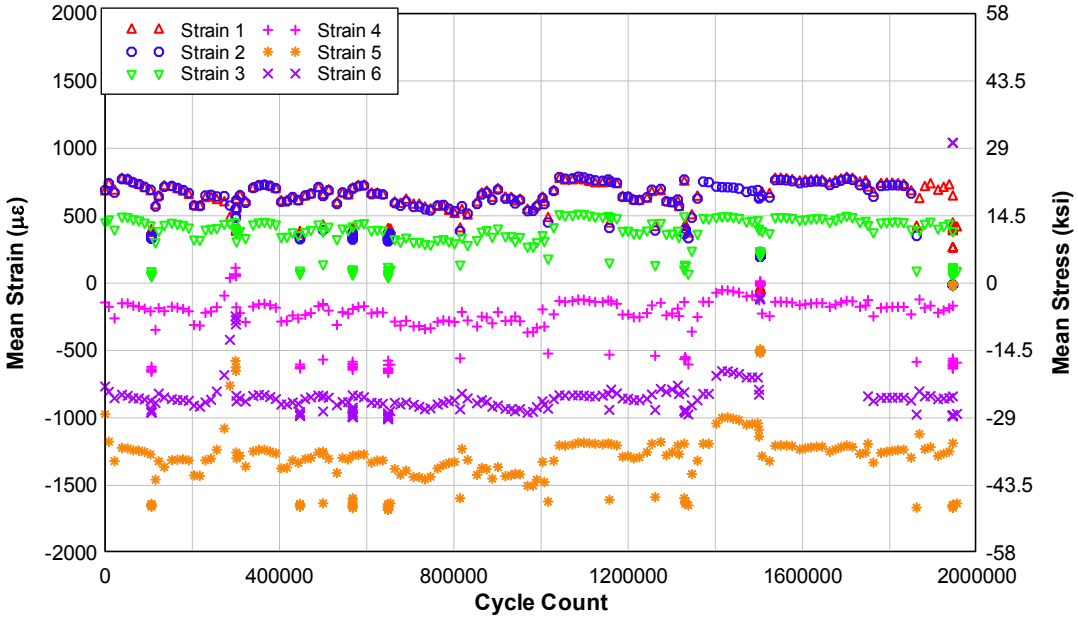

Figure 3.21: Example strain gage means during HCF test (specimen 6IT10 North end)

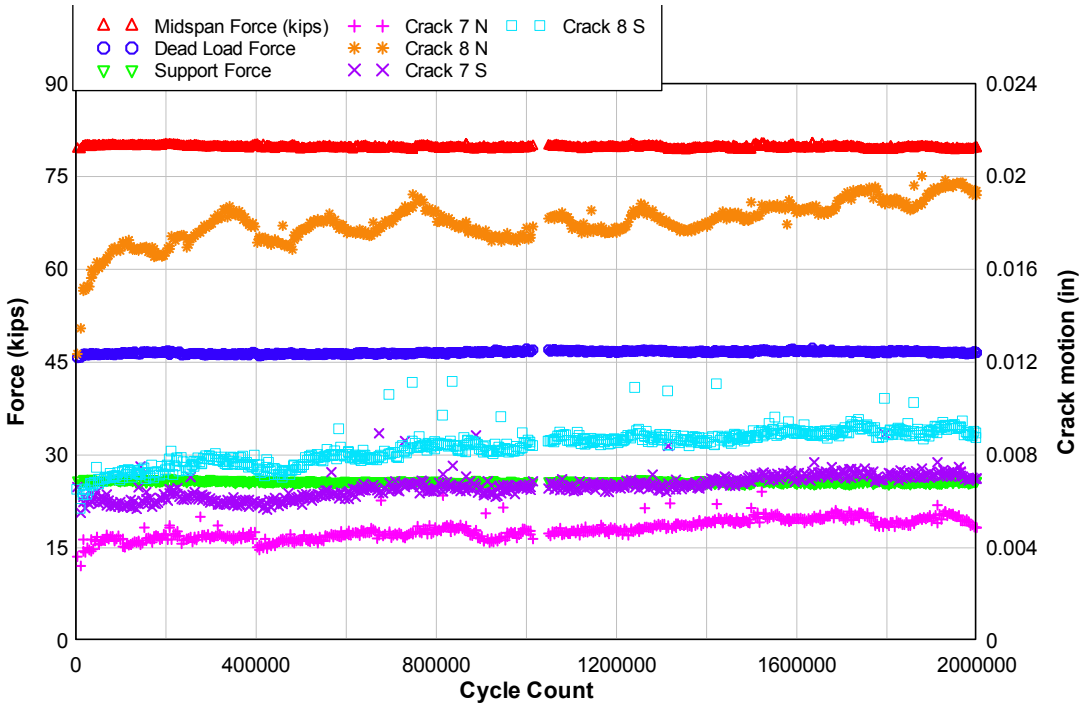

Figure 3.22: Example load and crack motion sensor ranges during HCF test (specimen 3IT12)

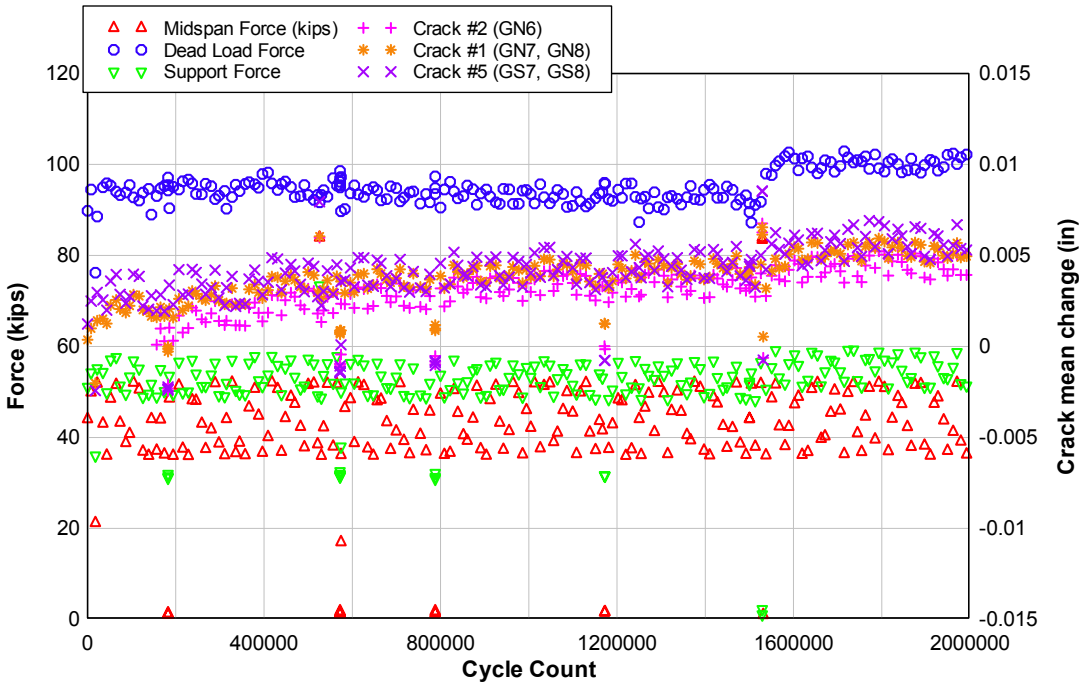

Figure 3.23: Example load and crack motion sensor means during HCF test (specimen 5IT12-B1)

Table 3.12a: Stirrup strain ranges during HCF interval tests

Specimen	Strain Gage	Check test											
		0k	100k	200k	300k	400k	500k	750k	1M	1.25M	1.5M	1.75M	2M
3IT12	GS1	22						16	16	20	13	18	
	GS2	178						165	162	157	160	153	
	GS3	270						269	271	265	272	263	
	GS4	252						252	248	247	257	244	
	GS5	451						456	447	463	444	457	
	GS6	148						138	126	139	130	122	
	GS7	392						390	385	391	386	389	
	GS8	438						451	436	455	440	462	
	GN1	19						17	15	19	22	15	
	GN2	22						17	22	36	26	20	
	GN3	0						0	0	0	0	0	
	GN4	285						297	286	287	286	292	
	GN5	871						851	0	0	0	0	
	GN6	0						0	0	0	0	0	
	GN7	602						611	600	604	610	608	
	GN8	0						0	0	0	0	0	
3T12	GS1	375								369	405		435
	GS2	63								77	103		108
	GS3	9								330	385		0
	GS4	220								212	234		260
	GS5	60								64	74		70
	GS6	0								0	0		0
	GS7	448								462	400		450
	GS8	476								494	432		469
	GN1	0								0	0		0
	GN2	284								287	323		327
	GN3	357								331	369		397
	GN4	657								633	640		696
	GN5	281								281	306		312
	GN6	3418								0	0		0
	GN7	414								383	374		408
	GN8	773								740	708		720
3IT18	GS1	19	22	30	20	24	19	18	19	29	24	33	31
	GS2	33	31	31	35	34	34	37	40	43	42	49	19
	GS3	766	697	14	192	729	336	37	15	903	921	929	0
	GS4	279	223	227	223	236	218	250	257	304	281	283	395
	GS5	27	22	22	22	27	24	31	32	41	34	32	40
	GS6	537	513	520	505	511	494	622	666	661	659	681	968
	GS7	969	890	920	897	917	876	1079	1123	1113	1103	1077	34
	GS8	864	773	795	774	791	760	910	944	955	952	977	1325
	GN1	23	15	22	21	21	14	21	25	25	35	33	25
	GN2	20	18	27	26	21	24	26	30	29	30	45	36
	GN3	832	938	934	946	915	940	895	894	869	901	924	910
	GN4	58	78	93	116	101	139	70	79	67	73	83	93
	GN5	25	24	30	24	39	21	24	30	31	26	29	36
	GN6	742	782	789	792	787	785	833	820	807	816	825	829
	GN7	1331	1493	1497	1510	1472	1490	1464	1410	1412	1433	1465	1459
	GN8	767	834	808	843	789	829	687	660	659	622	615	628
5IT12-B1	GS1		16		12		11	10	15			15	11
	GS2		20		16		14	9	17			15	13
	GS3		33		29		31	30	27			27	25
	GS4		123		125		121	117	111			106	116
	GS5		416		411		419	415	407			403	403
	GS6		539		545		570	573	587			628	596
	GS7		561		586		602	595	596			636	593
	GS8		702		713		723	709	713			725	691
	GN1		15		18		14	16	23			15	17
	GN2		17		21		24	18	19			21	28
	GN3		324		318		318	301	279			238	271
	GN4		360		354		357	341	331			307	317
	GN5		197		153		115	111	108			79	108
	GN6		627		632		640	635	605			618	621
	GN7		942		918		916	913	898			886	852
	GN8		630		605		593	589	590			558	546

Table 3.12a (continued): Stirrup strain ranges during HCF interval tests

Specimen	Strain Gage	Check test											
		0k	100k	200k	300k	400k	500k	750k	1M	1.25M	1.5M	1.75M	2M
6IT10	GS1	711	720	720	758	765	755	679	785	775	671	736	
	GS2	590	599	601	626	628	621	557	643	638	555	613	
	GS3	8	10	230	422	431	435	346	11	438	389	10	
	GS4	268	291	300	333	334	336	299	345	337	289	319	
	GS5	407	402	401	441	444	440	385	454	434	371	432	
	GS6	431	451	456	489	490	490	432	503	483	419	474	
	GN1	492	473	478	492	485	487	414	491	620	0	536	
	GN2	557	552	549	545	551	549	496	547	718	633	644	
	GN3	549	536	520	504	505	500	466	481	685	620	607	
	GN4	550	596	587	571	567	563	612	560	665	628	589	
	GN5	544	622	608	565	607	616	689	582	726	713	686	
	GN6	145	190	198	189	196	202	250	169	315	365	252	
6T10	GS1	677	643	624	629	625		689	699	697	674	628	674
	GS2	689	638	618	611	616		685	691	690	670	622	669
	GS3	321	23	242	361	10		12	12	10	12	10	11
	GS4	410	440	451	435	452		543	532	539	535	477	532
	GS5	415	402	406	394	403		487	479	486	480	429	479
	GS6	505	449	434	426	438		540	544	546	540	476	534
	GS7	407	334	315	308	316		427	431	433	426	365	414
	GS8	123	88	84	85	88		157	181	184	176	141	164
	GN1	481	419	382	381	387		530	546	546	533	437	525
	GN2	504	433	395	395	400		554	569	568	550	465	544
	GN3	386	339	314	317	319		461	474	478	468	395	462
	GN4	342	319	306	310	309		418	441	442	425	382	420
	GN5	445	422	423	420	424		439	437	441	434	426	427
	GN6	690	649	643	640	635		637	633	636	637	633	638
	GN7	1055	919	912	911	906		866	872	878	877	908	877
	GN8	732	740	746	738	734		694	679	680	681	693	668
8IT10	GS1			473	469	465	463	470	461			456	449
	GS2			313	318	300	303	301	288			283	271
	GS3			6	5	6	8	24	141			157	162
	GS4			326	346	358	459	547	539			571	573
	GS5			29	28	31	27	27	31			29	29
	GS6			573	567	555	553	552	555			547	540
	GS7			566	571	560	549	549	567			557	572
	GS8			501	506	492	479	476	498			487	499
	GN1			440	434	434	436	438	433			440	436
	GN2			557	548	544	545	554	545			560	539
	GN3			482	479	483	483	488	494			507	494
	GN4			294	282	285	284	290	296			339	322
	GN5			0	0	0	0	0	0			0	0
	GN6			824	795	786	790	781	784			799	768
	GN7			1078	1070	1054	1047	1036	1053			1062	1033
	GN8			518	510	518	522	522	540			547	542
9IT12-B1	GS1		398	391	406	388	392	413	391	368	427	404	411
	GS2		451	441	446	434	438	447	468	459	455	461	450
	GS3		0	0	0	0	0	0	0	0	0	0	0
	GS4		61	59	78	59	70	61	68	64	59	58	58
	GS5		2119	1946	1993	1983	1994	1768	428	188	164	156	170
	GS6		567	565	570	564	568	560	590	584	557	553	554
	GS7		804	796	799	795	795	771	814	806	767	752	766
	GS8		690	688	698	696	699	676	748	734	684	668	689
	GS9		493	496	499	501	503	483	573	561	483	480	487
	GN1		0	0	0	0	0	0	0	0	0	0	0
	GN2		484	482	495	487	492	510	499	504	531	524	514
	GN3		266	266	269	270	265	259	235	239	239	219	212
	GN4		256	256	276	258	265	256	265	271	269	272	265
	GN5		280	272	274	261	269	255	266	271	271	269	263
	GN6		647	640	635	628	629	609	695	691	600	596	591
	GN7		794	789	790	787	789	769	903	893	761	765	753

Table 3.12a (concluded): Stirrup strain ranges during HCF interval tests

Specimen	Strain Gage	Check test											
		0k	100k	200k	300k	400k	500k	750k	1M	1.25M	1.5M	1.75M	2M
9T12-B4	GS1	526	483	0	0	0	0	0		0	0	0	0
	GS2	183	49	137	36	30	139	37		38	39	51	43
	GS3	241	85	157	17	21	132	17		4	9	5	4
	GS4	234	181	223	186	193	295	207		253	252	248	267
	GS5	221	28	112	24	18	135	22		9	21	20	8
	GS6	720	841	810	804	818	815	883		992	1004	840	1148
	GS7	798	963	924	912	931	921	1019		1110	1113	948	1251
	GS8	551	526	513	503	504	498	523		585	580	464	612
	GN1	0	0	0	0	0	0	0		0	0	0	0
	GN2	24	8	7	9	11	10	0		0	0	0	0
	GN3	554	0	0	0	0	0	0		0	0	0	0
	GN4	178	124	221	31	33	192	27		29	27	30	30
	GN5	352	273	287	286	294	307	307		327	325	332	329
	GN6	907	849	791	799	800	803	819		989	984	667	1027
	GN7	1266	1266	1194	1201	1200	1205	1231		1480	1473	1073	1533
	GN8	813	789	770	766	766	785	809		874	841	698	897

After completion of the fatigue loading protocol, specimens were tested to failure using the previously described conventional loading history consisting of incrementally higher loads followed by unloading until failure. The applied shear and specimen displacement at the loading point of the specimens during precracking were combined with that measured during failure testing. This was performed by using the last displacement measurement recorded during precracking as the initial displacement for the failure test. Any offset produced by fatigue loading was ignored. The combined responses are shown in Figure 3.11 and do not indicate an abrupt change between the precracking and initial reloading responses during final testing. Photographs of the specimens after failure are shown in Figure 3.12. Other data from the failure tests are contained in Appendix A4.

Table 3.12b: Crack displacement ranges during fatigue interval tests

Specimen	Crack Gage	Check test											
		0k	100k	200k	300k	400k	500k	750k	1M	1.25M	1.5M	1.75M	2M
3IT12	#1	0.0047						0.0048	0.0055	0.0051	0.0057	0.0056	
	#2	0.0175						0.0188	0.0176	0.0186	0.0180	0.0194	
	#4	0.0074						0.0087	0.0086	0.0089	0.0091	0.0106	
	#5	0.0072						0.0069	0.0076	0.0071	0.0077	0.0083	
3T12	#1	0.0086								0.0087	0.0035		0.0090
	#2	0.0036								0.0034	0.0032		0.0038
	#4												0.0082
	#6												0.0077
3IT18	#2	0.0091	0.0122	0.0126	0.0137	0.0131	0.0141	0.0142	0.0134	0.0131	0.0134	0.0140	0.0137
	#3	0.0089	0.0095	0.0098	0.0098	0.0096	0.0094	0.0111	0.0110	0.0109	0.0116	0.0118	0.0118
	#4	0.0071	0.0082	0.0086	0.0084	0.0085	0.0081	0.0097	0.0100	0.0099	0.0104	0.0111	0.0132
	#5	0.0059	0.0064	0.0071	0.0067	0.0070	0.0072	0.0076	0.0078	0.0084	0.0086	0.0091	0.0096
	#6	0.0041	0.0051	0.0054	0.0054	0.0053	0.0054	0.0063	0.0066	0.0070	0.0073	0.0076	0.0078
5IT12-B1	#1		0.0044		0.0049		0.0051	0.0054	0.0052	0.0051	0.0054	0.0054	0.0053
	#2		0.0005		0.0065		0.0066	0.0070	0.0068	0.0065	0.0066	0.0066	0.0069
	#5		0.0087		0.0091		0.0096	0.0093	0.0097	0.0095	0.0092	0.0093	0.0089
6IT10	#2	0.0049	0.0066	0.0069	0.0069	0.0086	0.0091	0.0113	0.0113	0.0151	0.0157	0.0156	
	#3	0.0061	0.0067	0.0070	0.0065	0.0075	0.0071	0.0059	0.0075	0.0093	0.0078	0.0083	
	#4	0.0068	0.0085	0.0084	0.0083	0.0088	0.0086	0.0081	0.0087	0.0090	0.0085	0.0092	
	#5	0.0044	0.0050	0.0053	0.0049	0.0053	0.0058	0.0049	0.0057	0.0059	0.0054	0.0061	
	#6	0.0031	0.0041	0.0054	0.0045	0.0048	0.0050	0.0048	0.0056	0.0057	0.0055	0.0065	
6T10	#1	0.0055	0.0061	0.0064	0.0062	0.0063		0.0093	0.0098	0.0099	0.0100	0.0083	0.0101
	#2	0.0097	0.0110	0.0113	0.0118	0.0118		0.0133	0.0137	0.0141	0.0140	0.0133	0.0142
	#3	0.0081	0.0106	0.0108	0.0114	0.0114		0.0114	0.0129	0.0124	0.0111	0.0128	0.0127
	#4	0.0060	0.0066	0.0070	0.0074	0.0078		0.0090	0.0098	0.0099	0.0117	0.0097	0.0104
	#5	0.0027	0.0042	0.0045	0.0045	0.0052		0.0063	0.0065	0.0069	0.0069	0.0071	0.0074
	#6	0.0000	0.0000	0.0000	0.0000	0.0000		0.0000	0.0000	0.0000	0.0000	0.0000	0.0000
8IT10	#1			0.0093	0.0091	0.0098	0.0095	0.0091	0.0098			0.0103	0.0102
	#2			0.0072	0.0075	0.0080	0.0076	0.0077	0.0081			0.0085	0.0082
	#3			0.0087	0.0098	0.0086	0.0088	0.0088	0.0093			0.0096	0.0095
	#4			0.0069	0.0075	0.0072	0.0073	0.0072	0.0076			0.0088	0.0074
	#5			0.0050	0.0057	0.0057	0.0052	0.0055	0.0058			0.0069	0.0071
	#6			0.0076	0.0085	0.0077	0.0076	0.0078	0.0083			0.0083	0.0084
9IT12-B1	#1		0.0090	0.0094	0.0096	0.0097	0.0098	0.0099	0.0120	0.0122	0.0102	0.0103	0.0104
	#4		0.0141	0.0145	0.0147	0.0147	0.0147	0.0148	0.0164	0.0166	0.0146	0.0149	0.0159
	#5		0.0085	0.0086	0.0089	0.0088	0.0105	0.0089	0.0102	0.0103	0.0090	0.0090	0.0108
9T12-B4	#1	0.0086	0.0089	0.0086	0.0086	0.0086	0.0089	0.0097		0.0112	0.0137	0.0102	0.0111
	#2	0.0095	0.0117	0.0115	0.0123	0.0127	0.0130	0.0141		0.0113	0.0115	0.0083	0.0124
	#3	0.0077	0.0087	0.0164	0.0084	0.0086	0.0086	0.0086		0.0157	0.0167	0.0138	0.0179
	#4	0.0116	0.0134	0.0128	0.0129	0.0133	0.0132	0.0134		0.0162	0.0155	0.0140	0.0156
	#5	0.0089	0.0084	0.0079	0.0078	0.0082	0.0095	0.0077		0.0101	0.0101	0.0088	0.0107

3.8.3 Results

The specimens included both T and inverted-T configurations, stirrup spacings ranging from 10 to 18 in., as well as different flexural reinforcing bar details. Comparing specimen performance during high-cycle fatigue tests, specimens with flexural cutoffs and hooked bars (specimens 8IT10 and 9IT12-B1) did not exhibit significant differences from other specimens. However, the specimen with flexural bar cutoffs and straight-bar anchorage (9T12-B4) appeared to have higher rates of diagonal crack width growth as well as strain range and mean increases. Considering test durations when the dead load remained fairly constant (steady pressure in the applied dead load cylinder), the stirrup strain range increased along the eventual failure crack as shown in Figure 3.24. This diagonal crack intersected the flexural steel just past the cutoff location.

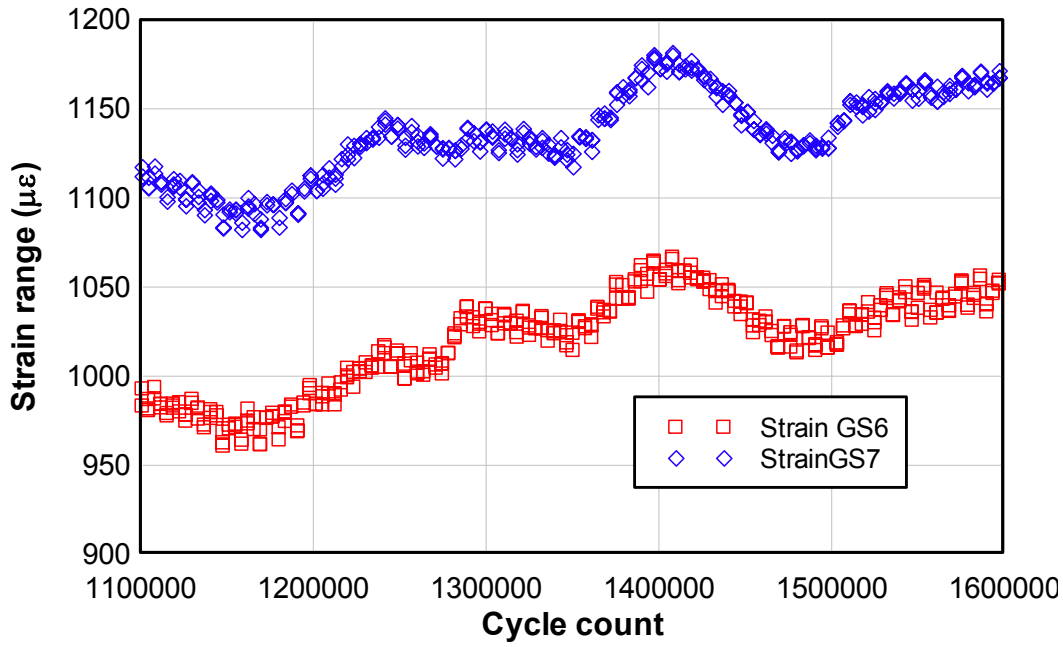

Figure 3.24: Increasing strain range in specimen 9T12-B4, having cut and straight bars during HCF test

On each specimen, at least one strain gage sensor measured a stress range of approximately 13.8 ksi at diagonal crack locations on the south half of the beam. The 13.8 ksi stress range is above the single highest stress range observed in the field testing portion of this research program. Further, based on field testing of three typical 1950's RCDG bridges, the 13.8 ksi stress range applied for 2,000,000 cycles corresponds to approximately 50 years of service life, using a linear damage model (Minor's Rule) and an equivalent constant amplitude fatigue stress derived from the variable amplitude strain field measurements at the highest strain location (Location #7 on McKenzie River Bridge).

On the north side, stress ranges were even higher, although the stress field was more complex due to the positioning of the dead load cylinder. During the warmer months, stress ranges in the stirrups at locations where concrete cover was removed show oscillation at approximately a 24-hour interval due to heating and cooling at the exposed surface. Adjustments to the dead load

cylinder also had a noticeable effect on stirrup stress ranges. As an example, Figures A6.13 and A6.15 in Appendix A6 show the effects of applied dead load increase at about 700,000 cycles, and Figures A6.25 and A6.27 show the effects of dead load decrease at about 500,000 cycles. Measured stress ranges remained fairly consistent during high-cycle fatigue as illustrated in Figure 3.25, where strains changed slightly over a long period of cyclic loading. There were also several instances of instruments going out of range due to the demanding test protocol.

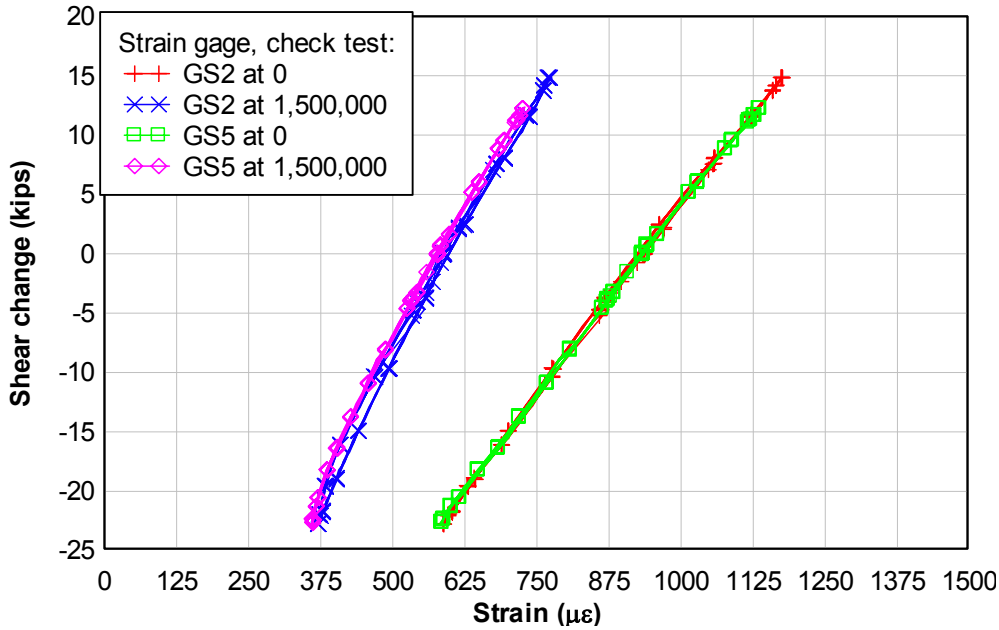

Figure 3.25: Measured strain comparing two interval tests for specimen 6IT10

Only small visible growths in crack width or extensions were observed over the 2,000,000 cycles for each specimen. Crack displacement tended to increase slightly, though typically not of a sufficient magnitude to be perceived using the visual ODOT crack comparator. Accounting for sensors and load fluctuations during the long-duration tests, the crack motion ranges typically increased, as shown in Table 3.10. These increases were attributed to bond slip of the stirrup relative to the concrete at the diagonal cracks. Concrete debris, shown in Figure 3.26a and b, and relative slip between the stirrup and concrete were visually observed at locations where concrete cover was removed to install strain gages on the stirrup leg.

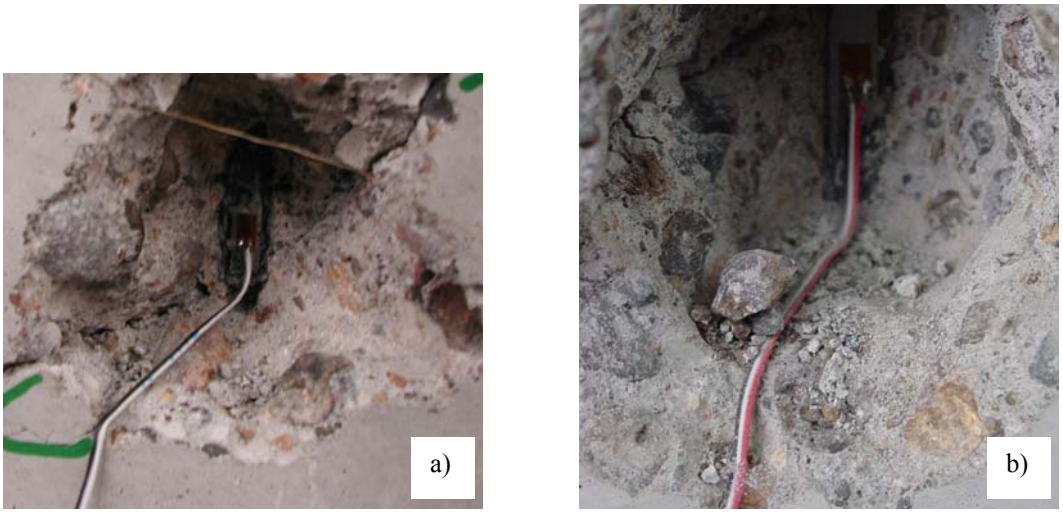

Figure 3.26: Example of debris associated with bond damage around stirrup legs: a) specimen 6T10; b) specimen 3IT12

Corresponding rebar strains did not change at the same rate as the crack displacements. Similar magnitudes of stirrup strain were produced even as diagonal crack displacements became larger, as shown in Figure 3.27. Comparison of the strain gage and associated crack motion sensor ranges in Figure 3.28, over the course of the fatigue test further illustrate this behavior.

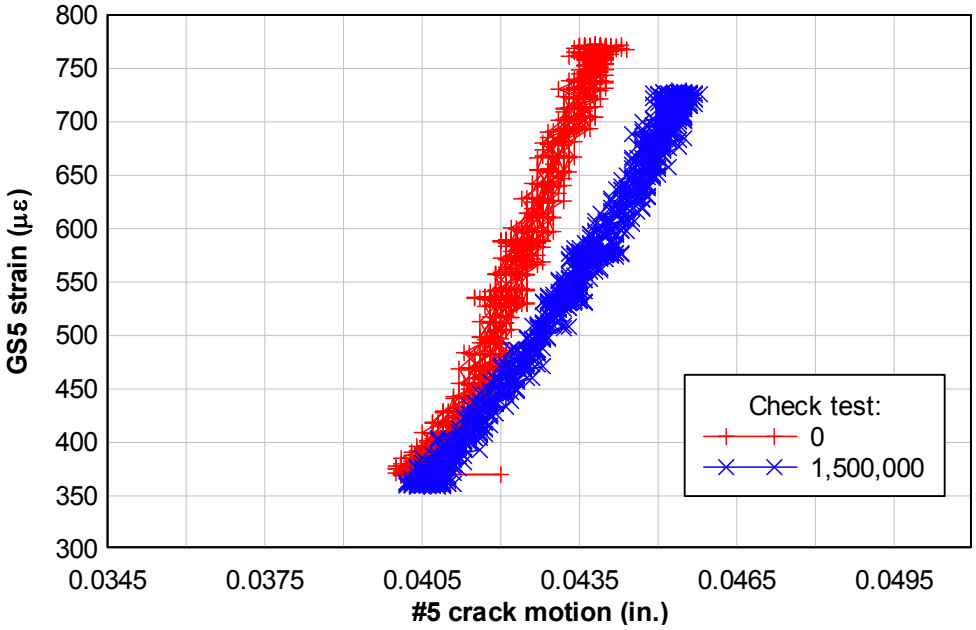

Figure 3.27: Strain gage and associated crack motion sensor at the eventual failure crack in specimen 6IT10. Note that after many cycles, less strain is needed to achieve the same crack movement

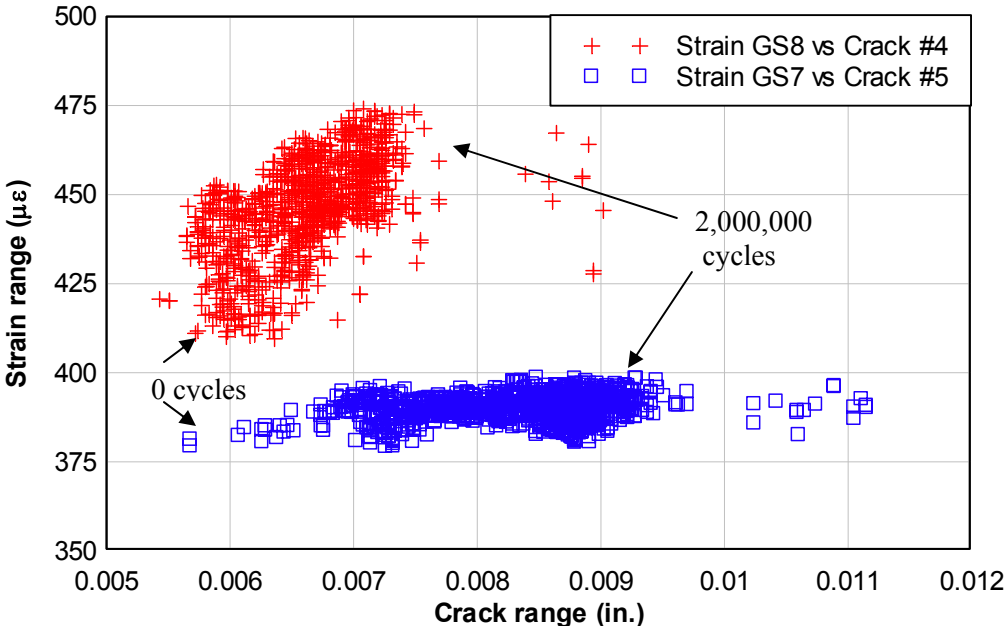

Figure 3.28: Changes in strain range and crack range for specimen 3IT12 over a 2,000,000 cycle HCF test

One sensor location shows the strain range increasing along with the crack range, while the other shows increasing crack motion with almost constant strain range. Thus, if the diagonal crack displacement increases without a corresponding increase in stirrup stress, the effective gage length of the rebar is likely increasing, indicating a reduction in bond. This degradation process was observed to be gradual. To evaluate the impact of stirrup debonding on the capacity and behavior of the girders, a series of tests was performed as described in the next section.

Metal fatigue of the stirrups occurred in only one specimen that contained the widest stirrup spacing considered in the HCF test series (3IT18). Testing at failure exposed two stirrups exhibiting cleavage failure surfaces instead of the ductile fracture surface commonly associated with previous ultimate strength tests as shown in Figure 3.29.

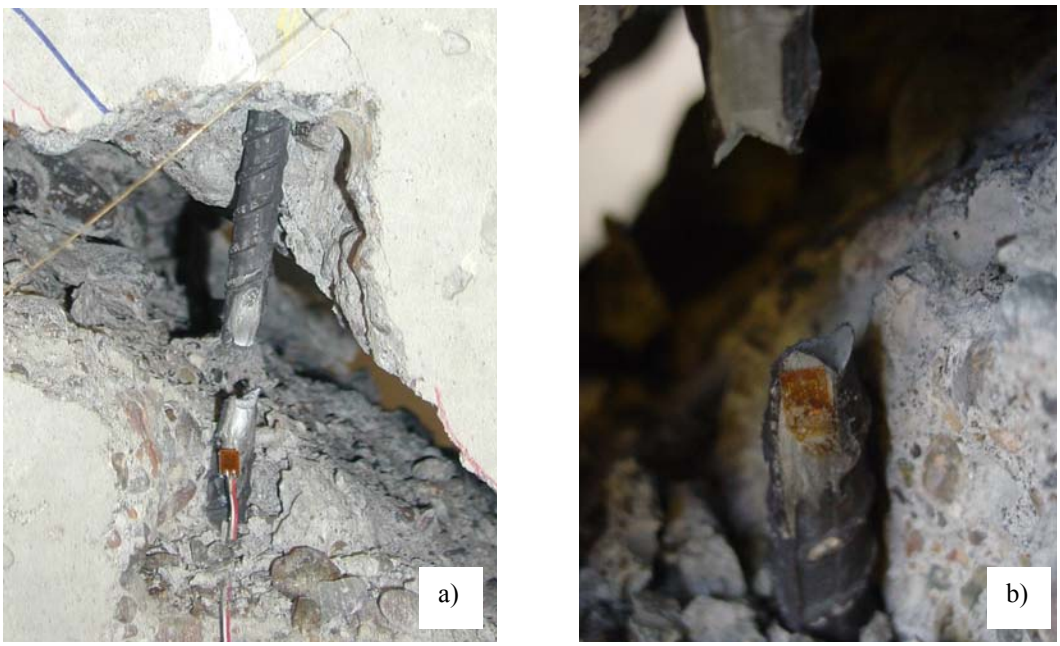

Figure 3.29: Ductile fracture of stirrup at ultimate strength: a) sensor GS8 on specimen 3IT18; b) another example from specimen 3IT12

One high-cycle fatigue fracture was located approximately 9 in. below strain gage GS2 on the east face stirrup leg and the other was located about 2 in. above GS7 on the west face stirrup leg; both are pictured in Figures 3.30 and 3.31.

Figure 3.30: Fracture surface on east leg of stirrup from high-cycle fatigue specimen 3IT18 at 9 in. below sensor GS2

Figure 3.31: Fracture surfaces on west leg of stirrup from high-cycle fatigue specimen 3IT18 at 2 in. above sensor GS7

The west face stirrup leg fracture occurred just after 1,750,000 cycles during fatigue testing as observed by the abrupt strain decrease in the stirrup and resulting increases in the neighboring stirrup strains and crack displacement sensor readings, as shown in Figures 3.32 and 3.33 for the crack motions and Figures 3.34 and 3.35 for the strain readings.

The measured stress range in stirrup GS7 was approximately 29 ksi as measured by the strain gage applied 2 in. above the eventual fracture location. The east stirrup leg fatigue fracture was not detected from the sensor measurements, but may have occurred at about the same time, so that the combined effect was blended into the measurements. The higher stress ranges carried by the adjacent stirrups would have caused these to fatigue at a higher rate and likely lead to their eventual fracture.

Subsequent strength testing of fatigued specimens did not indicate significant change in capacity as compared to the unfatigued specimens. However, to approximate the impact of very substantial stirrup debonding on the capacity and behavior of the girders, a series of tests was performed as described below.

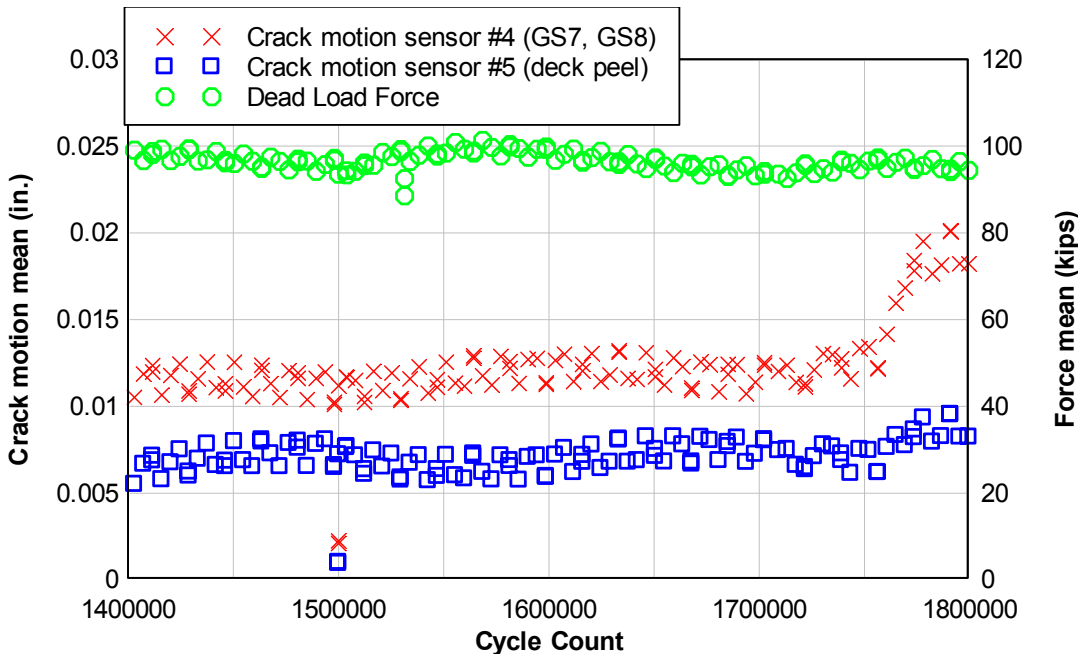

Figure 3.32: Detail from specimen 3IT18 load and crack motion sensor means. Note the change after 1,750,000 cycles

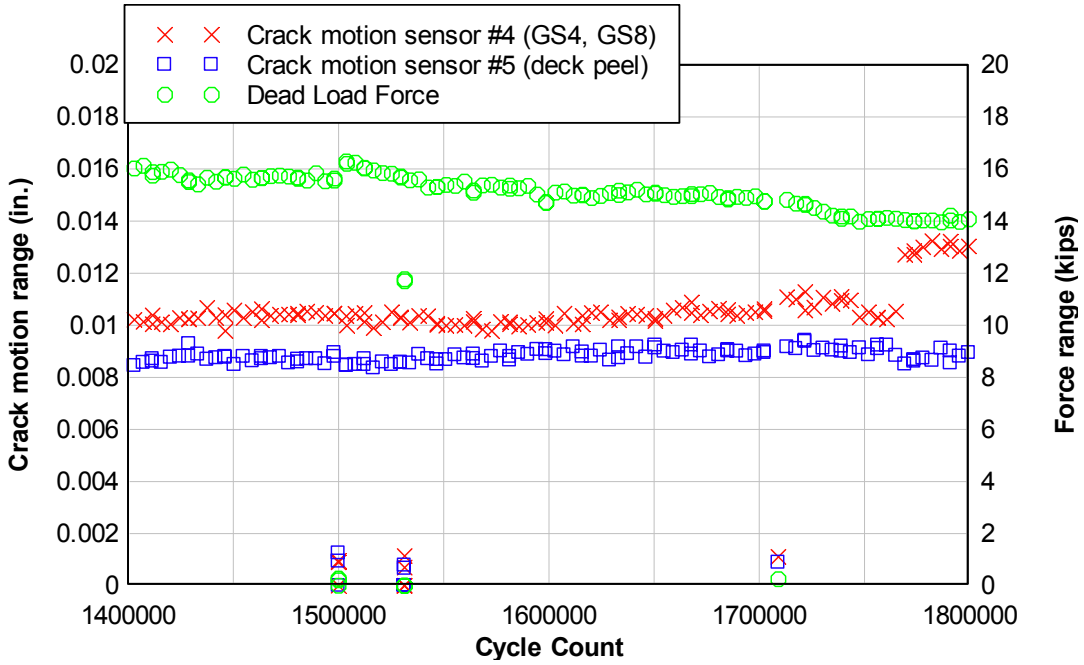

Figure 3.33: Detail from specimen 3IT18 Load and crack motion sensor ranges. Note the change after 1,750,000 cycles

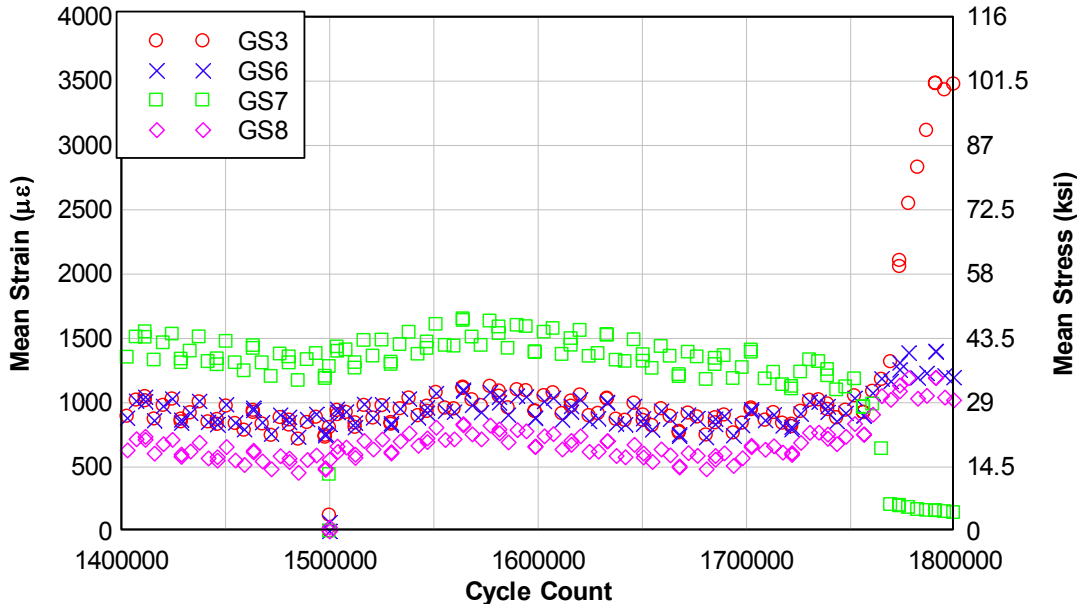

Figure 3.34: Detail from specimen 3IT18 South strain gage means. Note the change after 1,750,000 cycles

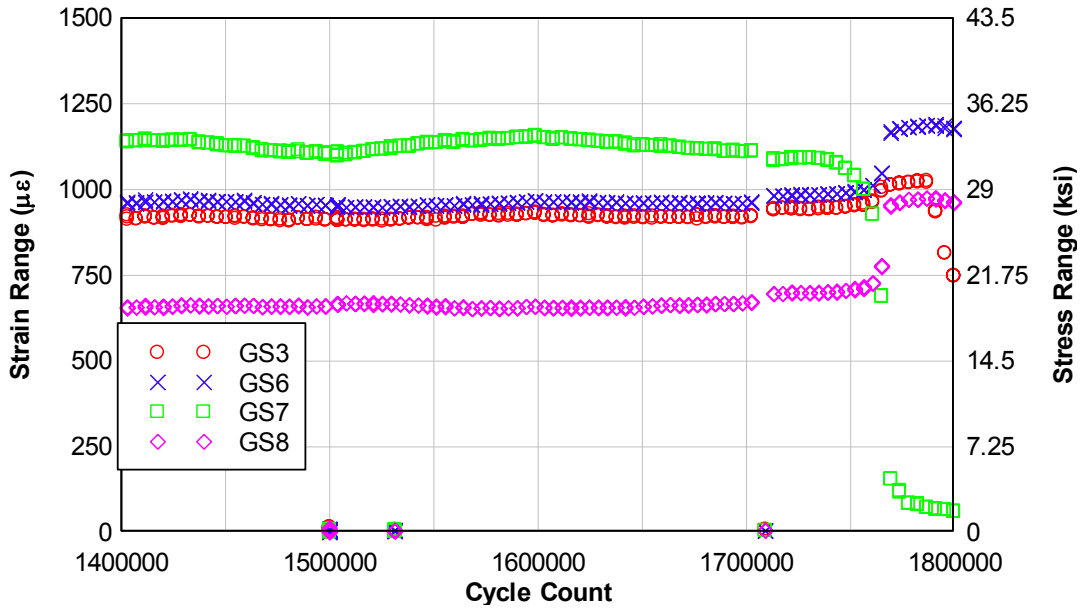

Figure 3.35: Detail from specimen 3IT18 South strain gage ranges. Note the change after 1,750,000 cycles

3.8.4 Debonded Stirrup Specimens

Based on the observed deterioration of the stirrup-concrete bond under high-cycle fatigue, a series of experiments was performed to assess the impact of stirrup debonding on the capacity and behavior of test specimens. During 2 million cycles of fatigue loading, the stirrups did not become fully debonded from the concrete along the entire leg length. However, if the high-cycle fatigue tests were permitted to be run continuously and at a sufficiently low threshold so as not to induce metal fatigue (stress range below 20 ksi) it could be possible to produce the condition of fully debonded stirrups. Due to the space, time, and equipment demands to achieve this condition, it was not possible to conduct these tests in the laboratory.

To simulate this effect, four specimens were constructed (7T6, 7T12, 7IT6, and 7IT12) with all the stirrup legs within the test span debonded from the concrete. The vertical straight leg portions of the stirrups were wrapped with plastic strand sheathing to prevent bond between the stirrup leg and surrounding concrete. The horizontal portion at the hooked end and the horizontal length between bends at the beam soffit were not wrapped. These specimens were tested using the control loading protocol described previously.

3.8.4.1 Debonded Stirrup Test Results

Experimental results from 5IT12-B4 specimen were used for comparisons of behavior between specimens with and without debonded stirrups, since these specimens had similar beam details and were subjected to the same test protocols. The stem concrete strengths of 5IT12-B4 and 7IT12 specimens were also similar, 4130 psi and 4165 psi, respectively.

Both specimens exhibited shear-compression failures with applied load of 405.4 kips for 5IT12-B4 specimen and 400.2 kips for specimen 7IT12. Failures occurred on the north end of both specimens. Specimen displacement under the load point at the failure load was 1.01 in. for the 5IT12-B4 specimen and 0.81 in. for the 7IT12 specimen. Fewer but wider diagonal-tension cracks were observed in 7IT12 specimen as shown in Figure 3.36.

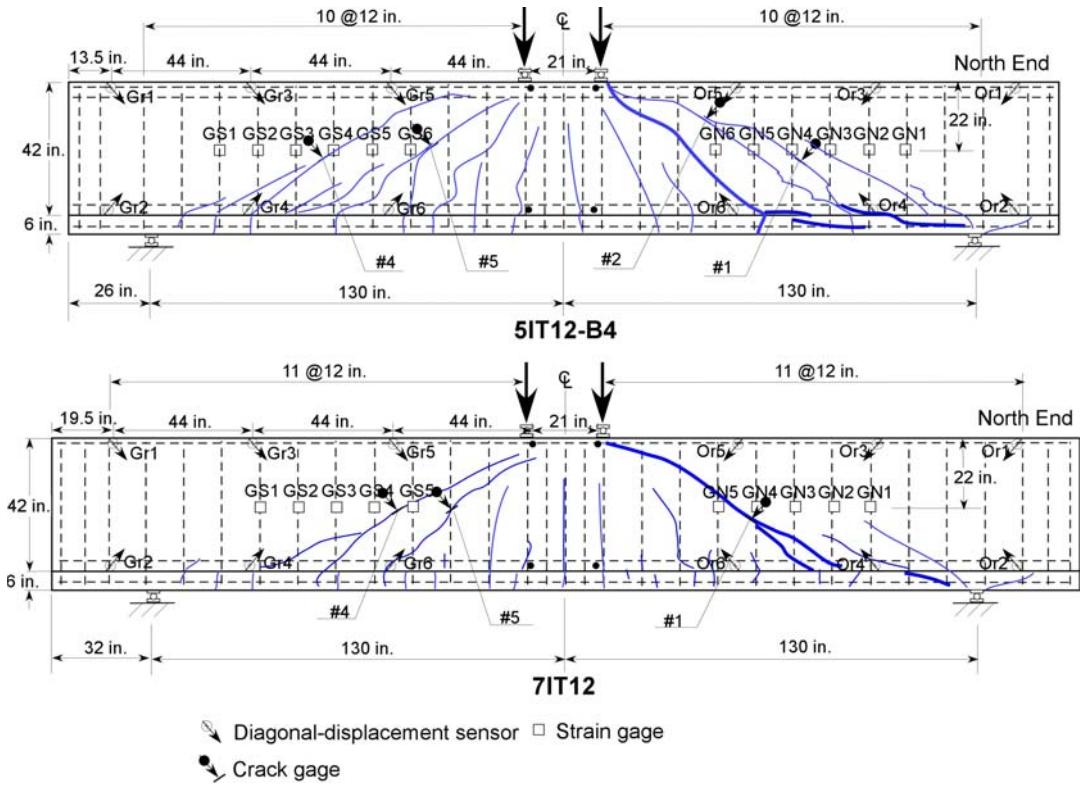

Figure 3.36: Crack pattern and instrument locations for 5IT12-B4 and 7IT12 specimens

The largest crack width measured with the visual crack comparator at the load step prior to failure was 0.124 in. for specimen 5IT12-B4 and 0.132 in. for specimen 7IT12. Specimen 5IT12-B4 was stiffer than 7IT12 specimen as shown in Figure 3.37. Although failure loads of both specimens were relatively similar, specimen 7IT12 was less ductile.

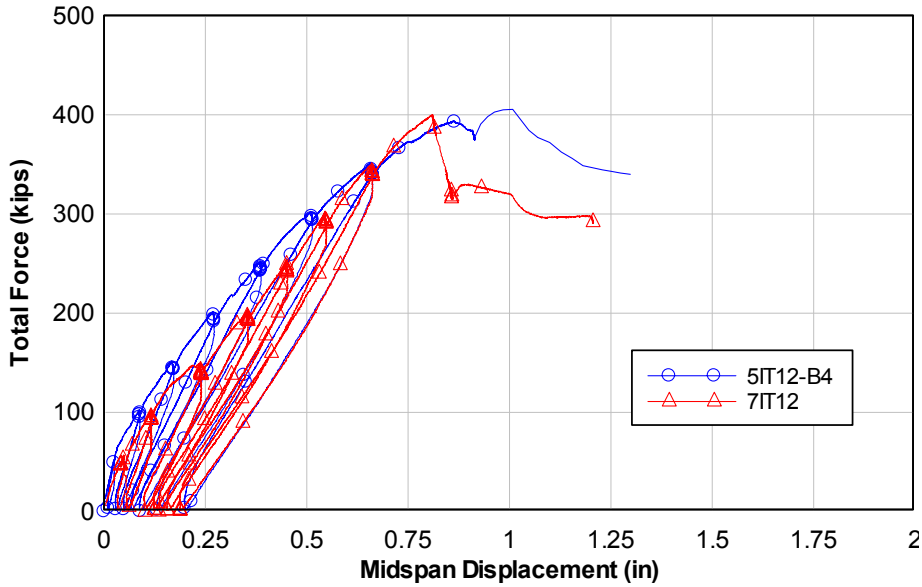

Figure 3.37: Load-midspan displacement plots for 5IT12-B4 and 7IT12 specimens

Diagonal-tension cracks in specimen 7IT12 formed earlier than those in 5IT12-B4 specimen, as indicated by the first abrupt change in stirrup strains shown in Figure 3.38a. Smaller crack widths at unloading were observed for the 7IT12 specimen due to the debonded stirrups as shown in Figure 3.38b. This was a result of reduced local stirrup yielding at crack locations due to the longer effective gage length of the stirrup leg.

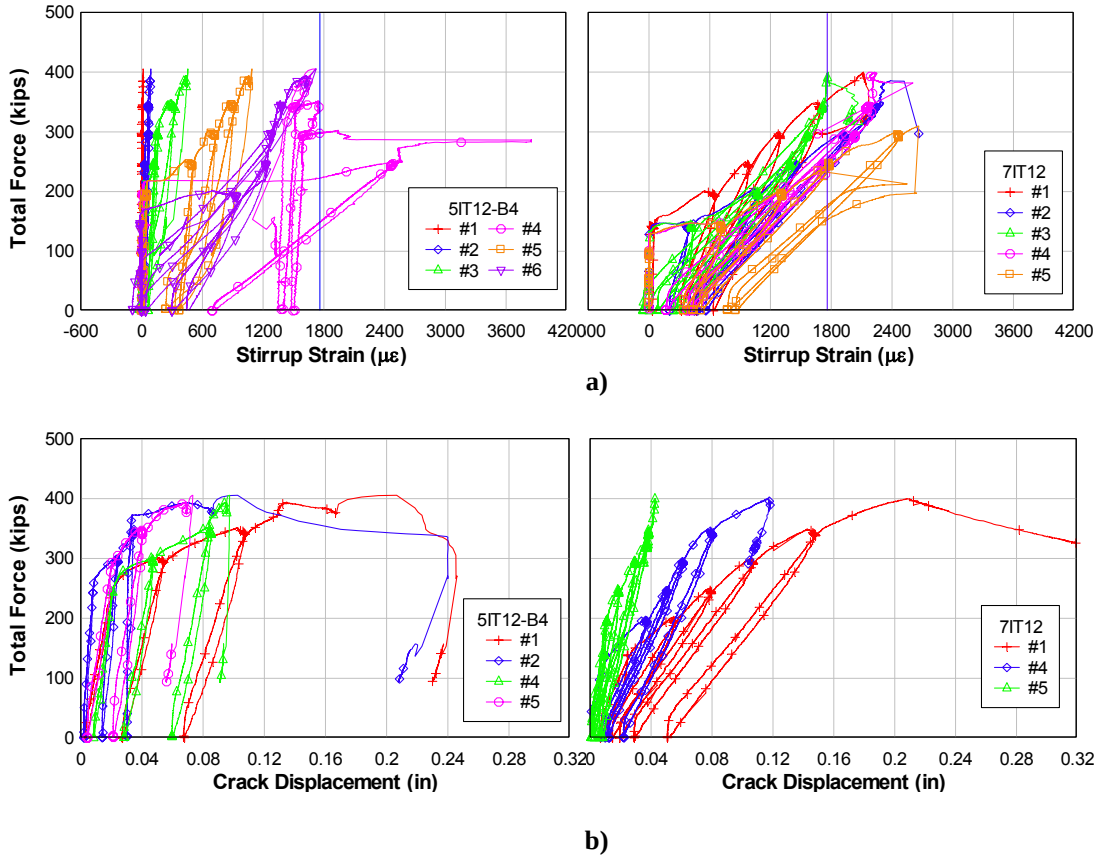

Figure 3.38b: Stirrup strains and crack displacements for 5IT12-B4 and 7IT12 specimens: a) stirrup strains in the north-end side; b) crack displacements

Typically, strain gages located near midheight of specimens with bonded reinforcing bars measured large strains in stirrups when diagonal-tension cracks form across or near the instrumentation locations on the stirrups, as occurred in specimen 5IT12-B4. Strain sensors GN1 and GN2 in specimen 5IT12-B4 indicated small strains throughout the test, as shown in Figure 3.38a, because they were not located near a diagonal crack. For specimen 7IT12, large stirrup strains were observed from sensors GN1-GN3 although no diagonal cracks formed near the strain gages.

Strains in all instrumented stirrups of specimen 7IT12 exhibited similar response for both loading and unloading and exceeded the yield strain indicated by a vertical line in Figure 3.38a. When strains in all stirrups across a diagonal-tension crack reach the yield stress for the debonded condition, the section is likely near failure. For specimen 5IT12-B4, failure occurred before the strain in sensor GN6 was close to the yield strain. Specimen 7IT12 failed after sensor GN3 reached the yield stress.

3.8.5 Conclusions

Full-size tests of conventionally-reinforced concrete (CRC) girders, designed and constructed to reflect 1950's vintage details and materials, were performed under high-cycle fatigue. Prior to fatigue loading, specimens were precracked to achieve desired crack widths corresponding to observed field conditions. High-cycle fatigue loading was applied to the precracked specimens with a constant amplitude load range of 80 kips for 2,000,000 cycles. The specimens were then tested to ultimate. A series of tests with fully debonded stirrups was also performed to simulate a condition of serious bond deterioration. Based on these tests, the following conclusions are presented:

- Repeated loading in the service range can lead to metal fatigue of embedded stirrups. Stress ranges needed to meet this condition exceeded 20 ksi and appear to be represented by fatigue data for reinforcing steel as discussed in the field testing section.

- Diagonal crack widths tended to increase under repeated loading.

- Stirrup strain range changes varied for different specimens, although in general these remained fairly similar from the start to the end of high-cycle fatigue testing.

- Flexural bar cutoffs combined with straight-bar anchorage appeared to have more rapid changes for both crack displacement as well as strain ranges and means than otherwise similar specimens with well-anchored flexural reinforcement.

- The mechanism for damage from high-cycle fatigue (if fracture is precluded) is bond fatigue at the stirrup/concrete interface.

- Bond fatigue may eventually lead to longer gage lengths for stirrups and reduced constraint at diagonal crack locations, thereby leading to wider diagonal cracks.

- Wider cracks resulting from bond deterioration under HCF may reduce capacity based on modified compression-field theory (MCFT). Analysis methods to account for bond deterioration are discussed in a subsequent section.

- The specimen with fully debonded stirrups exhibited only slightly reduced capacity than an otherwise similar specimen with bonded stirrups. Stirrup debonding resulted in fewer but wider diagonal cracks, although the overall specimen displacement was reduced at failure.

- For the specimens and loading conditions considered, HCF loading did not significantly diminish the capacity of the specimens, when metal fatigue of the stirrups was precluded.

3.9 MOVING LOAD TESTS

Moving load tests are described in a separate appendix to this report.